First principle Investigation Of Electronic Structure,Magnetic Property And Valley Hall conductivity In Monolayer And Bilayer MoS_2 Doped (Mn,V)

A Dissertation Submitted to the Department of Physics

Addis Ababa University

In Partial Fulfillment of the Requirement of the Degree

of Doctor of Philosophy in Physics

Department of Physics Addis Ababa University

Sintayehu Mekonnen

Addis Ababa, Ethiopia

February 2018

DECLARATION

I hereby declare that this PhD dissertation is my original work and has not been presented for a degree in any other university, and that all sources of material used for the dissertation have been duly acknowledged.

Name: Sintayehu Mekonnen

Signature: ——————

This PhD dissertation has been submitted for examination with my approval as university advisor.

Name: Prof.P.Singh

Signature: ——————

Addis Ababa University

Department of Physics

February 2018

Addis Ababa University
Department of Physics

This is to certify that the dissertation prepared by Sintayehu Mekonnen Hailemariam, entitled "First principle Investigation Of Electronic Structure,Magnetic Property And Valley Hall conductivity In Monolayer And Bilayer MoS_2 Doped (Mn,V)" submitted in fulfillment of the requirements for the degree of Doctor of Philosophy(Physics) complies with the regulations of the university and meets the accepted standards with respect to originality and quality.

by

Sintayehu Mekonnen

Addis Ababa University
Department of Physics

Approved by the Examination Committee

External Examiner	Dr.Sudip Chakraborty
Internal Examiner	Dr. Chernet Amente
Advisor	Prof. Pooran Singh
Chairman	Dr.Teshome Senbeta

Contents

Bibliography . . . . . .

1 Review Literature **1**

1.1 Structural and electronic property of Bulk MoS_2 1

1.2 Structural and electronic property of monolayer MoS_2 1

1.3 Structural and electronic properties of bilayer and few layer MoS_2 . . 3

1.4 Two dimensional dicolgenide semiconductors ,MoS_2,doped with transition metal elements 3

1.4.1 Dilute magnetic semiconductor property of transition-metal doped MoS_2 4

1.4.2 Magnetic exchange interaction in transition metal doped MoS_2 5

1.5 Valley degree of freedom in MoS_2 6

2 Many body system and Density functional theory **8**

2.1 Introduction to many body system 8

2.1.1 The Hartree approximation 9

2.1.2 The Hartree-Fock approximation 10

2.2 Density functioinal Theory 12

2.2.1 The Hohenberg-Kohn Theorems 12

2.2.2 The Kohn-Sham Equations 15

2.3 Self-consistent cycle and approximation for exchange-correlation energy (E_{XC}) 16

2.3.1 Local density approximation (LDA) 18

2.3.2 The generalized gradient approximation (GGA) 19

2.4 Spin polarized Density functional Theory 19
2.5 Density Functional Theory + Hubbard potential (U)approach 20
2.6 Plane Wave approximation 21
2.7 k point sampling and Brillouin zone integration 23
2.8 Pseudopotentials 24

3 Electronic structure and Magnetic property of Mn doped monolayer and Bilayer MoS_2 25

3.1 Unit cell parameter deterimination 25
3.1.1 plane wave cut off energy(ecut) and k-point sampling 25
3.1.2 Electronic properties of single and bilayer MoS_2 28
3.1.3 Interlayer distance dependent band structure in bilayer MoS_2 28
3.2 Computional details 30
3.3 Result and discussion 31
3.3.1 Defect formation energy and structural stability 31
3.3.2 Electronic Structures and magnetism Of single Mn doped monolayer and bilayer MoS_2 33
3.3.3 Magnetic interaction in monolayer MoS_2 doped with pair of Mn atoms 35
3.3.4 Magnetic interaction in bilayer MoS_2 doped pair of Mn atoms 37
3.3.5 Mechanism of exchange interaction 38
3.3.6 Ferromagnetic transition temperature (T_c) 43
3.3.7 Conclusion 47

4 Electronic structure and Magnetic property of Vanadium(V) doped monolayer and bilayer MoS_2 49

4.1 Result and Discussion 49
4.1.1 Defect formation energy and structural stability 49

4.1.2 Electronic structure and magnetic properties of pure and single V doped ML and BL MoS_2 . . . 51
4.1.3 Magnetic interaction in monolayer and bilayer MoS_2 doped pair of Vanadium atoms . . . 53
4.1.4 Ferromagnetic transition temperature (T_c) for Vanadium doped monolayer and bilayer MoS_2 . . . 56
4.2 Conclusion . . . 60

5 Valley and Spin Hall effect in doped monolayer MoS_2 61
5.1 Theoretical Model . . . 61
5.2 Berry potential . . . 64
5.2.1 Berry curvature in the vicinity of K^- and K^+ Valleys of doped Monolayer MoS_2 . . . 65
5.3 The Kubo formula and Anomalous Hall Conductivity . . . 66
5.4 Spin and valley Hall Conductivity . . . 68
5.4.1 Spin and Valley Hall conductivity in ML MoS_2 when Fermi level is in the gap . . . 69
5.4.2 Spin and Valley Hall conductivity in Mn doped ML MoS_2 at T=0 71
5.5 Discussion . . . 73
5.6 Conclusion . . . 75

6 Summary and future work 78
6.1 List of publications . . . 88

A Appendix 89
A.1 Derivation of Berry curvature in two dimensional k-space . . . 89

B Appendix 93
B.1 Linear response theory to derivative Kubo formula for Hall conductivity 93

List of Figures

1.1 History of molybdenum disulphide research for last 50 years (1964-2014) which shows the annual number of journal publications adopted from [27] 2

1.2 a)Raman spectra of the undoped and the Mn^{2+} doped MoS_2 nanostructures with a different doping concentration, b)magnetic properties of the MoS_2 and the 7% Mn doped MoS_2 [43]. 5

2.1 Algorithm for Self-consistent field theory in Hartree. 11

2.2 Self-consistent Kohn-Sham loop 17

3.1 Unit cell structure of single layer MoS_2 (a) top view (b) side view . . . 25

3.2 Convergence of total ground state energy of single layer MoS_2 with respect to :a)plane wave cut off energy (ecut), b) Brillouin sampling(k points),c)lattice parameter. 26

3.3 Band structure of single layer MoS_2:a)without considering spin-orbit coupling,b)considering spin-orbit interaction 27

3.4 Density of state in single layer MoS_2: a)Total density of states for both spin up and spin-down electrons, b)Partial density of states 27

3.5 Bilayer MoS_2 a) crystal structure b)Total Ground state energy versus interlayer distance 29

3.6 Interlayer distance dependent band gap in bilayer MoS_2:a)band structure at equilibrium interlayer distance,b)band structure at interlayer distance (d=6.65Å) 29

3.7 Optimized input structure for ML and BL MoS_2 : a,b and c) top view of $4\times4\times1, 5\times5\times1$ and $6\times6\times1$ pure ML supercells respectively ,(d,e and f) top view of two Mn doped $4\times4\times1$,$5\times5\times1$ and $6\times6\times1$ ML MoS_2,g)top view of $4\times4\times1$ pure BL MoS_2 ,h and i) side(xy) view and (xz) view of two Mn doped on different layers of BL MoS_2 32

3.8 Spin resolved total density of state for $4\times4\times1$ and $3\times3\times1$ ML MoS_2 : (a) Pure MoS_2, (b) one-Mn-doped $4\times4\times1$ MoS_2 ML and (c) one Mn-doped $3\times3\times1$ MoS_2 ML respectively. The blue and red lines represent the spin-up and spin-down components respectively.The zero energy represents the Fermi level. 39

3.9 Spin resolved total density of state for $4\times4\times1$ and $3\times3\times1$ BL MoS_2:(a) pure MoS_2,(b)One-Mn-doped on upper layer of BL $4\times4\times1$ MoS_2 and (c)two Mn-doped in upper layer of $4\times4\times1$ BL MoS_2 d)Two Mn-doped in different layers of $4\times4\times1$ BL MoS_2 ,e)Two Mn-doped in upper layer of $3\times3\times1$ BL MoS_2 respectively. 40

3.10 Band structure for $4\times4\times1$ ML MoS_2 : (a) and (b) pure MoS_2, (c) and (d) one-Mn-doped $4\times4\times1$ ML MoS_2 respectively. The blue and red lines represent the spin-up and spin-down components respectively.The zero energy represents the Fermi level. 41

3.11 Band structures of $4\times4\times1$ BL MoS_2 : (a) and (b) pure MoS_2, (c) and (d) one-Mn-doped in upper layer of BL MoS_2,and (e) and (f) two-Mn-doped BL MoS_2(in different layers).The blue and red lines represent the spin-up and spin-down components respectively. 42

4.1 Optimized input structure of ML and BL MoS_2: (a) top view pure ML MoS_2 , (b) top view for one V doped ML MoS_2, (c) top view for two V doped ML MoS_2 and (d) side view for two V doped in different layers of BL MoS_2 50

4.2 Spin resolved density of state for $4 \times 4 \times 1$ and $3 \times 3 \times 1$ ML MoS_2: (a) pure ,b)one-V-doped $4 \times 4 \times 1$ ML MoS_2, c) one V-doped $3 \times 3 \times 1$ ML MoS_2 respectively. The blue and red lines represent the spin-up and spin-down components respectively.The zero energy represents the Fermi level. 57

4.3 Spin resolved density of state for $4 \times 4 \times 1$ and $3 \times 3 \times 1$ MoS_2 (BL): (a) pure MoS_2, (b) one-V-doped $4 \times 4 \times 1$ MoS_2 BL , (c) one-V-doped $3 \times 3 \times 1$ BL MoS_2 and (d) two V-doped $3 \times 3 \times 1$ BL MoS_2 respectively. The blue and red lines represent the spin-up and spin-down components, respectively. The zero energy represents the Fermi level. 58

4.4 Band structures of $4 \times 4 \times 1$ ML and BL MoS_2 supercell: (a) and (b) pure ML MoS_2, (c) and (d) one-V-doped ML MoS_2 , (e) and (f) pure BL MoS_2, (g) and (h) one-V-doped BL MoS_2 respectively .The blue and red lines represent the spin-up and spin-down components respectively 59

5.1 The color on line: the left panel 2D first Brillouin zone with special k points. b_1 and b_2 are the reciprocal basis vectors. The two inequivalent valleys K and K^- are shown in black and their equivalent counterparts in gray,the right panel atomic orbitals weights in the energy bands of MoS_2 61

5.2 Electronic band structure near valley $K^{\pm}$: a) and b)for zero both spin-orbit coupling and hexchange field (lo=h_{ex}=0),c) and d) for spin-orbit coupling(lo=0.08eV,) and zero exchange field ,and e) and f) for spin-orbit coupling(lo=0.08eV) and exchange field(h_{ex}=0.2eV). Red: spin up electron(hole) states, blue: spin down electron(hole) states,right panel for K^+ and left panel for K^- valley. 76

5.3 Berry Curvature as function of ($\frac{ka}{\pi}$) for different values of exchange field(h_{ex}) ,right panel for K^+ and left panel for K^- valley. 77

List of Tables

3.1 Summary of Interlayer distance dependent band structure in bilayer MoS_2 30

3.2 Calculated values of formation energy ,E_F(eV), monolayer (ML) and bilayer (BL) MoS_2 doped with Mn under Mo rich and S-rich condition 34

3.3 Magnetic energy (ΔE) and magnetic moment (μ_m)for Mn doped monolayer(ML) MoS_2 36

3.4 Magnetic energy (ΔE) and magnetic moment (μ_m)for Mn doped bilayer(BL) MoS_2 38

3.5 The calculated ferromagnetic transition temperature T_c for Mn doped monolayer(ML) and bilayer(BL) MoS_2. 47

4.1 Calculated values of formation energy ($E_{form}(eV)$) V doped ML and BL MoS_2 under Mo rich and S-rich condition 51

4.2 Magnetic energy (ΔE) and magnetic moment (μ_m),for V doped ML MoS_2 54

4.3 Magnetic energy (ΔE) and magnetic moment (μ_m),for V doped BL MoS_2 54

4.4 The calculated ferromagnetic transition temperature T_c for pair of V doped ML and BL MoS_2 56

Abstract

In the first and second parts of this dissertation structural stability, electronic structure and magnetic interaction in transition metal(TM) atoms(V,Mn) doped monolayer (ML) and bilayer(BL) MoS_2 are studied within the density function theory(DFT) based on DFT+U formalism. It is found that,the injection of V and Mn atoms in Mo site of ML and BL MoS_2 introduces magnetism and turns semiconductor behavior of host MoS_2 to half metallic nature. The magnetic interaction between dopants in ML and BL MoS_2 are always ferromagnetic irrespective of dopant configurations. In contrast, in V doped case the magnetic interaction oscillates from ferromagnet to antiferromagnet depending on the separation between dopants. Moreover,it is found that interlayer interaction in doped BL MoS_2 system affects not only electronic structures but also the magnetic properties of the system. The calculated ferromagnetic transition temperature (T_C) in Mn doped ML and BL MoS_2 cases are found to be above the room temperature (RT), whereas in V doped cases T_C closer to RT. In addition, T_C increases with doping concentrations in a range of dilute limit (6.5$\%$) of magnetic atoms for doped ML and BL MoS_2,which agrees with latest experimental observed RT T_C .Therefore based on our result, we suggest that Mn and V doped ML and BL MoS_2 are promising candidates for 2D DMS for high temperature spintronics applications. In third part of this dissertation,using low energy effective tight binding model together with consideration of dopant introduced exchange field it is found that spin orbit coupling together with exchange energy determine the valley polarization which in turn controls valley and spin Hall conductivity in doped ML MoS_2 system. Our results form another important step towards information processing based on the valley degree of freedom.

Acknowledgements

First, my greatest regards to the Almighty for bestowing upon me the courage to face the complexities of life and complete my dissertation successfully.

I would like to express my cordial thanks to my dissertation advisor **Prof. P. Singh**, for formulating the PhD research problem and valuable guidance,and constructive criticism i received from him during the work of this dissertation. I appreciate him for his friendly approach and encouragement without any reservation during the whole period of the this research work.

I would also like to thank **prof. Pawel Harlyak** ,Ottawa university of Canada for inviting me to visit his distinguished quantum theory group and for his constructive ideas to work in this area.

It is also pleasure to thank **Dr.Manish Jain** for writing Consent Letter to join his computational condensed matter group in Indian institute of science (iisc.), for his friendly discussion and allowing me to share computational facilitates in his group .

It is also my pleasure to acknowledge financial support from Center for Science and Technology of the Non-Aligned and Other Developing Countries (NAM) fellowship during my six months stay in Indian institute of science(iisc.)

I would also like to thank **Dr.Teshome Senbeta** chairman of department of physics for his smooth discussion and facilitating all necessary conditions to complete my dissertation work. It is also my great pleasure to thank my wife **Hana Bekele** for her decision to mange my family during my stay in abroad. I would also like to thank **Wezro Tsilat** and all my friends for every thing they did . I would also like to convey my gratitude to the **Arbaminch University** for providing me financial support.

INTRODUCTION

The search for two-dimensional (2D) materials has been very intense for the past few years due to their potential applications [1]. Among the 2D materials graphene is known because of its unique electrical,thermal and mechanical properties [2] .However its gapless band structure is limiting its usefulness in semiconductor industry such as transistor technologies which need open band gap. To overcome this, it is important to find new 2D materials [3].On the contrary,layered transition metal dichlcogenides(TMDs),with chemical formula MX_2 where M denotes transitionmetal (TM):Molybdenum(Mo),Tungsten(W) etc.. and X represents chalcogen atoms like sulfur(S) ,Selenium(S) and tellurium(Te) are semiconductors whose band gap varies from direct to indirect depending on the number of layers [4]. Among the family,a few layer and monolayer MoS_2 have attracted great interest of researchers due to the following reasons; well-defined spin-splitting property [5], suitability for optoelectronic and nanoelectronic application [6],lubricant [7], used as catalyst [8], suitability for flexible, transparent and low-power devices in electronics [9]. In addition to this,these materials are stacked together with weak Van der Wall forces and their properties can be easily modulated by varying their thickness, crystal orientation and composition etc. However ,the pure monolayer(ML) and a few layer MoS_2 are a nonmagnetic semiconductor. However,for spintronics and for storage of magnetic information ferromagnetism is essential. Hence ,to broaden its application it is essential to introduce magnetism to this system. The main objective of this study is to introduce magnetism in ML and BL MoS_2 through substitutional doping so as to study structural, electronic and magnetic properties. This dissertation is organized in the following way:

In chapter one main properties of monolayer and few layer MoS_2 are reviewed on the basis of latest theoretical and experimental findings,

In chapter II the remarkable theorems of density-functional theory (DFT) which allow us to find ground-state properties of a system without dealing directly with the many-electron state are discussed in detail starting from properties of N interacting many-particle systems. In addition to this,the extended type of DFT: spin polarized DFT and implementation of DFT with on site Hubbard potential correction(DFT+U) formalism also discussed

In chapter III and IV ,first part of this work ,structural stability ,electronic structure and magnetic interaction in TM (Mn,V) doped ML and BL MoS_2 are studied using DFT. In addition, the effect of interlayer interaction on electronic structure and magnetic interaction are accessed . Finally the ferromagnetic transition temperature (Tc) are calculated for different dopant concentrations and its dilute magnetic semiconductor (DMS) properties are discussed. In chapter V ,anomalous spin Hall and valley Hall conductivity in the vicinity of $K^{\pm}$ Valleys of 2D hexagonal BZ are studied using low energy effective tight binding model together with Berry phase formalism,taking consideration of dopant introduced magnetic exchange field.

In chapter VI main findings of this work are summarized. The detail calculation of Berry curvature and liner response theory to calculate anomalous Hall conductivity are also described in in **appendix A.1** and **appendix B.1**

1

Review Literature

1.1 Structural and electronic property of Bulk MoS_2

The bulk MoS_2 is layerd material in which layers are stacked together with weak Van der Waal interaction [10],each layer of MoS_2 is composed of S-Mo-S stacks, where a single molybdenum atom is surrounded by six sulfur atoms. Depending on the coordination of Mo atoms within a single layer and the stacking order of single layers, there are three known polytypes of MoS_2 namely: triangular(T),hexagonal(2H) and rhombohedral(3R) structure. However,due to its naturally abundant and application hexagonal(2H) MoS_2 polytype structure has received an attention [11]. The corresponding bravis lattice is hexagonal and belongs to space group of crystal $P6_3$/mmc(D6h non-symmorphicgroup). The three basic vectors define the physical dimension of unit cell are : $\vec{a}_1 = \left(a, 0, , 0\right)$, $\vec{a}_2 = \left(\frac{1}{2}a, \frac{\sqrt{3}}{2}a, 0\right)$,$\vec{a}_3 = \left(0, 0, c\right)$ respectively .Hence the unit cell of MoS_2 is characterized by the in plane lattice parameter(constant) which is found to be 3.18 Å theoretically [12] and ranges 3.18-3.2 Å experimentally [13]and the out-of plane-lattice constant (c).In other words ,the crystal structure of MoS_2 can be specified as a stacking of quasi 2D S-Mo-S layers along the c direction,thus inherent weakness of the interlayer interactions can result in different stacking sequences and also enable to get monolayer or single layer from its bulk . Pristine bulk 2H-MoS_2 is a diamagnetic semiconductor with indirect band gap of 1.29 eV [14] and 1.3 eV [15].

1.2 Structural and electronic property of monolayer MoS_2

Recently, monolayer(ML) MoS_2 with direct band gap has been fabricated by mechanical exfoliation [16] and chemical vapor deposition [17]. The ML MoS_2 consists

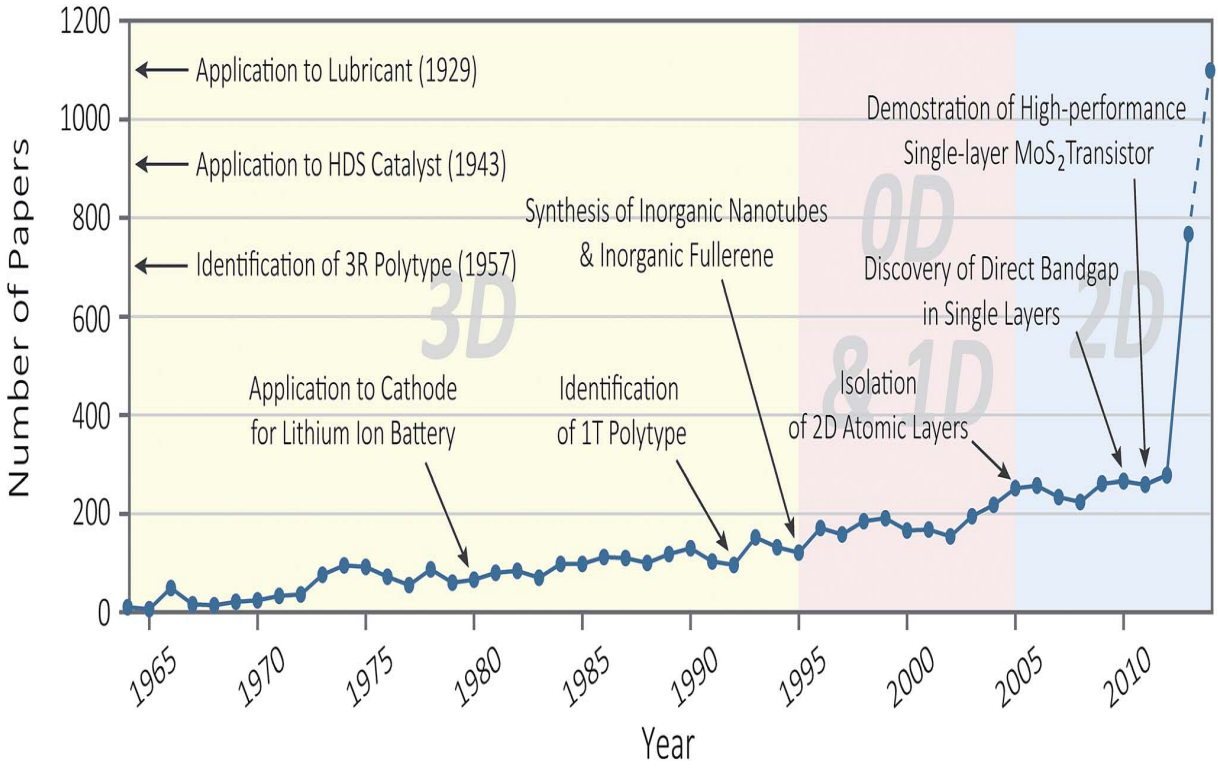

Fig. 1.1: History of molybdenum disulphide research for last 50 years (1964-2014) which shows the annual number of journal publications adopted from [27]

.

of a single layer of Mo atoms sandwiched between two layers of sulfur(S) atoms in a trigonal prismatic structure [18]. The unit cell of ML MoS_2 are characterized by in plane primitive vectors a=b=3.18 Å [19] and thickness of two sulfur atoms (S-S bond length) approximately 3.13 Å [20]. Moreover,the ML MoS_2 are characterized by direct band gap ranging from 1.75-1.9Å [21–23] which is situated at K high symmetry points of 2D hexagonal Brillouin zone. Therefore,the unique future of transition from bulk to its ML may be characterized by: band gap increase in magnitude and becomes direct which is resulted from absence of interlayer interaction in ML MoS_2 [23],ii) strong spin-orbital coupling in ML MoS_2 induced by split-valence band which also makes ML MoS_2 better for spintronics applications [24, 25], iii) broken inversion symmetry which also makes ML MoS_2 interesting for spin physics [26].

1.3 Structural and electronic properties of bilayer and few layer MoS_2

The double-layer or bilayer(BL) MoS_2 is constructed by adding another S-Mo-S layer on ML. Interestingly, in few-layer MoS_2 the size and the nature of the band gap depends on the number(N) of MoS_2 layers, with a transition between a direct gap in ML(N = 1) compounds to a smaller indirect gap for N $\geq$2 [14,28]. Theoretical calculations [29,30] and experimental [15,21] studies have predicted that the stacking sequence or patterns in BL MoS_2 plays an important role in its electronic band structure. In contrast to ML system, BL MoS_2 are inversion symmetric. Recently,breaking of inversion symmetry by application of electric field has been proposed [32] such method remove the inversion symmetry of the BL system by modifying the electron density [32]. Moreover,for layered materials, the interlayer van der Waals (vdW) interaction is undoubtedly a crucial determinant of the physical properties. This is especially true for MoS_2 material [33, 34]. In addition to this,experimental studies have found that the relative rotation angle in bilayer MoS_2 significantly modifies the direct(indirect) band gap and interlayer coupling [35–37]. More recently [38] ,it has been reported interlayer distance in BL MoS_2 to be 0.689nm using the 'VdW-DF-D2' method theoretically [29] and 0.68nm experimentally [40]. Despite of its indirect band gap,few-layer MoS_2), still have attractive properties for various electronic devices application due to its narrow band gap which can be tunable by electric field [41] and higher carrier mobility compared to single layer MoS_2 [42].

1.4 Two dimensional dicolgenide semiconductors ,MoS_2,doped with transition metal elements

The clean ML and BL MoS_2 are a nonmagnetic semiconductors [43–45].Thus, no magnetism hampers their application in spintronic devices. Hence to broaden its application especially in spintronics it is essential to introduce the magnetic dopant in pure system which can modulate electronic and magnetic properties. Recently,severals groups have reported experimentally [43] and theoretically feasibility of ML MoS_2

by substitutional doping with different transition metal(TM): Mn [44, 45] ,Co [46] Fe BL MoS_2 [47],Ni doped MoS_2 [48],and Re doped MoS_2 [49]. Besides to substitutional doping with TM,doping with nonmetal elements [50] ,transition metal-adsorbation [51–53] and external strain [54] are other proposed methods to introduce magnetism. However,the detail investigation of magnetic interaction between dopants and the effect of layers on their magnetic proprieties are still open questions [43, 45, 47].

1.4.1 Dilute magnetic semiconductor property of transition-metal doped MoS_2

The important parameter of a dilute magnetic semiconductor (DMS) is the Curie temperature (TC) below which the system develops a long-range ferromagnetic ordering [55]. It is worth mentioning that,ferromagnetic transition temperature(Tc) in three dimensional(3D) DMSs,in well studied type of DMSs like $Ga_{1-x}Mn_xAs$ is less than 200K which is far from room temperature [55] but for practical application we need T_c which exceeds room temperature . As a result of this,the search for DMSs has more recently been extended to 2D transition metal dichlcogenides (TMDs) like MoS_2, $MoSe_2$,and WS_2 doped transition metal [43, 44]. The realization of two dimensional DMS and half-metallic behavior has received attention not only to enhance T_c but also due to both in fundamental aspects of physics [56–58] and for prospective applications such as the integration between 2D semiconductors and magnetic data storage enables the development of two dimensional spintronics devices such as spin valve and spin based transistors [59]. It has been reported theoretically 2d DMS in ML MoS_2 by replacing Mo by other transition metal atom [34, 60] and their result demonstrate that room temperature 2d DMS can be achieved for the dopant concentrations in the range of 10-15 $\%$

.Besides , more recently room temperature ferromagnetism has been reported in manganese oxide doped MoS_2 experimentally [61].

The experimental measured intensity versus Raman shift for pure and Mn doped

MoS_2 are shown in Fig.(1.2a) confirms that electronic state can be altered in the presence of magnetic impurities .On the other hand,the magnetic susceptibility of pure and Mn doped MoS_2 are displayed in Fig.(1.2b) ,for the undoped MoS_2 shows very low susceptibility dominated by a Curie-Weiss paramagnetic behavior while for the 7% Mn doped MoS_2 nano structure the magnetic susceptibility is much higher than that of the undoped one indicating tunability of magnetic property by dopant atoms.

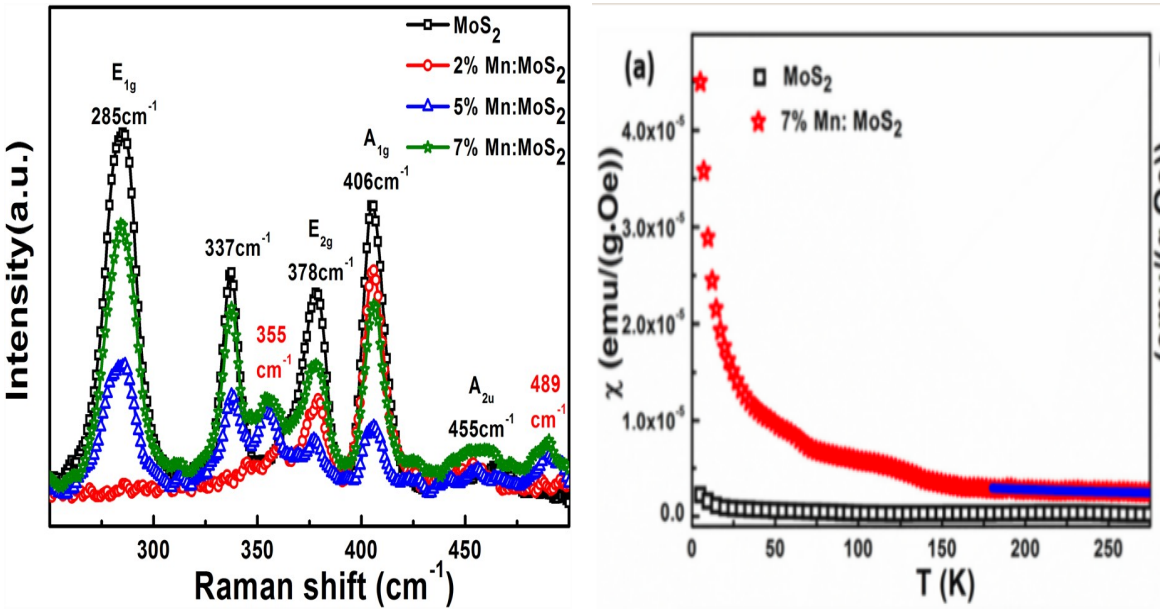

Fig. 1.2: a)Raman spectra of the undoped and the Mn^{2+} doped MoS_2 nanostructures with a different doping concentration, b)magnetic properties of the MoS_2 and the 7% Mn doped MoS_2 [43].

1.4.2 Magnetic exchange interaction in transition metal doped MoS_2

There are two kinds of interaction between two electrons ;repulsive coulomb interaction and exchange interaction which occurs as a result of Pauli exclusion principle in quantum mechanics. The physical understanding of the exchange mechanisms involved is a very delicate and difficult problem, since no simple and elementary magnetic interaction exists [62]. There are different exchange mechanism in which pair of dopant communicate to each others; Zener-RudermanKittelKasuyaYosida (RKKY) [63],Zeners pd exchange [64–66] and superexchange [67, 68], etc are pro-

posed to explain exchange interaction in dilute magnetic semiconductors (DMSs) like (II-VII and III-VI). However,the clear cut mechanism of ferromagnetism in transition metal doped dichlcogenides are not well understood ,but based on phenomenological observation some studies propose double exchange [69]and superexchange interaction [70].

1.5 Valley degree of freedom in MoS_2

The charge and spin degrees of freedom (DOF) of electrons are at the heart of moden electronics as they form the basis for a wide range of applications, such as transistors, photodetectors, and magnetic memory devices. In addition to this,electrons in two-dimensional (2D) crystals that have a honeycomb lattice structure possess an extra valley DOF in addition to charge and spin [71]. Valley is a quantum number defined in an electronic system whose band structure contains energetically degenerate but non-equivalent structures due to a certain crystal structure. Among various material candidates for valleytronics, spatial inversion symmetry broken two dimensional (2D) honeycomb lattice systems such as gapped graphene and ML MoS_2 are predicted to be the most useful. These systems have two valleys called K and K'. The use of Valley index as a potential information carrier was first suggested in the studies of of conventional semiconductors such as AlAs and Si [72]. On the other hand,the presence of a valley-dependent orbital magnetic moment in graphene with gap suggests that currents flow perpendicular to applied electric field even in the absence of a magnetic field, named as the 'valley Hall effect'. The valley Hall effect was first time observed in gaped graphene(graphene with substrate).However, due to the small value of the gap, this effect has not yet been observed experimentally. Recently,photogenerated valley Hall conductivity was observed in ML MoS_2 [73]. MoS_2 ML have two important distinctions from graphene [72]. First,inversion symmetry is explicitly broken in ML MoS_2, which can give rise to the valley Hall effect where carriers in different valleys flow to opposite transverse edges when an in-plane electric field is applied [74]. Inversion symmetry breaking

can also lead to valley dependent optical selection rules for interband transitions at K points [75]. Second,MoS_2 has a strong spin-orbit coupling (SOC) originated from the d orbitals of the heavy metal atoms(Mo) [24] ,and can be an interesting platform to explore spin physics and spintronics applications absent in graphene due to its vanishing SOC [76, 77]. As far as both valleys are concerned,due to time reversal symmetry analogy to paramagnetic and paraelectric materials,pristine MoS_2 ML is paravalley materials. Therefore, the major challenge in valleytronics is to break the degeneracy between the two prominent K^+ and K^- valleys. Recent experimental investigation demonstrated that means optical orientation of the valley polarization [78–81],by applied electric field [82] ,by electron-electron interaction [83] , means of external magnetic field [84–87].In present work, we are proposing other approach of breaking of valley degeneracy between two prominent valleys (K^- and K^+) so as to introduce valley polarization by dopant introduced internal magnetic exchange field(h_{ex})

2

Many body system and Density functional theory

2.1 Introduction to many body system

The description of the physical properties of interacting many-particle systems has been one of the most important goals of physics. All electrons(Ne) and all nuclei(Nn) are quantum mechanical particles,forming an interacting (Ne + Nn) many-body system .The problem is to derive the properties of many-particle systems from the quantum mechanical laws of nature, this requires the solution of a the Schrdinger equation of 3N spatial variables and N spin variables (for electrons) where N is the number of particles in the system. We know that in real solid 10^{23} electrons interact to each other and with ion-cores to form crystal. In practice it is impossible task to solve wave equation for 10^{23} interacting electrons and ion cores,as result of this, the Schrödinger Wave equation for many body problems subjected to some reasonable approximation to reduce it to solvable problem. The time-independent, non-relativistic Schrödinger equation for Hamilton operator for a system containing N electrons and M nuclei is given by

$$\left(\hat{T}_e + \hat{T}_N + \hat{V}_{e-e} + \hat{V}_{N-N} + \hat{V}_{e-N}\right)\Psi = E_N\Psi, \tag{2.1}$$

Where the kinetic energy operator for electron $(\hat{T}_e)$ and nuclei $(\hat{T}_N)$ respectively are given by

$$\hat{T}_e = \sum_i^N \frac{-\hbar^2}{2M_e} \bigtriangledown_i^2 . \tag{2.2}$$

$$\hat{T}_N = \sum_i^N \frac{-\hbar^2}{2M_N} \bigtriangledown_i^2 . \tag{2.3}$$

The potential acting on electrons due to the nuclei ($\hat{V}_{e-N}$),electron-electron interaction ($\hat{V}_{e-e}$)and nucleus nucleus interaction ($\hat{V}_{N-N}$) respectively are given by

$$\hat{V}_{e-e} = \frac{1}{4\pi\varepsilon_0} \sum_{i=1}^{Ne} \sum_{j>i}^{Ne} \frac{e^2}{|r_i - r_j|}. \tag{2.4}$$

$$\hat{V}_{N-N} = \frac{1}{4\pi\varepsilon_0} \sum_{i=1}^{N_e} \sum_{j>i}^{N_n} \frac{Z_i Z_j e^2}{|R_i - R_j|}. \tag{2.5}$$

$$\hat{V}_{e-N} = -\frac{1}{4\pi\varepsilon_0} \sum_{i=1}^{N_e} \sum_{j=i}^{N_n} \frac{Z_j e^2}{|r_i - R_j|}. \tag{2.6}$$

Although the Hamilton operator is known, Eq. (2.1) is too complex to be solved due to the large number of variables the wave function Ψ(r) depends on. First step in simplifying Eq. (2.1) is the Born-Oppenheimer approximation . Since the nuclei are much heavier than the electrons (almost a factor of $\sim$ 1800), it is assumed within the Born-Oppenheimer approximation, that the response of the electrons to an external perturbation is much faster than the response of the nuclei. Thus,the electrons would be able to follow any movement of the nuclei quasi instantaneously and might then be considered as basically moving in a constant field generated by the nuclei at fixed positions. The kinetic energy term T_N for the nuclei in Eq. (2.3) is set to zero and the repulsion term for the nuclei, V_{N-N}, enters the total energy as a constant and therfore, with help of this first approximation the electronic Schrödinger Eq.(2.1) is reduced to,

$$\hat{H}_e \Psi(r_i) = \left(\hat{T}_e + \hat{V}_{e-e} + \hat{V}_{ex} \right) \Psi_e(r_i) = E_e \Psi_e(r_i). \tag{2.7}$$

with the electronic Hamilton operator $\hat{H}_e$,the electronic wave function $\Psi_e(r_i)$ and the electronic energy E_e ,Eq. (2.7) is simple compared to Eq.(2.1).However,solving Schrödinger equation is very difficult to solve for more than 2 electrons ,hence to handle this we need further approximation.

2.1.1 The Hartree approximation

Hartree introduced in 1927 a procedure, which he called the self-consistent field method, to approximate the Schrödinger equation. The simplest approximation is

multi electron system is the Hartree approximation. Accordingly,the electron wave function in Eq.(2.7) can be approximated as

$$\Psi_e(r_1, r_2...r_N) \approx \Psi_e(r_1)\Psi_e(r_2)...\Psi_e(r_N). \tag{2.8}$$

from which it allows that the electron are independent and interact only via the mean field coulomb potential resulting from ion-electron interaction. This yields one- electron Schrödinger equations of form

$$\left(-\frac{\hbar^2}{2M_e} \bigtriangledown^2 + V_{eff}(r) \right) \Psi(r_i) = E_i \Psi(r_i), \tag{2.9}$$

where V(r) is the potential in which the electron moves; this inculdes both the nuclear-electron interaction

$$\hat{V}_{N-e}(r) = -e^2 \sum_{R}^{Ne} \frac{1}{|r-R|}. \tag{2.10}$$

and the mean field arising from the N-1 other electrons. This other electrons are smear out into a smooth negative charge density n(r') leading to a Hartree potential in the form of

$$\hat{V}_{electron}(r) = -e \int dr' n(r') \frac{1}{|r-r'|}, \tag{2.11}$$

where total electron density is given by

$$n(r) = \sum_{i}^{occ} |\Psi(r_i)|^2. \tag{2.12}$$

In Eq.(2.12) the sum over runs over all occpaied states. While this functional form is fairly convenient, it has at least one major shortcoming: it fails to satisfy the antisymmetry principle, which states that a wavefunction describing fermions should be antisymmetric with respect to the interchange of any set of space-spin coordinates.

2.1.2 The Hartree-Fock approximation

The correlation resulting from the Coulomb repulsion for all electrons of like and unlike spins is missing in elctron Hamiltonian in Eq. (2.7). Hatrtree-Fock was introduced the concept of electron correlation. In other words,the Hartree-Fock method

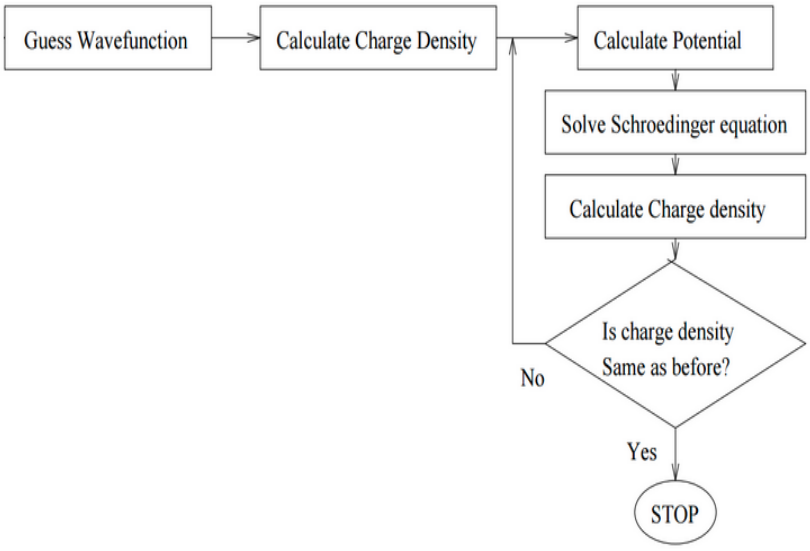

Fig. 2.1: Algorithm for Self-consistent field theory in Hartree.

is itself an extension of the Hartree method where the many-electron wave-function is assumed to be a simple product of one-electron orbitals also electron correlation is taken under consideration. The Harttee-Fock approach is a better approach,which correctly takes into account the antisymmetric nature of the trivial wave functions. The Pauli exclusion principles demands that the many body wave function must be antisymmetric with respect to interchange of any two electron coordinates

$$\Psi_e(r_i, r_j) = -\Psi_e(r_j, r_i) \tag{2.13}$$

which clearly cannot be satisfied by the Eq.(2.8) of Hartree approximation. This indistingushability condition can be satisfied by forming a slater determinant of single-particle orbitals,

$$\Psi_e(r_1, r_2....r_N) = \frac{1}{\sqrt{N!}}\phi_e(r_1)\phi_e(r_2)...\phi_e(r_n), \tag{2.14}$$

where the orbital ϕ_e is the product of spatial coordinate $\Psi_e(r)$ and either the spining up function α or spining down function β i.e ϕ_e=$\Psi_e(r)\alpha$. Using Eq.(2.14) into Schrdinger wave equation decouples into usual Hartree term and the new exchange

term as,

$$\left(\hat{T}_e + \hat{V}_H + \hat{V}_{ex}\right)\phi_n(r) - \sum_m \int dr' \frac{\phi_m^* \phi_n(r')}{r - r'} \phi_m(r) = E_n \phi_n(r). \tag{2.15}$$

Where the Hartree potential is given by Eq.(2.11).The Eq. (2.15) is an effective one particle wave equation and the extra term is called exchange potential and creates the repulsion between electrons of like spins .From orthogonality of wave function this extra term can survive only index m=n (for the same spin state). The Hartree Fock equation deals exchange exactly; however,one of the celebrated failure of Hartree-Fock equation is neglect more detailed correlation due to many body effects. On the other hand,these so-called wave function based methods are mainly used for calculating atoms and molecules (containing up to 50 atoms). Due to this limitation , we need other approach which can be used to calculate increasing number of atoms. One such refinement is given by the density functional theory (DFT) [89, 90] which is discussed in next section in detail.

2.2 Density functioinal Theory

In DFT the quantum mechanical theory is reformulated to model the electrons as a compound cloud, an electron gas. The reformulation focuses on the density of electrons, rather than on individual electrons . In this particular section Algorithm in density functional theory and some common approximation implemented in DFT are discussed in detail.

2.2.1 The Hohenberg-Kohn Theorems

In 1964 Hohenberg and Kohn formulated two theorems, which formally justified the use of the electron density as basic variable in determining the total energy and which became the foundation of modern density-functional theory [89]. They have developed two theorems which are basis for formulation of DFT:(i) there exists a one-to-one correspondence between external potential V(r) and electron density n(r); and (ii) the ground state electron density can be found by using a variational principle. According to varitional Principe we know that ground state energy E_0

is always less than or equal to expectation value of Hamiltonian $\hat{H}$ with the trivial wave function i.e

$$E_0 < \langle \Psi | \hat{H} | \Psi \rangle. \tag{2.16}$$

The first theorem can be proved by assuming that there are two different external potential say, V_{ex1} and V_{ex2} ;that give the same ground state electron density $n_o(r)$ the associated Hamiltonians,$\hat{H}_1$ and $\hat{H}_2$ will therefore have different grounds state wave functions,$\Psi(r_1)$ and $\Psi(r_2)$ using Eq. (2.16) we have

$$E_{01} < \langle \Psi_2 | \hat{H}_1 | \Psi_2 \rangle = E_{01} < \langle \Psi_2 | \hat{H}_1 + \hat{H}_2 - \hat{H}_2 | \Psi_2 \rangle \tag{2.17}$$

$$E_{01} < \langle \Psi_2 | \hat{H}_1 | \Psi_2 \rangle = \langle \Psi_2 | \hat{H}_2 | \Psi_2 \rangle + \langle \Psi_2 | \hat{H}_1 - \hat{H}_2 | \Psi_2 \rangle \tag{2.18}$$

Eq. (2.18) is simplified to

$$E_{01} < \langle \Psi_2 | \hat{H} | \Psi_2 \rangle = E_{02} + \int n(r)(V_{ex1} - V_{ex2}) dr \tag{2.19}$$

where E_{o1} and E_{o2} are ground state energies of $\hat{H}_1$ and $\hat{H}_2$ respectively.Similarly,

$$E_{02} < \langle \Psi_1 | \hat{H}_2 | \Psi_1 \rangle = E_{01} < \langle \Psi_2 | \hat{H}_2 + \hat{H}_1 - \hat{H}_1 | \Psi_2 \rangle \tag{2.20}$$

$$E_{02} < \langle \Psi_1 | \hat{H}_2 | \Psi_1 \rangle = \langle \Psi_1 | \hat{H}_1 | \Psi_1 \rangle + \langle \Psi_1 | \hat{H}_2 - \hat{H}_1 | \Psi_1 \rangle$$

$$E_{02} < \langle \Psi_1 | \hat{H}_2 | \Psi_1 \rangle = E_{01} + \int n(r)(V_{ex2} - V_{ex1}) dr \tag{2.21}$$

After adding Eq.(2.19)and Eq.(2.21) we get

$$E_{01} + E_{02} < E_{02} + E_{01}, \tag{2.22}$$

which is an obvious contradiction. Follow that there is no possibility for two different external potential that can give the same n(r). Thus n(r) uniquely determines Vex(r) and all ground state properties.Hence the term for external potential V_{ex} is easily rewritten in terms of density as

$$V_{ex} = \int n(r_i) V(r) dr \tag{2.23}$$

Therefore,for given external potential we can write the total electron energy E_e explicitly as function of the electron density n(r):

$$E_e[n] = T[n] + V_{ex}[n] + V_{ee}[n] \tag{2.24}$$

$$= \int n(r)v(r)dr + F_{HK}[n] \tag{2.25}$$

where

$$F_{HK}[n] = T[n] + V_{ee}[n], \tag{2.26}$$

where $F_{HK}[n]$ is only dependent on n(r) and independent from any external potential v(r). Thus $F_{HK}[n]$ is a universal functional of n(r),in the sense that it has the same dependence on the electron density for any system independent of the external potential concerned.If it were known we would have solved the Schrödinger equation exactly , The exact density dependence of this functional is,however, unknown. The major challenge of DFT is determination of the explicit form of universal functional $F_{HK}[n]$. The second Hohenberg-Kohn theorem is try to answer question how can we be sure that a certain density is the ground-state density that we are looking for? . According to the second Hohenberg-Kohn theorem,the total energy will reaches the minimum only when the electron density is the ground-state electron density.On the other hand, the ground state energy can be obtained variationally, with the density that minimizes the total energy being the exact ground state density. This is nothing but the variational principle.

$$E_0 \leq E[n] = T[n] + V_{ex}[n] + V_{ee}[n]. \tag{2.27}$$

Now the many-electron problem with 10^{23} variable in three-dimensions turn into a problem with just one variable in three-dimensions. Although these two theorems prove the existence of a universal functional, they do not give any idea as to the nature of the functional, or how to actually calculate the ground state density.In order to do so, we must discuss the Kohn-Sham formulation [90]. This is based upon a sleight of hand whereby we map the fully interacting system of N-electrons

onto a fictitious auxiliary system of N non-interacting electrons moving within an effective Kohn-Sham potential, $v_{KS}(\mathbf{r})$, thereby coupling the electrons. The single-particle Kohn-Sham orbitals are constrained to yield the same ground state density as that of the fully-interacting system, so the Hohenberg-Kohn-Sham theorems are still valid.

2.2.2 The Kohn-Sham Equations

Almost exactly a year after the Hohenberg-Kohn theorems were published, the DFT was first time applied into practical electronic structure theory in 19 65 by Kohn and Sham [90]. Their approach centers on mapping the full interacting system, onto a virtual non-interacting system,quite similar with Hartree -Fouck approximation. However,Kohn-Sham equation incorporate the correlation of electrons in addition to exchange energy. Hence,according to Kohn-Sham , the energy functional can be written as

$$E_n = \int n(r)V(r)dr + F_{HK}[n(r)]$$

$$= \int n(r)V_{ex}(r)dr + T_s[n(r)] + \int\int \frac{n(r)n(r')drdr'}{|r-r'|} + E_{EX}[n(r)], \tag{2.28}$$

where $V_{ex}(r)$ is the external potential, the third part of Eq.(2.28) is the classical Coulomb interaction energy for the electron density with itself (the Hartree energy), Whereas ,the kinetic energy of non-interacting electrons whose total ground state density is exactly n(r) is given by

$$T_s(n) = -\frac{1}{2}\sum_{i=1}^{N}\int \phi_k^*(r) \bigtriangledown^2 \phi_k^*(r)dr. \tag{2.29}$$

Where the effctive potential energy functional can be written in separted form as:

$$V^{eff}[n(r)] = \int n(r)V_{ex}(r)dr + \int\int \frac{n(r)n(r')drdr'}{|r-r'|} + E_{XC}[n(r)]. \tag{2.30}$$

where,XC functional represents everything that can not be exactly expressed in KS theory: electron correlation energy, exchange energy and the component of kinetic energy arising from these effects ,these interactions are combined into a single entity called the exchange-correlation energy $E_{XC}[n(r)]$. If the energy expression in

Eq. (2.28) is minimized with respect to stationary density n(r), the effective Kohn-Sham potential, which is minimization of effective potential energy can be written as

$$v^{eff} = \frac{\delta V^{eff}}{\delta n} = \int \frac{\delta n(r) V_{ex}(r) dr + E^{Hart.}[n(r)] + E_{ex}[n(r)].}{\delta n(r)}$$
$$= V(r) + \int \frac{n(r')dr'}{|r - r'|} + V_{xc}(r), \tag{2.31}$$

here, V_{xc} is exchange-correlation potential. It is a variational derivative of the exchange-correlation energy, E_{xc} ,

$$V_{XC}(r) = \frac{\delta E_{ex}[n(r)]}{\delta n(r)}. \tag{2.32}$$

this led to basic equation in Kohn-Sham DFT which is the one-electron Schrödinger like equation expressed as:

$$\left(\frac{-\bigtriangledown^2}{2M_e} + V_{eff}\right)\phi_i = \epsilon_i \phi_i \tag{2.33}$$

Where the Kohn-Sham one electron orbitals(ϕ_i) and the corresponding electron number density is given by

$$n(r) = \sum_{i=1}^{N} |\phi_i|^2 \tag{2.34}$$

The total energy of system is given by

$$E_s = \sum_i \epsilon_i \tag{2.35}$$

Note that the V_{eff} depends on n(r) through Eq. (2.30)

2.3 Self-consistent cycle and approximation for exchange-correlation energy (E_{XC})

In principle, the Kohn-Sham equations provide a theoretically exact method for finding the ground state energy of an interacting system provided that the form of E_{XC} is known. Unfortunately, the form of E_{XC} is in general unknown , hence Eq.(2.33) can be solved iteratively. A self consistent iterative procedure would start from an initial electron density that can be used to calculate the Kohn-Sham potential. Then, through solution of Eq.(2.33), and use of the relation in Eq.(2.34) we can

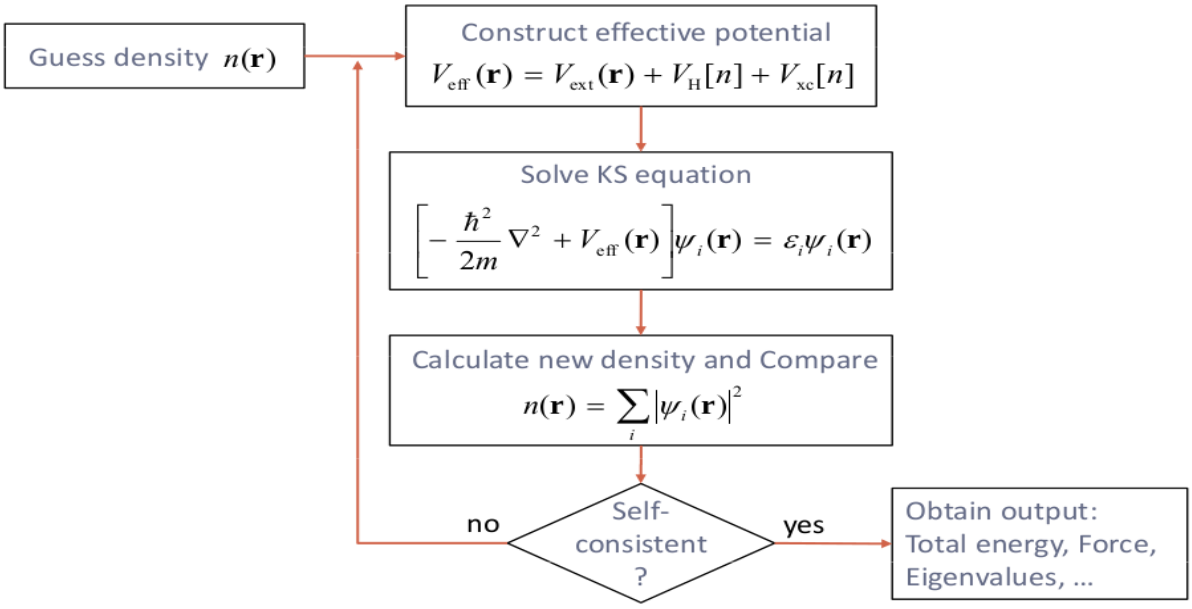

Fig. 2.2: Self-consistent Kohn-Sham loop

obtain a new electron density. Eq.(2.34), reveals that the ground state density is the density that minimize the total energy,such ground state density $n_0(r)$ can be found by iterative scheme which works towards self consistency ,th self consistence cycle are listed below:

1. Start with initially guessed density.
2. Insert this density,into equation (2.31) and construct new effective potential v_{eff} (r) ,that depends on density n(r).
3. Using $v_{eff}[n(r)]$ obtained from step two,solve Kohn-sham orbital equation ,Eq.(2.33)
4. Compute the new Kohn-sham orbitals using Eq.(2.34).

If the initial and new densities are identical, then the ground state density has been found and the iterative processes stooped . Otherwise, one must select a new trial density through minimization of the total energy and continue to repeat the iterative procedure. In electronic structure calculations E_{XC} is most commonly approximated within the local density approximation(LDA) or generalized-gradient approximation (GGA) and extension of those,LDA+U and GGA+U method respec-

tively.Hence in next section those approximation are discussed in detail.

2.3.1 Local density approximation (LDA)

In this approximation the contribution to E_{xc} from any region of space only depends on the density in that region, so this is usually called the local density approximation(LDA). Assuming that,inhomogeneous system is divided into infinitesimal volume,and the electron density in each of infinitesimal volume is assumed to be constant. Hence the exchange correlation energy for density within each of volume is then considered as exchange correlation energy obtained from the homogeneous electron gas from that density. In the LDA and LSDA XC functionals are functionals of the density only and can thus be written as E_{XC} [n(r)]:

$$E_{XC}[n(r)] = \int \varepsilon_{XC}^{uniform}(n(r))n(r)dr. \tag{2.36}$$

Here, $\varepsilon_{XC}^{uniform}(n(r))$ is the exchange-correlation energy per particle of an uniform electron gas of density n(r). This energy per particle is weighted with the probability n(r) that there is an electron at this position,(r). The quantity $\varepsilon_{XC}^{uniform}(n(r))$ can be split into exchange and correlation contributions,

$$\varepsilon_{XC}^{uniform}(n(r)) = \varepsilon_{X}^{uniform}(n(r)) + \varepsilon_{C}^{uniform}(n(r)) \tag{2.37}$$

The exchange part, X , which represents the exchange energy of an electron in a uniform electron gas of a particular density,n(r), the explicit form of $\varepsilon_{X}^{uniform}[n(r)]$ is given by [91].

$$\varepsilon_{X}^{uniform}[n(r)] = -\frac{3}{4}(\frac{3}{\pi})^{\frac{1}{3}} \int n(r)^{\frac{4}{3}}dr. \tag{2.38}$$

Eq.(2.38) was originally derived by Bloch and Dirac in the late 1920's. However,the explicit form of expression for correlation part ,ε_C,is unknown and more accurate estimation is made by using quantum Montecarlo simulation. LDA, has a tendency to favor more homogeneous systems and it gives good approximation for molecules and solids whose orbitals lie on s or p. It also follows that the exchange-correlation energy per particle is constant in space. In other words, LDA uses only the local value of the electron density.

2.3.2 The generalized gradient approximation (GGA)

The first logical step to go beyond LDA is the use of not only the information about the density n(r) at a particular point r, but incorporate the density with information about the gradient of the charge density, ∇n(r) in order to account for the non-homogeneity of the true electron density. Thus,we rewrite the exchange-correlation energy in the following form termed generalized gradient approximation (GGA). The GGA more accurate approximation than LDA and the expression for $\mathrm{E}_{XC}[n(r)]$ is given by

$$E_{XC}^{GGA}[n(r)] = \int f^{GGA}(n(r), \bigtriangledown n(r))dr. \tag{2.39}$$

Within GGA the exchange energy, $\varepsilon_X[n(r)]$,takes the form [92]

$$E_X^{GGA}[n(r)] = \int n(r)\varepsilon_X^{uniform}(n(r))F_X^{GGA}(g)dr \tag{2.40}$$

where $F_X^{GGA}(s)$ is the exchange enhancement factor and tells us how much exchange energy is enhanced over its LDA value for given n(r) and here g is a dimensionless reduced gradient.

2.4 Spin polarized Density functional Theory

The Generalization of DFT to spin-polarized systems,the charge density is argumented by magnetization density ,m(r). The basic variables of spin-density-functional theory are the scalar electronic density n(r) and the vector of the magnetization density m(r). Therefore,DFT can be reformulated in terms of this scalar field, a spin up density $n_\uparrow(r)$ and spin-down density $n_\downarrow(r)$.Then

$$n(r) = n_\uparrow(r) + n_\downarrow(r) \tag{2.41}$$

$$m(r) = n_\uparrow(r) - n_\downarrow(r) \tag{2.42}$$

In spin polarized DFT,the Hohenberg-Kohn theorem is generalized to state that the true ground state energy is variational functional of the spin densities. The coulomb terms remain functional of the total density,but the kinetic term(T) and exchange-correlation part E_{XC} become functional of the two densities. For spin polarized DFT

the energy functional in Eq.(2.28) now modified to

$$E[n^{\alpha\beta}(r)] = T_s[n^{\alpha\beta}(r)] + \int\int \frac{n(r)n(r')drdr'}{|r-r'|} + \int V_{ex}^{\alpha\beta} n^{\alpha,\beta}(r)dr + + E_{xc}[n^{\alpha\beta}(r)], \quad (2.43)$$

where α and β are spin indices and can have two values either$\uparrow$ or $\downarrow$ and the kinetic energy functional and electron density are given by

$$T_s(n) = -\frac{1}{2}\sum_{i=1}^{N} \int \phi_k^{*\alpha}(r) \bigtriangledown^2 \phi_k^{*\alpha}(r)dr. \quad (2.44)$$

$$n^{\alpha\beta}(r) = \sum_{i=1}^{N} \phi_k^{*\alpha}(r)\phi^{*^\beta}. \quad (2.45)$$

where the sum over includes all occupied orbitals.This, leads to The Kohan-Sham equations

$$-\bigtriangledown_r^2 \phi_i^{\alpha}(r) + \sum_{\beta} V_{eff}^{\alpha\beta}\phi^{\beta}(r) = \epsilon_i \phi_i^{\beta}(r) \quad (2.46)$$

The effective one particle potential in Eq.(46) is given by

$$v_{eff}^{\alpha\beta} = \delta^{\alpha\beta}e^2 \int \frac{n(r')dr'}{|r-r'|} + V_{ex}^{\alpha\beta}(r) + V_{xc}^{\alpha\beta}(r). \quad (2.47)$$

2.5 Density Functional Theory + Hubbard potential (U)approach

The description and understanding of electronic properties of strongly correlated materials is a very important and long standing problem for abinitio calculations. Pure LDA and GGA is not always accurate enough for calculating sensitive property like spin state energetic and band gap of d and f metals [92–94]. The LDA+U method consists in a correction to the LDA (or GGA) energy functional to give a better description of electronic correlations. Since the LDA(GGA) often fails to describe systems with localized (strongly correlated) d and f electrons [94].

$$H_{Hub} = t\sum_{\langle i,j\rangle}(c_{i,\sigma}^{+}c_{j,\sigma+h.c}) + U\sum_{i} n_{i\uparrow}n_{i\downarrow}. \quad (2.48)$$

Where $\langle i,j\rangle$denotes nearest-neighbor atomic sites,$c_{i,\sigma}^{+}, c_{j,\sigma}$, and $n_{i,\sigma}$ are electronic creation,annihilation and number operators for electrons of spin σ on site i respectively and U and t are on site Hubbard potential and hoping integral respectively.

In virtue of the strong localization, the Coulomb repulsion is only accounted for between electrons on the same atom through a term proportional to the product of the occupation numbers of atomic states on the same site, whose strength is U. In general,the balance between U and t controls the behavior of these systems and the character of their electronic ground state. Thus there are two regimes:$t >> U$ regime dominated by single-particle terms of energy is generally well described by approximate DFT only,the opposite one $(t << U)$ is more problematic and insulating character of ground state energy dominate . Therefor ,to account correctly the behavior of electrons in this regime U correction applied to a generic approximate DFT functionals, aimed to improve the accuracy of DFT functionals in describing the ground state of correlated systems [93–95].In the DFT+U method, non correlated s and p electrons are described by the usual DFT approach,and strongly correlating d and f electrons are described by an approximate Hartree-Fock method that considers the Hubbard-type one-site interaction between these correlating electrons [96].

2.6 Plane Wave approximation

It is formidable task to handle an infinite number of non-interacting electrons moving in the static potential,since infinite number of electrons (say more than 10^{23}) means infinite number of wave function must be calculated and since each electronic wave function extends over the entire system, the basis set required to expand each wave function is infinite.Therefore,a most important step for solving Kohn-Sham equations is to find a suitable basis set for the expansion of wave function,making use of suitable basis set that describes the behavior of the electrons leads to find easily solution of KS Eq.(2.23). In principle any of basis function may be used to expand the wave functions: exponential,Gaussian ,polynomial,slater type of orbitals ,plane Wave (PW) etc.. However,in condensed matter physics most of materials like to have their atoms arranged in some kind of regular,repeating pattern and the nuclei are arranged in a periodically repeating pattern. Hence, taking

account of those periodicity,the problems can be easily tackled by applying Bloch's theorem which states :for the periodic system,the potential is periodic i.e,

$$V(r+R) = V(r). \tag{2.49}$$

where R is bravais lattice vector. We know that from the Hohenberg-Kohn theorems,if the potential is periodic,so the density is also periodic and it can be expressed

$$n(r+R) = n(r). \tag{2.50}$$

Moreover,the electron density also related with wave function through the relation ,Eq.(2.34). The Bloch's theorem also says that the eigenfunctions of the one electron Hamiltonian can be written as the product of plane wave ($e^{ik.r}$) and a function $u_{n,k}(r)$ having the same periodicity as the potential V(r),

$$\phi_{n,k}(r) = e^{ik.r} u_{n,k}(r), \tag{2.51}$$

where $u_{n,k}(r+R) = u_{n,k}(r)$ can be expanded using a basis set which is consistes of discrete set of plane waves whose wave vector are reciprocal lattice vectors (G) of crystals ,whereas index k represents a set of plane waves within each primitive unit cell and each k the index n is a second quantum number,the so called band index. Now expanding the periodic function ,$u_{n,k}(r)$, with plane vectors reciprocal lattice vectors (G) of the periodic crystal as

$$u_{n,k}(r) = \sum_G C_{n,G} e^{iG.r}, \tag{2.52}$$

where $C_{n,G}$ are complex Fourier coefficient,and the sum is over all wave vectors and each of Fourier basis functionals $e^{iG.r}$ represents a plane wave traveling in space ,perpendicular to the wave vector G. Using Eq.(2.52) into Eq.(2.51) the electronic wave function can be rewritten as

$$\phi_{n,k}(r) = \sum_G C_{n,G+k} e^{i(G+k).r}. \tag{2.53}$$

Using eq.(2.54),one electron Schrödinger like equation with an effective periodic potential,Kohn-Sham potential(V_{eff}),defined in Eq.(2.33) can be rewritten as ,

$$\sum_{G'}\left[\frac{\hbar^2}{2m_e}|k+G'|^2\delta_{GG'}+V_{eff}(G-G')\right]C_{n,G+k}=\epsilon_n C_{n,G+k}. \tag{2.54}$$

Where $\delta_{GG'}$ is Kronecker delta and reflects that the kinetic energy is diagonal and ϵ_n are electronic energies.Here the sum over G' tells that one needs an infinite number of plane waves to solve Eq.(2.54) in principe.However,the coefficient $C_{n,k+G}$ for the plane waves with small kinetic energy are typically more important than those with large kinetic energy.Thus the plane wave basis set can be truncated to include only plane waves that have kinetic energies less than a particular energy cut off (E_{cut})

$$\frac{\hbar^2|k+G|^2}{2M_e}\leq E_{cut}. \tag{2.55}$$

However,employing a finite basis set introduces other sources of inaccuracy ,which can be reduced by increasing the number of plane waves or E_{cut}. Therefore,appropriate convergence tests have to be required in order to find an E_{cut} that is sufficiently converged to compute the property of interest with required accuracy.

2.7 k point sampling and Brillouin zone integration

Properties like the electron density,total energy, etc .. can be evaluated by integration over $\vec{k}$ inside the Brillouin zone (BZ)also the quality of those calculation also depends on choosing appropriate k-points(Brillouin integration). In principle we need to integrate over all possible k when constructing the density, fortunately the wavefunctions change slowly as we vary k,so we can approximate the integral with a summation the electronic wave functions at k points that are very close together will be almost identical and hence, it is possible to represent the electronic wave function over a region of k space by the wave function at a single k point. Hence the electronic states at only finite number of k points are required to calculate the electronic potential.On the other hand ,a uniform mesh of k- points can be generated

by Monkhorst-Pack procedure,

$$\vec{k}_{n_1,n_2,n_3} = \sum_{i=1}^{3} \frac{2n_i - N_i - 1}{2N_i} \vec{G}_i. \tag{2.56}$$

Where N_i is the number of $\vec{k}$ points in each direction and $n_i = 1, 2...N_i$ and G_i are reciprocal lattice vectors. In this dissertation 2D grid k points generated by Monkhorst-pack procedure [97] are employed after making convergence test with respect to total ground state energy.

2.8 Pseudopotentials

The core electrons of an atom are computationally expensive with plane wave basis sets because they are highly localized and hence very large number of plane waves are required to expand their wave functions. Furthermore, the contributions of the core electrons to bonding compared to those of the valence electrons is usually negligible. In fact,the primary role of the core electron wave functions is to ensure proper orthogonality between the valence electrons and core states. Consequently, it is desirable to replace strong Coulomb potential due to nucleus and tightly bound atomic core electrons with a pseudopotential that has the same effect on the valence electrons [98].There are essentially two kinds of pseudopotentials, norm-conserving soft pseudopotentials and Vanderbilt ultrasoft pseudopotentials [99] .In norm-conserving pseudopotentials, the charge enclosed in the pseudopotential region is the same as that enclosed by the same space in an all-electron calculation. In ultrasoft pseudopotentials, this requirement is relaxed and charge augmentation functions are used to make up the difference. As its name implies, this allows a ”softer” pseudopotential to be generated, which means fewer planewaves are required to expand it.

3

Electronic structure and Magnetic property of Mn doped monolayer and Bilayer MoS_2

3.1 Unit cell parameter deterimination

In this section,all parpameters used for nexst section calculations are determined by making convergence test:total ground state energy with respect to plane wave cutoff energy(e_{cut}),total ground state energy with respect to k point sampling and total ground state energy with respect to interlayer distance of BL MoS_2.

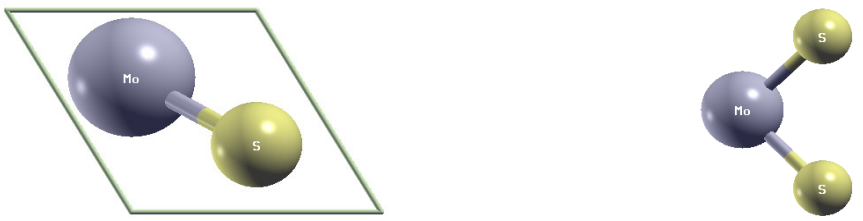

(a) (b)

Fig. 3.1: Unit cell structure of single layer MoS_2 (a) top view (b) side view

3.1.1 plane wave cut off energy(ecut) and k-point sampling

The magnitude of any error in the total energy or the total energy difference due to inadequacy of the k point sampling can always be reduced to zero by using a denser

set of k points. Therefore, it is crucial to test the convergence of the results with respect to the number of k points in general. The calculated plane wave ecut of energy,K point sampling and the converged values of lattice parameter are displayed in the Fig.(3.2). As shown in Fig (3.2*c*) ,the calculated equilibrium lattice constant is

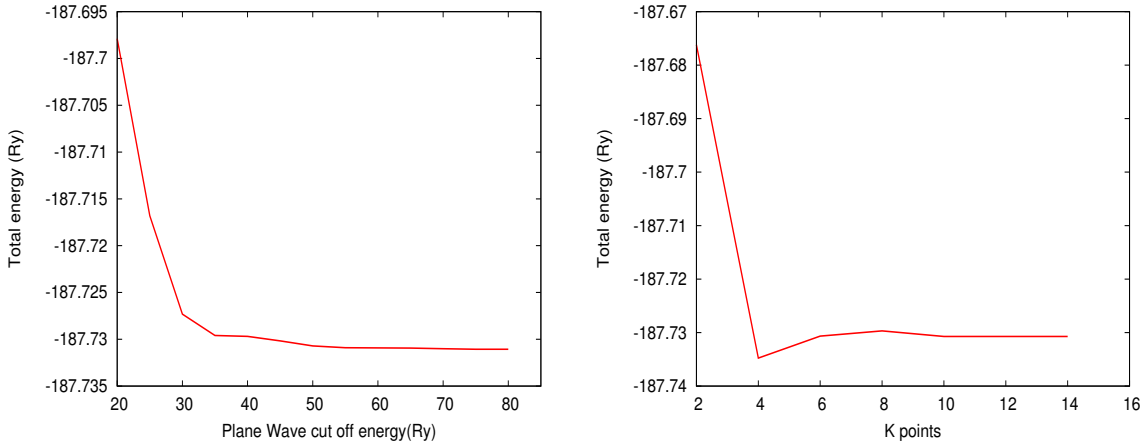

(a) (b)

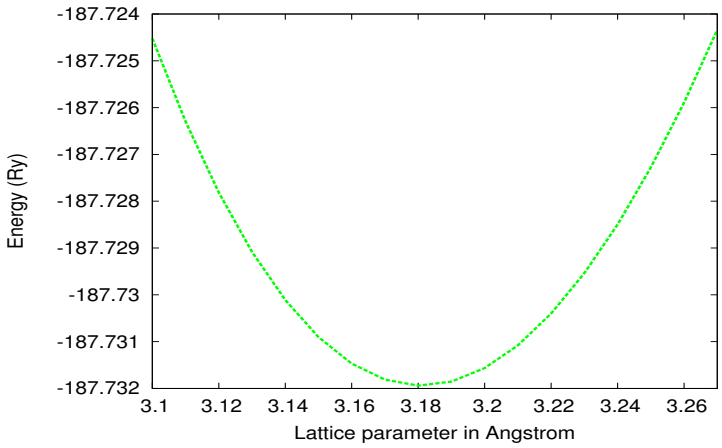

(c)

Fig. 3.2: Convergence of total ground state energy of single layer MoS_2 with respect to :a)plane wave cut off energy (ecut), b) Brillouin sampling(k points),c)lattice parameter.

found to be 3.18Å which is reasonably agrees with experimental value ranging from 3.16 Å [34] to 3.2Å [23] and theoretical value 3.18 Å [19]

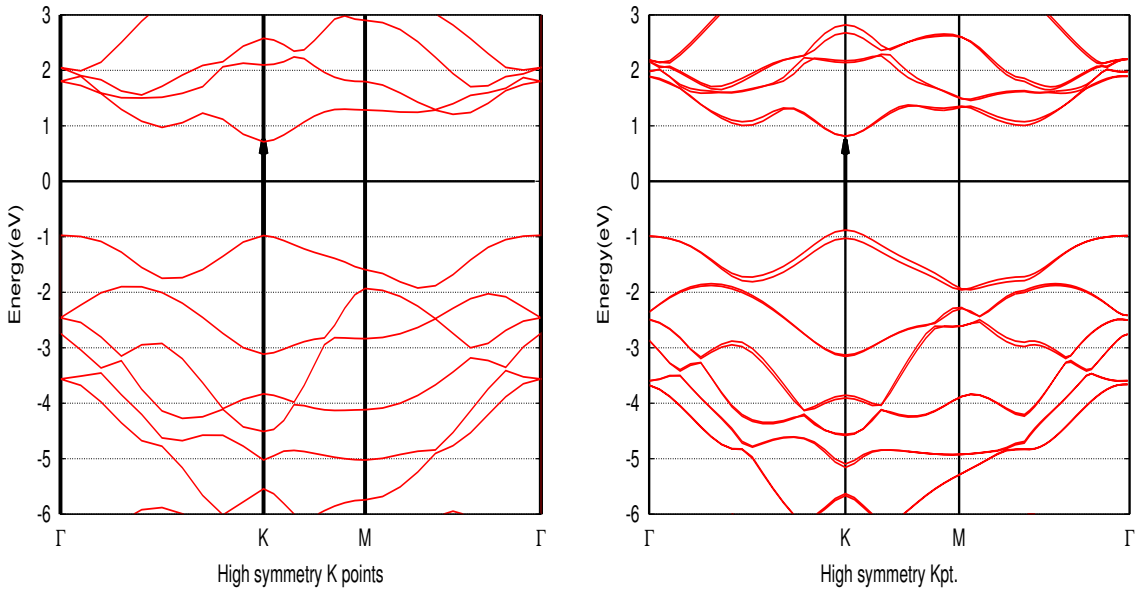

(a) (b)

Fig. 3.3: Band structure of single layer MoS_2:a)without considering spin-orbit coupling,b)considering spin-orbit interaction

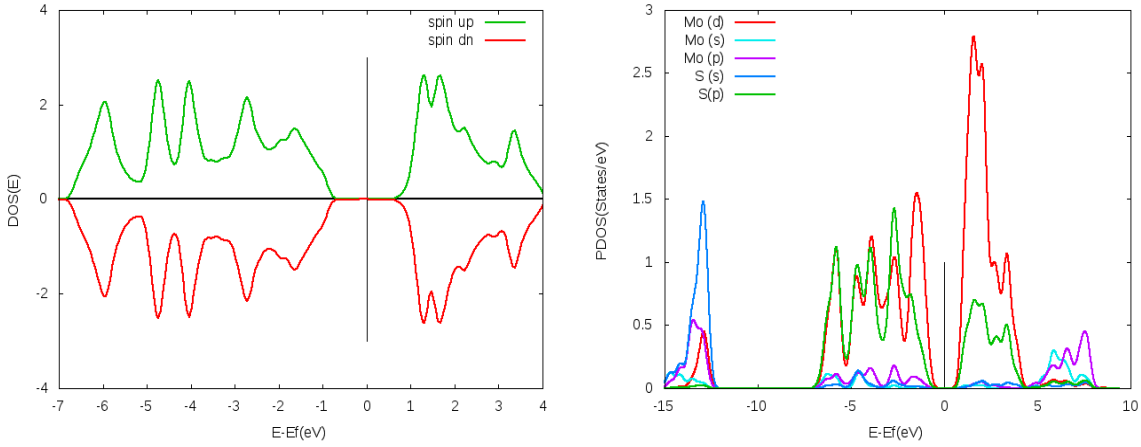

(a) (b)

Fig. 3.4: Density of state in single layer MoS_2: a)Total density of states for both spin up and spin-down electrons, b)Partial density of states

3.1.2 Electronic properties of single and bilayer MoS_2

Since the electronic structure are crucial to the understanding of the properties of the different structures the calculated electronic band structure the total spin polarized density of states DOS and partial density of states for ML and BL unit cell are displayed in Figs.(3.3) and (3.4). As shown in Fig.(3.3a) and Fig. (3.3b), the calculated band gap of ML MoS_2 of 1.75 eV closer with experimental optical band gap 1.9eV [21] and in good agreement with theoretical value of 1.75-1.9 Å [21–23]. Moreover,in Fig.(3.3a) the electronic band structure of monolayer MoS_2 without considering spin orbit coupling(SOC) direct band gap of 1.75 eV is obtained between the valence band maximum and conduction band minimum at the K-point, and all bands are found to be spin degenerate. When the SOC is turned on Fig.(3.3b) top valence bands displays a significant splitting ($\sim$ 150meV) at the K-point due to the breaking of spatial inversion symmetry (E(k, $\uparrow$)-E(k, $\downarrow$)). In sharp contrast, the top valence bands are spin degenerate at the Γ and M points. This is because Γ and M points are time-reversal invariant while K-point is not. However,as previous studies show that spin-orbital coupling has no significant effect on their magnetic exchange interaction [88] hence it is convenient to ignore for magnetic calculation in next sections. On the other hand,the total spin polarized density of state plot in Fig.(3.4a), show that nonmagnetic semiconductor behavior of pure single layer MoS_2 since spining up and down states are symmetric. Therefore, it is essential to introduce magnetism to break symmetry of those degenerate states. In addition ,the calculated partial density of state,Fig.(3.4b),indicates that much contribution for state near Fermi level is derived from molybdenum d-orbitals.

3.1.3 Interlayer distance dependent band structure in bilayer MoS_2

The theoretical calculations have predicted that the stacking sequence and interlayer distance in BL MoS_2 plays an important role in its electronic band structure [15]. Hence it is essential to determine equilibrium interlayer distance of BL MoS_2

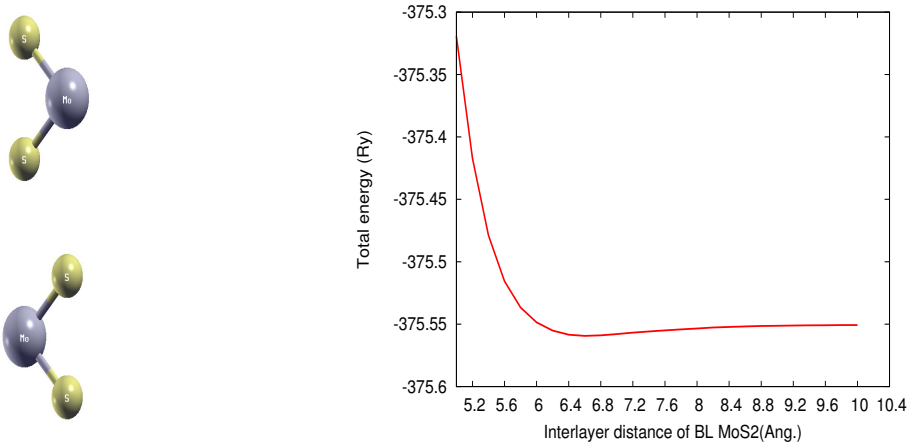

(a) (b)

Fig. 3.5: Bilayer MoS_2 a) crystal structure b)Total Ground state energy versus interlayer distance

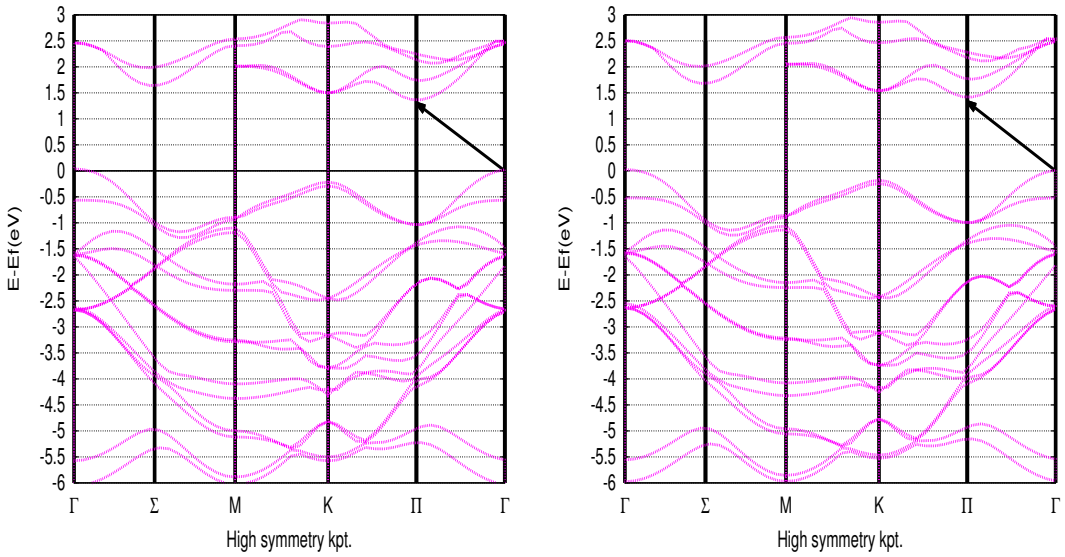

(a) (b)

Fig. 3.6: Interlayer distance dependent band gap in bilayer MoS_2:a)band structure at equilibrium interlayer distance,b)band structure at interlayer distance (d=6.65Å)

for further use. As shown Fig.(3.5*b*) ,the calculated equilibrium interlayer distance of BL MoS_2 is 6.543Å in reasonably agreement with experiment value of 0.68nm [40] and previous theoretical value 0.69nm [29] calculated using the 'VdW-DF-D2' method. The band gap calculated at this interlayer distance is 1.3 eV which is closer with previous reported value of 1.29Å [100]. Furthermore,the band gap increases with increasing interlayer distance as shown in Figs .(3.6*a*) and (3.6*b*).

Table 3.1: Summary of Interlayer distance dependent band structure in bilayer MoS_2

Interlayer distance (Å)	Band gap(eV)
6.55	1.30
6.61	1.32
6.65	1.33

3.2 Computional details

The first-principles calculations were carried out by using the Quantum espresso code within the density function theory(DFT) based on the DFT+U formalism [101].Electron-ion interactions were described by the Ultrasoft pseudopotentials (USPP) [99] and generalized gradient approximation of the Perdew-Burke-Ernzerhof using (PBE-GGA)formula for the electronic exchange-correlation potential. It is worth notify, that the GGA calculations, for example, for ABO_3 perovskites underestimate the band gap value, while the hybrid B3PW and B3LYP functionals allows to achieve much better agreement with the experiment for the band gap values [123, 124]. To overcome this on site Hubbard potential correction with a common U value of 3.0 and 4.0 eV was assigned to Vanadium(V) and manganese(Mn) 3d states respectively to handle highly correlated state of impurities. The plane wave basis set with cutoff energy of 60Ry used after performing convergence test. For 2D ML and BL a unit cell with periodic boundary condition is adopted to simulate the infinite x-y plane. For the BL

MoS_2,Grimmes DFT-D2 dispersion correction [102] is applied to account for the long-range Vander Waals interactions between different layers. To investigate the doping effects of Mn impurities on ML and BL MoS_2, supper cell with different sizes were employed and atomic position for those supercells were generated by making use of python code. 20Å thickness vacuum region was used for monolayer MoS_2 calculations to isolate the single layer along the z-axis and ensure no interaction take place between the layers . Integrations over the Brillouin zone (BZ) are sampled based on a Monkhorst-Pack 2D grid [103] which varies from $4 \times 4 \times 1$to $3 \times 3 \times 1$ for structural relaxation and $12 \times 12 \times 1$ to $9 \times 9 \times 1$ for density calculation respectively depending on the size of the supercells.

3.3 Result and discussion

3.3.1 Defect formation energy and structural stability

The relative stability of the doped structure is determined from the formation energy [104, 105]. Following [104],the formation energy of neutral Mn dopant atom can be calculated using the following relation

$$E_{form} = E_{Tot}(Mn, MoS_2) - E_{Tot}(MoS_2) - \sum_i n_i(\mu_{Mn} - \mu_{Mo}), \tag{3.1}$$

where E_{Tot}(Mn,MoS_2) and E_{Tot}(MoS_2) are total energy of doped and pure ML(BL) MoS_2 respectively,n_i is the corresponding number of species that have been added to or removed from the supercell and μ_{Mn} and μ_{Mo} are chemical potential of Mn and Mo respectively. We consider Mo rich and S rich condition for chemical potential calculation of Mo, in Mo rich condition, the chemical potential for μ_{Mo} is obtained from its bulk BCC Mo [104], where as under S- rich condition μ_{Mo} is obtained from energy difference between formula unit of MoS_2 and the most stable form of sulfur molecular (ring form of sulfur molecules) [106]. On the other hand, the relative stability of BL MoS_2 supercell is tested by calculating the energy difference between

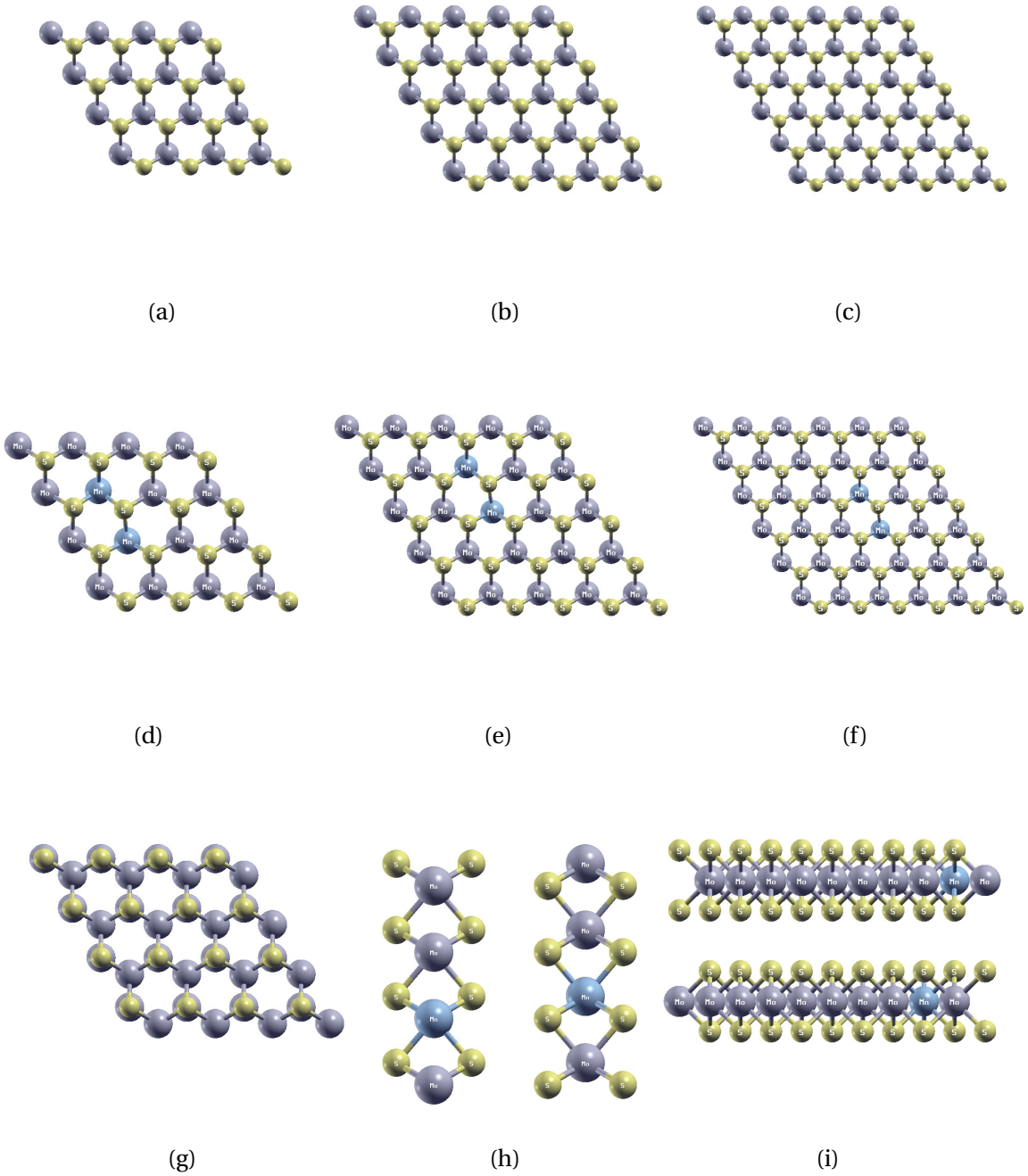

Fig. 3.7: Optimized input structure for ML and BL MoS_2 : a,b and c) top view of $4 \times 4 \times 1, 5 \times 5 \times 1$ and $6 \times 6 \times 1$ pure ML supercells respectively ,(d,e and f) top view of two Mn doped $4 \times 4 \times 1$,$5 \times 5 \times 1$ and $6 \times 6 \times 1$ ML MoS_2,g)top view of $4 \times 4 \times 1$ pure BL MoS_2 ,h and i) side(xy) view and (xz) view of two Mn doped on different layers of BL MoS_2

the BL supercell and two fold of corresponding ML as

$$E_{bind} = E_{BL} - 2E_{ML}, \tag{3.2}$$

where E_{bind} is binding energy of BL MoS_2 supercell E_{BL} and E_{ML} are the total energy of supercell in BL and ML phase respectively. We found that -12.0315 eV and -21.38 eV for supercell of $3\times3\times1$ and $4\times4\times1$ respectively. The result reveals the BL MoS_2 is energically more stable than ML. The calculated formation energy for different impurity concentrations and doping sites are summarized in table.(3.2), all calculated values under S-rich condition are negative which shows that doping Mn under S-rich condition ML and BL MoS_2 is energetically more favorable in compared with Mo-rich condition in agreement with other studies on Mn doped ML MoS_2 [107]. On the other hand, the least formation energy -2.014 eV is obtained in doping singe Mn on Mo site of $4\times4\times1$ BL MoS_2 supercell,hence doping Mn on supercell of $4\times4\times1$ is energically favorable than doping on $3\times3\times1$. In other word ,lowest formation energy implies that dopants will be bonded closer and stronger to Mo atoms.

3.3.2 Electronic Structures and magnetism Of single Mn doped monolayer and bilayer MoS_2

To investigate the effects of doping single Mn atoms on the electronic and magnetic properties of ML and BL MoS_2, we considered models of $4\times4\times1$ and $3\times3\times1$ supercell in which one of the Mo atoms of super cell is replaced by one of 3d TM (Mn)resulting concentration of magnetic dopant 3.125 % and 5.55 % respectively in BL and 6.25 % and 11.11 % ML MoS_2 phase respectively. As seen from table (3.3) and table (3.4),the total magnetic moment of the system 1 μ_B after introducing single Mn in super cell of $3\times3\times1$ and $4\times4\times1$ in ML phase and 1 μ_B and 1.02 μ_B respectively its BL phase and hence the system become magnetic. Now we turn to investigate the effect of the impurity atoms on electronic properties of ML and BL MoS_2, where we calculated spin polarized electronic state of pure and doped system. As shown from total spin polarized density of state (DOS) plot for pure ML and

Table 3.2: Calculated values of formation energy ,E_F(eV), monolayer (ML) and bilayer (BL) MoS_2 doped with Mn under Mo rich and S-rich condition

supercell	doping site	(Mo rich)$E_F(eV)$	(S rich)$E_F(eV)$
$3\times3\times1$ ML	1Mn	2.5533	-0.1062
$3\times3\times1$ ML	N	3.4952	-1.8210
$3\times3\times1$ BL	1Mn	1.908	-0.7523
$3\times3\times1$ BL	N	3.4019	-1.9173
$3\times3\times1$ BL	updn(do)	3.9779	-1.3432
$4\times4\times1$ ML	1Mn	1.7299	-0.92752
$4\times4\times1$ ML	N	3.0246	-2.2936
$5\times5\times1$ ML	N	2.04	-3.2776
$6\times6\times1$ ML	N	1.52456	-3.7930
$4\times4\times1$ BL	1Mn	1.8677	-0.7919
>>	N	3.3067	-2.0144
>>	updn(do)	3.7319	-1.5873

BL MoS_2 respectively on Figs.(3.8a) and (3.9a), for both cases,the Fermi level is located at the middle and spin up and spin down state are symmetric indicating the pure ML and BL MoS_2 are nonmagnetic semiconductor. However,after introducing single Mn the spin degeneracy of the band structure is broken and the minority of states remain semiconductors whereas, the majority(spin up state) impurity state is formed in vicinity of Fermi level as a result it behaves as metallic. Leading to magnetic and half metallic behavior of total DOS Figs.(3.8b). In addition to this impurity states are broadened toward the conduction band minimum (CBM) with increasing impurity concentration from (0 to 11.11 $\%$) for doped ML Figs.3.8($a-c$) and 3.9($a-e$) for BL which is in broad agreement with properties of dilute magnetic semiconductors [108]. Furthermore, in order to understand the nature of energy band structure and impurity state,the energy band structure for pure and single Mn doped in $4\times4\times1$ ML and BL MoS_2 supercell are plotted. As shown from Figs.(3.10) and (3.11) both valence band maximum (VBM) and conduction band minimum

(CBM) are located at K high symmetry point for pure and doped ML MoS_2 system indicating that the type of band gap is direct in nature. However,in Mn doped ML MoS_2 the Fermi energy closer to CBM for spin up(majority of state) Figs.(3.10c) and (3.10d) compared to pure system ,Figs.(3.10a) and (3.10b) which suggests that the doped system more likely to n-type of semiconductors. Contrary to ML MoS_2 the BL MoS_2 and its doped system is characterized by indirect band gap see Figs.3.11$(a-f)$,thus VBM and CBM are located at Γ and K high symmetric points respectively .As shown From those aforementioned figures, impurity bands are appear nearer to Fermi level in the case of majority state (spin up) but not in minority(spin down) state energy band structures. Thus, the occurrence of impurity bands at the Fermi level with different symmetries (spin up and spin down) confirm that Mn doped ML and BL MoS_2 are magnetic and half metallic nature which is much better for spintronic applications as dilute magnetic semiconductors. The origin of magnetism can be explained as an isolated Mn^{+2} atom has a Ar($3d^5 4s^2$) configuration one electron more than the Mo atom with electron configuration Ar($3d^{10} 4s^2 4p^6 4d^4 5s^2$) thus extra electron is responsible for observed defect state in the gap. Thus ,Mn^{+2} ions possesses spin magnetic moment $5\mu_B$ and therefore, incorporation of Mn^{+2} ions into ML and BL MoS_2 is expected to change its magnetic properties.

3.3.3 Magnetic interaction in monolayer MoS_2 doped with pair of Mn atoms

To determine the stable magnetic ground state, the possible magnetic state either ferromagnetic(FM) or anti-ferromagnetic(AF) is studied by calculating the total energy difference of the two configurations at the same impurity separation (d). We define magnetic energy (Δ E^d) as

$$\Delta E^d = E^d_{FM} - E^d_{AF}. \tag{3.3}$$

where E^d_{FM} and E^d_{AF} are the total energies of the supercell in ferromagnet(FM) and antiferromagnet(AFM) states with a pair of dopants separated by atomic distance d. We have employed models:$6 \times 6 \times 1$,$5 \times 5 \times 1$, $4 \times 4 \times 1$ and $3 \times 3 \times 1$ ML MoS_2

Table 3.3: Magnetic energy (ΔE) and magnetic moment (μ_m)for Mn doped monolayer(ML) MoS_2

supercell	distance(d)	impurity(%)	ΔE(eV)	$\mu_m(\mu_B)$
$3 \times 3 \times 1$	single	11.11		1.00
>>	N	22.22	-0.18444	2.32
>>	NN	22.22	-0.212240	2.000
>>	NNN	22.122	-0.132042	1.74
$4 \times 4 \times 1$	single	6.25		1.00
>>	N	12.5	-0.21007	2.07
>>	NN	12.5	-0.177582	2.00
>>	NNN	12.5	-0.0849	2.00
$5 \times 5 \times 1$	N	8	-0.1636	2.46
$6 \times 6 \times 1$	N	5.5	-0.15295	2.39

supercells,resulting in doping concentrations of 5.5 %, 6.25 % , 11.11 % and 22.22% respectively up on substituting a pair of Mn atoms on Mo sites. Three configurations with different Mn-Mn separations were considered: Nearest neighbor configurations(N) in which the two Mn atoms are in the nearest neighboring position with Mn-Mn distance of 3.4 Å, the second nearest neighbor configurations(NN) in which the two Mn atoms are in the next nearest-neighboring position with Mn-Mn distance of 5.5 Å, and the third nearest neighbor configuration(NNN) in which the distance between the two doped Mn atoms at 6.4Å. The calculated magnetic energy (ΔE) and magnetic moment (μ_B) for aforementioned configurations and impurity concentrations are summarized in Table. (3.3),the calculated ΔE for all three configurations and for all dopant concentrations are negative which means the ferromagnetic states are more favorable energetically and our results agree with previous results [105]. In addition to this,the calculated magnitude of magnetic energy ,ΔE,drop with increase in separation distance from 3.4Å to 6.4Å.

3.3.4 Magnetic interaction in bilayer MoS_2 doped pair of Mn atoms

Using Eq.(3.3) and following similar procedure for ML MoS_2 doped system in section 3 ,magnetic energy,ΔE, are calculated for pair of Mn doped BL MoS_2 using $5\times5\times1$, $4\times4\times1$ and $3\times3\times1$ model supercells resulting doping concentrations of $4\%, 6.25\%$ and 11.11% up on introducing a pair of impurity atoms in Mo sites. Unlike case of ML five potential doping configurations have been considered here (i) two Mn dopants in the same layer and nearest neighbor configuration(N),(ii) two Mn dopants in the same layer and second nearest neighbor configuration(NN),(iii) two Mn dopants in the same layer and third nearest neighbor configuration(NNN), (iV) two Mn dopants in different layers and dopants are separated by equilibrium interlayer distance (d_0=6.53Å) two Mn dopants in different layers and atomic distance between dopants 7.8Å denoted by updn(d1). All calculated values are summarized in table (3.4). As shown in table (3.4) ,the calculated ΔE for all impurity configurations and concentrations are also negative indicating that ferromagnetic coupling is always favorable irrespective of the position and concentration of magnetic dopants. In addition to this,the magnitude of magnetic energy (Δ E) decreases as distance between dopants (d) increases(on going from N to NNN). Before proceeding to investigate the role of interlayer interaction in BL MoS_2 sysetm on magnetic interaction between dopants ,it is convenient to understand the magnetic interaction between a pair of dopants in bilayer MoS_2 system which are placed in different layers (one in upper layer the other one lower layer) as shown in input structure Figs.(3.7h) and (3.7i) which has not been reported before even for other system. We found that ΔE =-0.006 and -0.0025 eV for two dopants separated by d_0=6.53 Å (at equilibrium interlayer distance) and d_1=7.8Å,respectively. The result reveals that two dopant in different layer interact ferromagnetically and the strength of ferromagnetism is suppress with atomic distance. Moreover,to understand how the states are distributed,the spin polarized total density state (DOS) are ploted.As

Table 3.4: Magnetic energy (ΔE) and magnetic moment (μ_m)for Mn doped bilayer(BL) MoS_2

supercell	distance(d)	impurity(%)	ΔE (eV)	$\mu_m(\mu_B)$
3X3X1	single	5.55		1.00
>>	N	11.11	-0.192	2.13
>>	NN	11.11	-0.232	2.000
>>	NNN	11.11	-0.13046	1.83
>>	updn(do)	11.11	-0.0085	2.00
>>	updn(d1)	11.11	-0.0033	2.000
4X4X1	single	3.125		1.02
>>	N	6.25	-0.2137	2.03
>>	NN	6.25	-0.1690	2.00
>>	NNN	6.25	-0.08217	2.06
>>	updn(do)	6.25	-0.006	2.00
>>	updn(d1)	6.25	-0.0025	2.00
$5X5X1$	N	4	-0.1654	2.00

shown in DOS plot in Fig .(3.9c) and energy band structure plot Figs.(3.11e) and (3.11f) the system become magnetic and half metallic similar with doping a pair of Mn in the same layer. This investigation will be base line for experimentalist to control magnetism of this system by doping transition metals regardless of where the dopants are injected either same layer or different layer of BL MoS_2,this also makes the physics of system under investigation more interesting on to how two dopant in different layers separated by $\sim$ 8Å are communicating .

3.3.5 Mechanism of exchange interaction

Understanding mechanism of exchange interaction between dopants which stabilize either ferromagnetism or anti ferromagnetism in doped system is other issue [110],since there are two sub system, host with paramagnetic back ground and

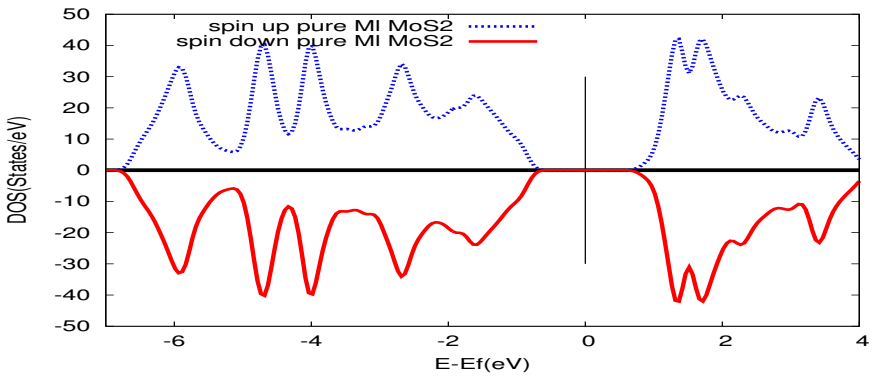

(a)

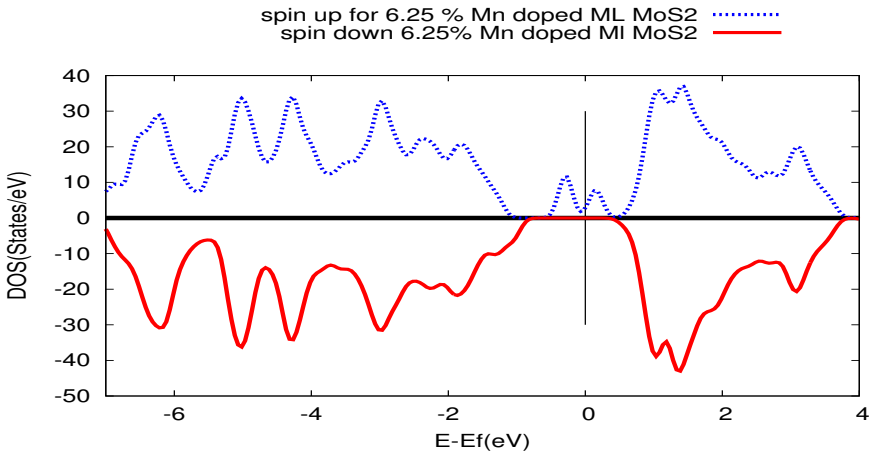

(b)

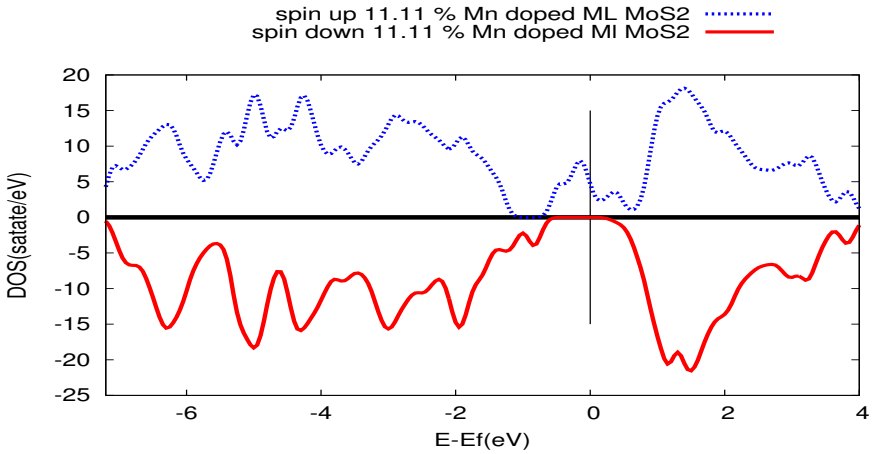

(c)

Fig. 3.8: Spin resolved total density of state for $4 \times 4 \times 1$ and $3 \times 3 \times 1$ ML MoS_2 : (a) Pure MoS_2, (b) one-Mn-doped $4 \times 4 \times 1$ MoS_2 ML and (c) one Mn-doped $3 \times 3 \times 1$ MoS_2 ML respectively. The blue and red lines represent the spin-up and spin-down components respectively.The zero energy represents the Fermi level.

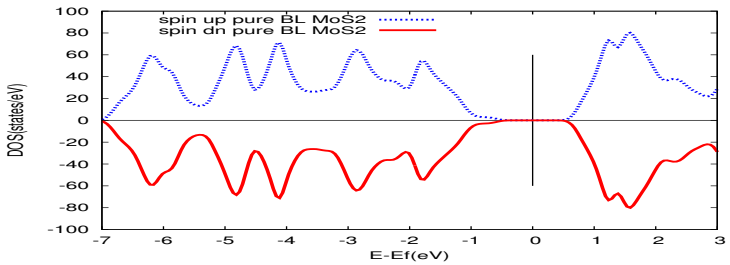

(a)

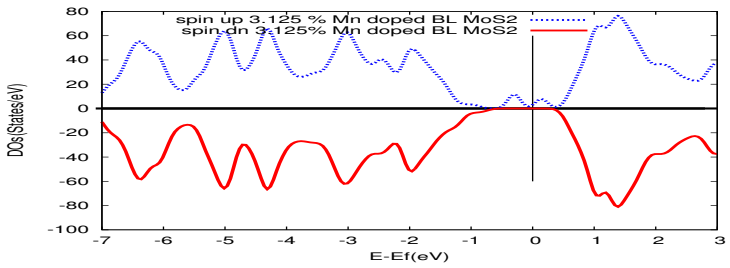

(b)

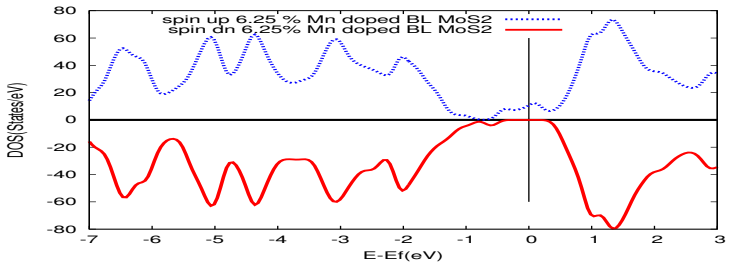

(c)

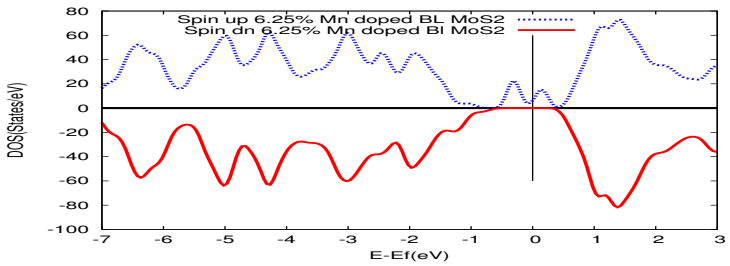

(d)

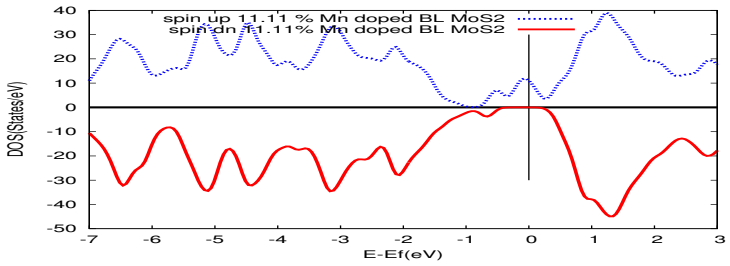

(e)

Fig. 3.9: Spin resolved total density of state for $4\times4\times1$ and $3\times3\times1$ BL MoS_2:(a) pure MoS_2,(b)One-Mn-doped on upper layer of BL $4\times4\times1$ MoS_2 and (c)two Mn-doped in upper layer of $4\times4\times1$ BL MoS_2 d)Two Mn-doped in different layers of $4\times4\times1$ BL MoS_2 ,e)Two Mn-doped in upper layer of $3\times3\times1$ BL MoS_2 respectively.

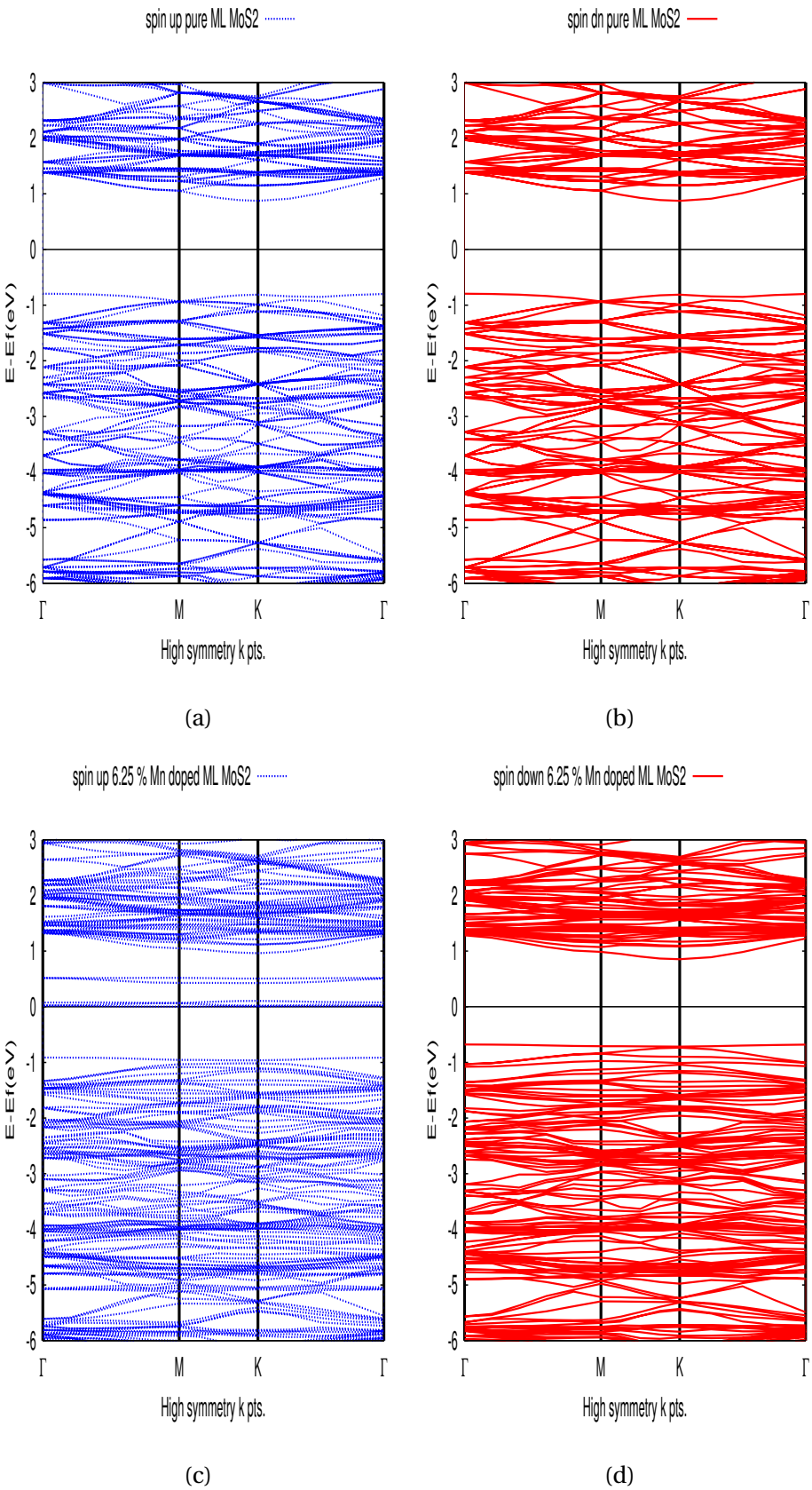

Fig. 3.10: Band structure for $4\times4\times1$ ML MoS_2 : (a) and (b) pure MoS_2, (c) and (d) one-Mn-doped $4\times4\times1$ ML MoS_2 respectively. The blue and red lines represent the spin-up and spin-down components respectively.The zero energy represents the Fermi level.

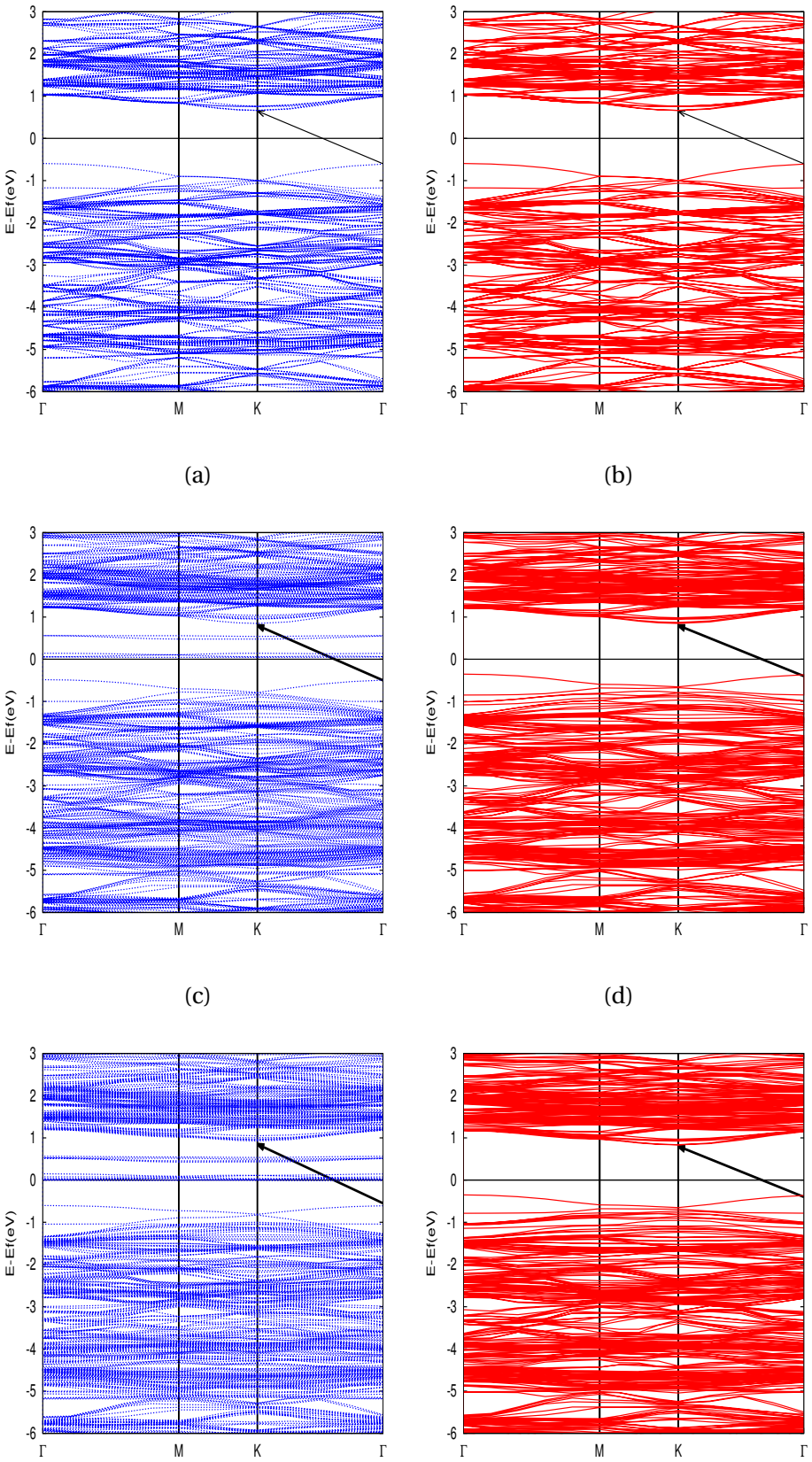

Fig. 3.11: Band structures of $4\times4\times1$ BL MoS_2 : (a) and (b) pure MoS_2, (c) and (d) one-Mn-doped in upper layer of BL MoS_2,and (e) and (f) two-Mn-doped BL MoS_2(in different layers).The blue and red lines represent the spin-up and spin-down components respectively.

the system of doped magnetic ions these two sub systems interact with each others. There are different competing magnetic interactions in doped system like Mn doped MoS_2 system. Based on Goodenough- Kanamori-Anderson rules [111, 112] state that the magnetic ion-ligand-magnetic ion angle is 180^0 of two magnetic ions with partially filled d shells is strongly antiferromagnetic. Whereas the magnetic ion-ligand-magnetic ion angle

is 90^0 is ferromagnetic superexchange based on the relaxed Mn impurity pair form a Mn-S-Mn complex with a bond angle of 93^0 closer to 90^0 thus the Anderson Goodenough-Kanamori rule preferred magnetic alignment for two neighboring Mn atoms is ferromagnetic which can be postulated as 3d state of Mn atom interact antiferromagnetically with one of sulfur(S) atom 3p state then this state further interact with other Mn 3d state ,in this way the two impurity-atoms communicate ferromagnetically indirectly in the presence of mediating sulfur 3p state and with aid of periodicity of crystals the process will be extended to entire the supercell.

3.3.6 Ferromagnetic transition temperature (T_c)

According to Weiss theory ferromagnetic materials contain in addition to any external applied magnetic field B_{ex}, an internal molecular field B_{in} which is proportional to its magnetization

$$B_{in} = n_W M_s. \tag{3.4}$$

where n_w is molecular field constant whose origin can be understood by introducing the idea of Heisenberg exchange field. On the other hand, the spin Hamiltonian of magnetic atoms localized at lattice site i,j is given by Heisenberg Hamiltonian

$$\hat{H} = -2\sum_{i>j} J_{ij} S_i.S_j, \tag{3.5}$$

where J_{ij} is the exchange coupling constant for the spins of magnetic atoms on site i and j ,and the summation is over all sites of magnetic atoms. Consider that the magnetic moment of magnetic atom in doped system,are given by $\mu_i = g\mu_B S_i$ and

assuming this moment interact with effective field (B_{in}) yields Hamiltonian,

$$\hat{H} = g\mu_B S_i B_{in} \tag{3.6}$$

where g and μ_B are the Lande g factor and Bohr magneton, respectively. Equating Eqs.(3.5) and (3.6),the molecular field B_{in} could be thus defined as

$$B_{in} = -\frac{2}{g\mu_B}\sum_j J_{ij}S_j \tag{3.7}$$

The effective field as defined in Eq.(3.7) is complicated and depending on the neighboring spin operators $S_{i+\delta}$ .However mean field theory replaces this quantity with its thermal average as

$$B_{in} \approx -\frac{2zJ_0}{g\mu_B} < S_j > . \tag{3.8}$$

Where J_0 is exchange interaction of nearest pair of Transition metal(TM) spins and related to the overlap of the charge distribution of nearest spins. On the other hand, at finite temperature (T) the magnetization of TM atoms doped in MoS_2 at site j defined by

$$M = N\langle\mu\rangle = -Ng\mu_B\langle S_j\rangle \tag{3.9}$$

where N is the concentration of magnetic ions in system. Using Eq.(3.9) into Eq.(3.8) we have

$$B_{in} = \frac{2zJ_0}{Ng^2\mu_B^2}M \tag{3.10}$$

Comparing Eq.(3.4) and Eq.(3.10) we shall extract molecular field constant

$$n_w = \frac{2zJ_0}{Ng^2\mu_B^2} \tag{3.11}$$

After some mathematical steps magnetization at finite temperature in Eq.(3.9) can be obtained as

$$M = N\langle\mu\rangle = Ng\mu_B S B_s(u), \tag{3.12}$$

where $B_s(u)$ is the Brillouin function and is defined by

$$B_s(u) = \frac{2S+1}{2S}cot(\frac{2S+1}{2S})u - \frac{1}{2S}cot(\frac{1}{2S})u,$$

and $u = \frac{g\mu_B S B_{in}}{K_B T}$. Now using properties of Brillouin function,

$$B_s(u)_{u\to 0} = \frac{S+1}{3S}u \tag{3.13}$$

Substitution of Eq.(3.13) into Eq.(3.12) yields,

$$M \approx \frac{N\mu_B^2 g^2 S(S+1)B_{in}}{3K_B T} \tag{3.14}$$

On the other hand,the magnetic susceptibility (molar) is defined as

$$\chi_M = \frac{M}{B} = \frac{N\mu_B^2 g^2 S(S+1)}{3K_B T} \tag{3.15}$$

Then the susceptibility obeys a Curie law ,

$$\chi_M = \frac{C_m}{T} \tag{3.16}$$

From Eqs.(3.15 and 3.16) we can extract Curie constant $C_m = \frac{N\mu_B^2 g^2 S(S+1)}{3K_B}$. Now considering the magnetization of ferromagnet for $T > T_c$ in the presence of an external magnetic field B_{ex} . The magnetization M is described by

$$M = \frac{C_m}{T}(B_{in} + B_{ex}) \tag{3.17}$$

Using Eq.(3.4) into Eq.(3.17) after few rearrangement,we obtain the magnetic susceptibility χ_m as

$$\chi_m = \frac{M}{B_{ex}} = \frac{C_m}{T-\Theta}. \tag{3.18}$$

where $\Theta = n_w C_M$ is Curie-Weiss temperature.$\Theta = T_c$ in mean field theory and can be found using the expression for C_w obtained in so far and n_W as

$$K_B T_c = \frac{2zJ_o S(S+1)}{3}. \tag{3.19}$$

If the term S(S+1)and z is included in the exchange coupling constants as it is usually done when the $J_o's$ are determined from first-principles calculations [113] and Eq.(3.19) becomes

$$T_c K_B = \frac{2}{3}J_o \tag{3.20}$$

In addition to this in supercell approach exchange constant(J_0) ,in Eq.(3.19) are replaced by magnetic energy (the energy difference between ferromagnetic(FM) and antiferromagnetic(AFM)states) which can be obtained directly from first principle calculation using spin polarized DFT.Therefore, using $J = \frac{\Delta E}{N_{imp}}$ [114]into Eq.(3.19) we have

$$\frac{3}{2}T_c K_B = -\frac{\Delta E}{N_{imp}}. \tag{3.21}$$

where ΔE=E_{FM}-E_{AFM} and N_{imp} is number of TM impurities doped in supercell. Now using the value ΔE for first nearest neighbor impurity configurations(N) in table .(3) and N=2, we have calculated T_c for ML and BL MoS_2 doped system for different impurity concentrations . However,it is well known that the magnetic ordering in doped system is strongly influenced by percolation, thus mean-field approximation cannot capture this behavior and tends to overestimate T_c in these systems [44]. To overcome this,we made use of some empirical relation which connects the mean field value critical temperature (T_c^{MFA}) with corrected critical temperature (T_c^{corr}) as T_C^{corr} =(0.506)T_c^{MFA} [115], where T_c^{corr} is exact (corrected) critical temperature calculated using Ising model for hexagonal lattice and T_c^{MFA} is predicted critical temperature using mean field theory as discussed earlier. The calculated result presented in table(3.5). As shown in table(3.5) the calculated T_c 5.5% Mn doped monolayer MoS_2 found to have 299K in agreement with latest experimental observation of room temperature T_c [109]. Moreover, for high concentration both in Mn doped ML and BL MoS_2 T_c exceeds the room temperature (RT) and a non monotonic behavior of T_c is observed,T_c increases with Mn concentrations in a range of dilute limit (0 to 6.25 $\%$) and then decrease with further increasing Mn concentration above this value (6.25 to 11.11$\%$). Thus our result indicates that ferromagnetism in this system is tunable by controlling the concentration of magnetic dopants (Mn). Moreover,ferromagnetism share some of properties of DMSs like Mn doped (III-V) [116].

Table 3.5: The calculated ferromagnetic transition temperature T_c for Mn doped monolayer(ML) and bilayer(BL) MoS_2.

System	impurity(%)	ΔE (eV)	$T_c^{MFA}(K)$	T_c^{corr}	Experimental
ML MoS_2 doped Mn	5.5	-0.153	591	299	300K [109]
>>	8.00	-0.163	630	319	
>>	12.50	-0.210	811	410	
>>	22.22	-0.184	711	360	
BL MoS_2 doped Mn	4.00	-0.166	641	324	
>>	6.25	-0.214	827	418	
>>	11.11	-0.192	742	38	

3.3.7 Conclusion

In conclusion,we have shown that Mn dopant in ML and BL MoS_2 are energetically favorable to occupy the substitutional lattice site(Mo) under sulfur(S) rich regime than Mo rich condition. It is found that Mn doping in ML and BL MoS_2 induces magnetism and turns semiconductor property of pure system to half metallic nature with n-type of conductivity.

Besides, we found that the magnetic interaction between dopants in ML and Bl MoS_2 are always ferromagnetic irrespective of dopant configurations and concentrations and the strength of ferromagntism decays with atomic distance between the dopants.

We also found that interlayer interaction in Mn doped BL MoS_2 affects its magnetic interaction between the dopants,this implies that the layer number may have an important effect on magnetic properties of Mn-doped MoS_2 system.

The calculated ferromagnetic transition temperature (T_c) in Mn doped ML and BL MoS_2 are found to be above room temperature (RT). Moreover, in ML phase T_c at impurity concentration of 5.5 % is found to be 299K which is in reasonable agreement with latest experimental observation of RT T_c in Mn doped system [109]. We

propose ferromagnetic super exchange mechanism is primarily responsible for ferromagnetic interaction between a pair of dopants in nearest neighbor configuration.

Based on our result, we suggest that Mn doped ML and BL MoS_2 are promising candidates for 2D dilute magnetic semiconductors(DMSs) for high temperature spintronics applications.

4

Electronic structure and Magnetic property of Vanadium(V) doped monolayer and bilayer MoS_2

4.1 Result and Discussion

4.1.1 Defect formation energy and structural stability

To understand relative stability of dopant atom (V) in ML and BL MoS_2, dopant formation energy (E_{form}) calculation are carried out using similar approach in chapter three as

$$E_{form} = E_{tot}(V, MoS_2) - E_{tot}(MoS_2) - \sum_i n_i(\mu_V - \mu_{Mo}). \tag{4.1}$$

Where E(V,MoS_2) and E(MoS_2) are total energy of V doped and pure ML(BL) MoS_2 respectively,n_i is the corresponding number of species that have been added to or removed from the super cell and μ_V and μ_{Mo} are chemical potential of V and Mo respectively. We have also considered both Mo rich and S rich condition for chemical potential calculation of Mo. The calculated dopant formation energy for different doping sites and dopant concentrations are summarized in table (4.1). As shown from table (4.1) all calculated dopant formation energy are negative in both Mo rich and S rich growth condition indicating that Vandium(V) doping on ML and BL MoS_2 for different configuration and dopant concentrations is energetically favorable in both S-rich and Mo-rich growth conditions and hence V dopants are strongly bonded with host system(MoS_2)orbitals which are actively involving in electronic and magnetic properties .However,all calculated values under S-rich condition are

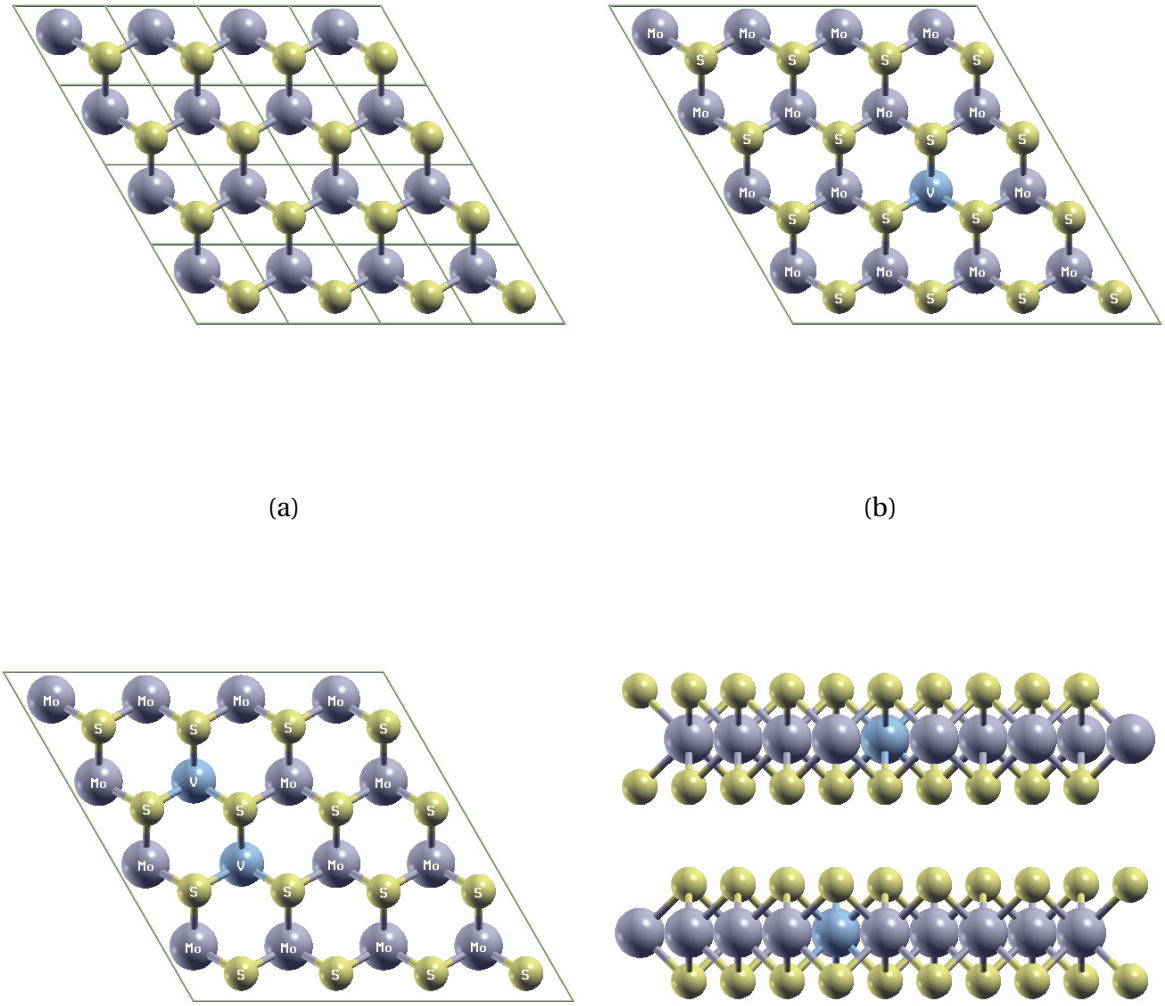

(a) (b)

(c) (d)

Fig. 4.1: Optimized input structure of ML and BL MoS_2: (a) top view pure ML MoS_2 , (b) top view for one V doped ML MoS_2, (c) top view for two V doped ML MoS_2 and (d) side view for two V doped in different layers of BL MoS_2

more negative than Mo-rich condition which reveals that V doping under S-rich condition of ML and BL MoS_2 is energetically more favorable than under Mo-rich growth condition.

Table 4.1: Calculated values of formation energy ($E_{form}(eV)$) V doped ML and BL MoS_2 under Mo rich and S-rich condition

supercell	doping site	(Mo rich)$E_F(eV)$	(S rich)$E_F(eV)$
$3\times3\times1$ ML	1V	-5.358	-8.017
>>	N	-3.538	-8.857
$4\times4\times1$ ML	1V	-1.601	-4.260
>>	N	-3.416	-8.735
$3\times3\times1$ BL	1V	-5.352	-8.012
>>	N	-10.635	-15.950
$4\times4\times1$ BL	1V	-4.879	-7.539
>>	N	-3.246	-8.566
>>	updn(d0)	-10.739	-15.058

4.1.2 Electronic structure and magnetic properties of pure and single V doped ML and BL MoS_2

To investigate the effects of doping on the electronic and magnetic properties of ML and BL MoS_2,we considered models of $4\times4\times1$ and $3\times3\times1$ supercell in which one of the Mo atoms of super cell is replaced by one of 3d TM (V),resulting concentration of magnetic dopant 3.125 % and 5.555 % respectively in ML and 6.25 % and 11.11 % BL MoS_2 phase respectively. In terms of geometry,our DFT+U calculation for single V doped ML and BL MoS_2 shows that,the bond length of Mo-S dramatically shortens to 2.35 Å,as compared with value 2.41 Å of pristine MoS_2 Fig.(4.1a) and (4.1b) but maintain the original prismatic configuration which makes the candidates good for applications in 2D materials. We now turn to investigate the magnetic properties of the doped system,as seen from tables .(4.2) and (4.3) ,the total magnetic moment within the super cell is 0.96 and 0.98 μ_B after introducing single V in $4\times4\times1$ ML and BL MoS_2. Therefore, system become magnetic. To get detail about how the state is

distributed we have plotted spin polarized total density of states (DOS) for pure and single V doped $4 \times 4 \times 1$ and $3 \times 3 \times 1$ MoS_2 supercells. As seen from Figs.$(4.2a)$ and Fig.$(4.3a)$,the nature of DOS for up and down spin channels are symmetric for pure ML and BL MoS_2 system,thus symmetric behavior of up and down spin channel of total DOS indicates that these materials bear non magnetic semiconductor nature. However, after introducing single V in molybdenum(Mo) sites, the spin degeneracy of the band structure is broken and the majority(spining up) states remain a semiconductors whereas,in minority (spin down state) some additional peaks appear closer to valence band maximum (VBM) and some states cross Fermi level as shown in Fig.$(4.2b)$ and Fig.$(4.4c)$ indicating metallic behavior of minority states and which suggest that half metallic and magnetic behavior of over all system. On the other hand,the shift of Fermi level to Valence band maximum(VBM) after injection of V compared to pure MoS_2 system reveals that V doping introduces holes(p-type of conductivity). Similar behavior is also observed form DOS plot of single V doped BL MoS_2 Figs.$4.3(a-d)$ except magnitude of band gap is suppressed in going from ML to BL due to confinement effect. In addition to this,the impurity states broaden its size toward valence band minimum (VBM) with increasing impurity concentration from 0 $\%$ to 11.11 $\%$ in ML doped system Fig.$4.2(a-d)$ as well as BL Fig.$4.3(a-d)$,reflecting that magnetism in this system can be controlled by dopant concentrations in broad agreement with properties of dilute magnetic semiconductors (DMS) like Mn doped GaAs [116, 117]. Further more, the energy band structure plot for pure and single V doped ML and BL MoS_2 supercell are displayed in Fig.(5). It is clearly seen that VBM and CBM are located at K high symmetric points of hexagonal BZ for pure and doped ML MoS_2 system Fig.$(4a-4d)$, indicating that the type of band gap is direct in nature. On the other hand,in V doped ML MoS_2,the Fermi energy shifted down to VBM Figs.$(4c)$ and $(4d)$ compared to pure system which also further confirm that p-type of semiconductor behavior of V doped ML MoS_2 system.In addition to this,the spin degeneracy in up state and down state is broken

see Figs.(4c) and (4d) and the system becomes magnetic. Contrary to ML MoS_2 BL MoS_2 and its doped system is characterized by indirect band gap see Figs.4.4($e-h$). The origin of magnetism seems to be,an isolated vanadium(V) atom has a electron configuration Ar ($3d^3 4s^2$) with one electron less than the molybdenum(Mo) atom with electron configuration configuration Ar($4s^2 3d^{10} 4p^6 45s^2 4d^4$), hence substitution of V with Mo introduces deficiency of single electron(hole).Thus hole wave function overlap with nearest neighbor sulfur p-orbitals and Mo d orbitals resulting in calculated magnetic moment of $\sim 1\mu_B$ to system.

4.1.3 Magnetic interaction in monolayer and bilayer MoS_2 doped pair of Vanadium atoms

The magnetic interaction between dopants in doped ML and BL MoS_2 system is studied by calculating the magnetic energy (ΔE), the total energy difference of the two configurations (ferromagnetic (FM) and antiferromagnetic (AFM) at the same impurity separation), as defined in Eq.(3.3) of chapter three. Employing model supercells: $4\times4\times1$ and $3\times3\times1$ with impurity concentrations of 6.25 $\%$ and 11.11 $\%$ respectively up on doping a pair of magnetic impurity atoms (V) on its ML phase and 3.25 $\%$ and 6.25 $\%$ BL phase respectively. Using those model supercells,We have calculated ΔE for four possible impurity configurations: two V dopants in the same layer and nearest neighbor configuration(N),two V dopants in the same layer and second nearest neighbor configuration(NN),two V dopants in the same layer and third nearest neighbor configuration(NNN) and two V dopants in different layers and separated by equilibrium interlayer distance(d0=6.53Å) for Bl phase only. The calculated results for pair of V doped MoS_2 in its ML and BL phases respectively are summarized in tables .(4.2) and .(4.3) .The magnetic energy(Δ E) for the nearest neighbor(N) and third nearest neighbor (NNN) configuration are negative for both ML and BL phases which reveals that ferromagnetic interaction is favorable in agreement with previous report on vanadium(V) doped ML MoS_2 [105].

Table 4.2: Magnetic energy (ΔE) and magnetic moment (μ_m),for V doped ML MoS_2

supercell	distance(d)	impurity(%)	ΔE(eV)	μ_m (μ_B)
$4 \times 4 \times 1$	single	6.25	-	0.98
>>	N	12.5	-0.1247	1.97
>>	NN	12.5	0.00147	1.96
>>	NNN	12.5	-0.0247	1.95
33X1	single	11.11	-	0.81
>>	N	22.22	-0.1462	1.84
>>	NN	22.22	0.0082	1.75

Table 4.3: Magnetic energy (ΔE) and magnetic moment (μ_m),for V doped BL MoS_2

supercell	distance(d)	impurity(%)	Δ E(eV)	μ_m (μ_B)
$4 \times 4 \times 1$	single	3.125		0.96
>>	N	6.25	-0.0958	1.23
>>	up-dn	6.25	0.0065	1.48
$3 \times 3 \times 1$	single	5.55		0.81
>>	N	11.11	-0.131	1.47
>>	NN	11.11	0.029	1.28
>>	NNN	11.11	-0.030	1.47

Whereas,second nearest neighbor configuration (NN) are positive for all cases indicating that antiferromagnetic state is favorable. Therefore, unlike case of Mn doped MoS_2 system the magnetic interaction in V doped ML(BL) MoS_2 osculates from FM to AF depending on distance between a pair of dopants. However,in similar trend with Mn doped system in chapter three, the magnitude of ΔE is decreases with increasing separation (moving from N to NNN). In order to understand the detail about ferromagnetic(FM) interaction between the two nearest neighbor (N) V dopants in ML and BL MoS_2 the total spin polarized density of states (DOS) are plotted for first nearest neighbor(N) impurity configuration Fig.(4*c*) and our calculated result show that the dopants interact ferromagnetically . We further extend investigation by doping pair of magnetic impurities in different layers of BL MoS_2 ,distance between impurities (d0=6.53 Å, see input structure Fig.(4.1*d*), the calculated magnetic energy ΔE = 0.006eV table .(4.3) which indicates that in contrast to

Mn doped BL system,the magnetic ground state for two dopant placed different layer are antiferromagnetic. We further investigate the role of interlayer interaction in BL MoS_2 on its possible magnetic interaction(FM/AF) by making comparison of magnetic energy Δ E of pair of Vanadium(V) doped monolayer(ML) MoS_2 with its corresponding bilayer(BL) using model supercells. The results are also summarized in tables .(4.2) and (4.3) respectively. For instance ,the calculated magnetic energy (ΔE) are -0.1247,and-0.1462 eV for a pair of V doping in first nearest neighbor configurations(N) in $4 \times 4 \times 1$ and $3 \times 3 \times 1$ ML MoS_2 supercells respectively table (4.2). Whereas -0.0958 and -0.131 eV for a pair of Vanadium doping in nearest neighbor configuration(N) in $4 \times 4 \times 1$ and $3 \times 3 \times 1$ BL MoS_2 supercells respectively, table (4.3). Hence,the results show that ferromagnetism is more stable in Vanadium doped monolayer(ML) MoS_2 than BL MoS_2. The origin of discrepancy in magnetic energy,ΔE, seems to be from interlayer interaction in BL MoS_2 . Therefore,we report that interlayer interaction in V doped BL MoS_2 system affects the magnetic interaction between dopants More recently ,similar finding has been reported in iron doped BL MoS_2 [47]. Interestingly,the role of interlayer interaction on magnetic interaction of Mn doped BL MoS_2 are quite different from V doped BL MoS_2 system since the former becomes more ferromagnetic in the presence of interlayer interaction (on going from monolayer to bilayer) whereas the later becomes antiferromagnetic on going from monolayer to bilayer, this makes the physics of system under investigation more interesting. We note that ,this should not be surprised since the magnetic interaction even well studied DMSs are not well understood due to different computing interactions in doped system as mentioned in literature part of this work. Finally, based on Goodenough-Kanamori-Anderson rules discussed in section three,thus bond angle (V-S-V) calculated 85^0 which is closer to 90^0 ensures that ferromagnetic super exchange interaction is primarily responsible for magnetic interaction in nearest neighbor dopants. But also superexchange interaction may stabilize ferromagnetic or antiferromaggnetic ground state for two magnetic dopoants

based on magnetic ion-legand-magnetic ion configurations [101, 102].

4.1.4 Ferromagnetic transition temperature (T_c) for Vanadium doped monolayer and bilayer MoS_2

Curie temperature (T_C) below which the system develops a long-range ferromagnetic ordering are estimated using expression $\frac{3}{2}k_BT_c = -\frac{\Delta E}{N}$,as discussed in chapter three in detail .Using the value Δ E calculated from DFT+U formalism for first nearest neighbor impurity configurations(N) in tables (4.2) and (4.3) and N=2 number of vanadium atom introduced in ML and BL MoS_2 system, we have calculated T_c for monolayer(ML) and bilayer(BL) MoS_2 doped system for different impurity concentrations.The calculated Tc using mean field theory and corrected are summarized in table (4.4),our result reveals that,at high concentration of magnetic impurity (22.22 $\%$) for V doped ML MoS_2 are found to be closer to room temperature. Moreover T_c increases with doping concentrations for both V doped monolayer(ML) and bilayer(BL) phases, indicating that ferromagnetism in this system is tunable by controlling the concentration of magnetic dopants (V).Therefore ,our result endorses that V doped ML and BL MoS_2 other 2D dilute magnetic semiconductors(DMS) for spintronics applications.

Table 4.4: The calculated ferromagnetic transition temperature T_c for pair of V doped ML and BL MoS_2

System	impurity($\%$)	ΔE(eV)	T_c^{MFA}(K)	T_c^{cor}(K)
V doped BL MoS_2	6.25	-0.966	371	187
>>	11.11	-0.131	506	256
V doped ML MoS_2	12.5	-0.125	479	242
>>	22.22	-0.147	564	285

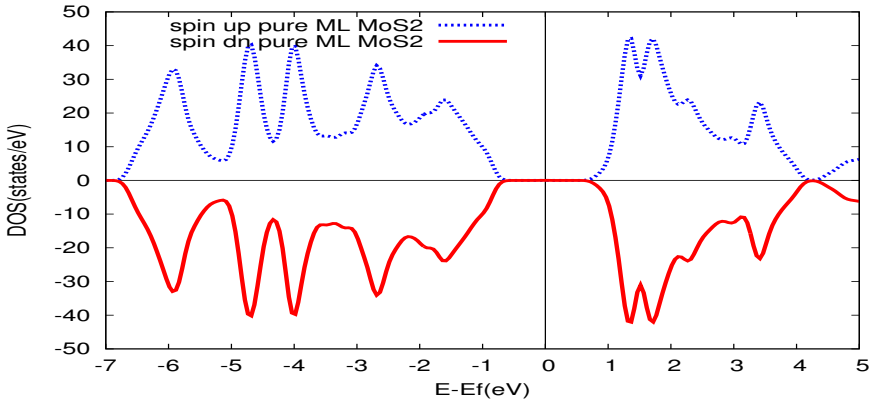

(a)

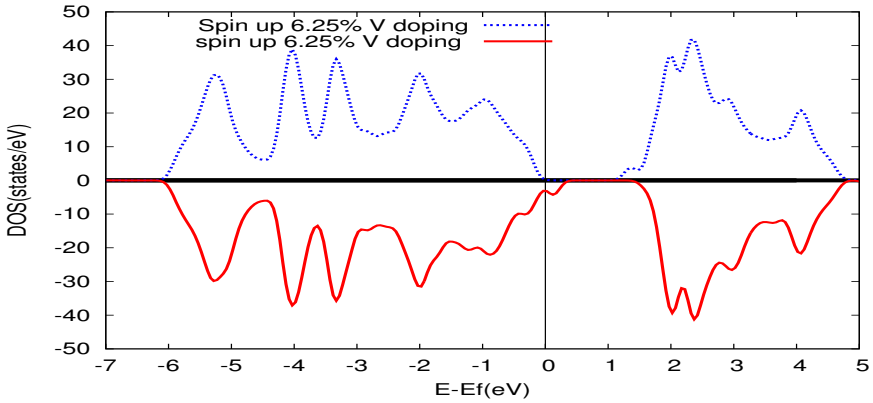

(b)

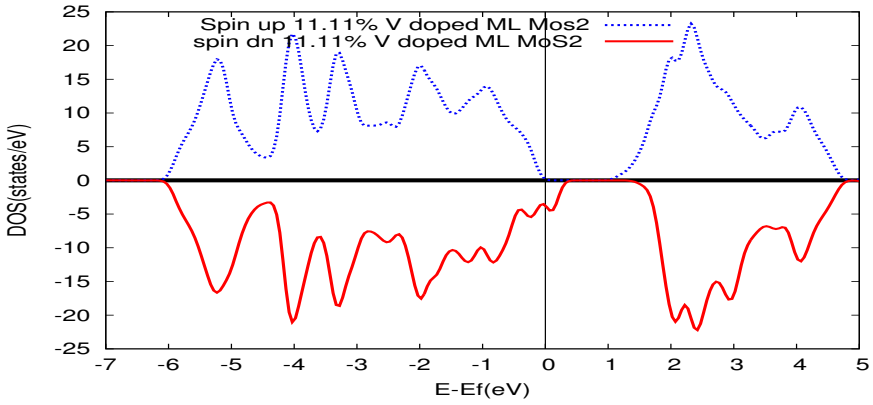

(c)

Fig. 4.2: Spin resolved density of state for $4 \times 4 \times 1$ and $3 \times 3 \times 1$ ML MoS_2: (a) pure ,b)one-V-doped $4 \times 4 \times 1$ ML MoS_2, c) one V-doped $3 \times 3 \times 1$ ML MoS_2 respectively. The blue and red lines represent the spin-up and spin-down components respectively.The zero energy represents the Fermi level.

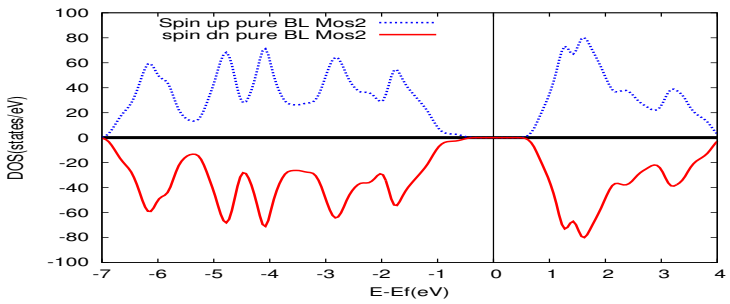

(a)

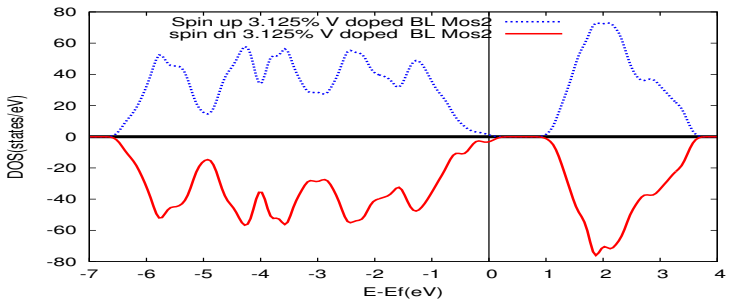

(b)

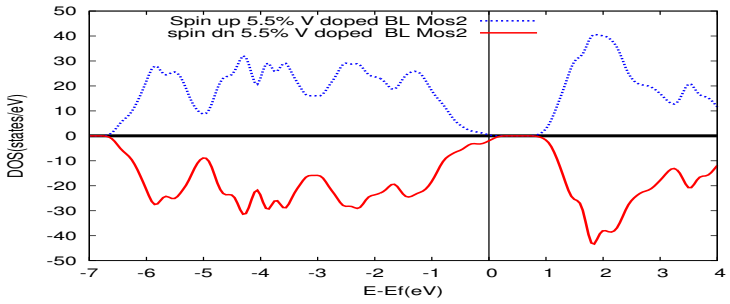

(c)

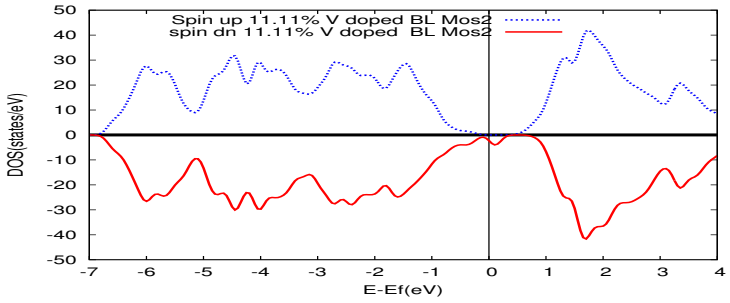

(d)

Fig. 4.3: Spin resolved density of state for $4 \times 4 \times 1$ and $3 \times 3 \times 1$ MoS_2 (BL): (a) pure MoS_2, (b) one-V-doped $4 \times 4 \times 1$ MoS_2 BL , (c) one-V-doped $3 \times 3 \times 1$ BL MoS_2 and (d) two V-doped $3 \times 3 \times 1$ BL MoS_2 respectively. The blue and red lines represent the spin-up and spin-down components, respectively. The zero energy represents the Fermi level.

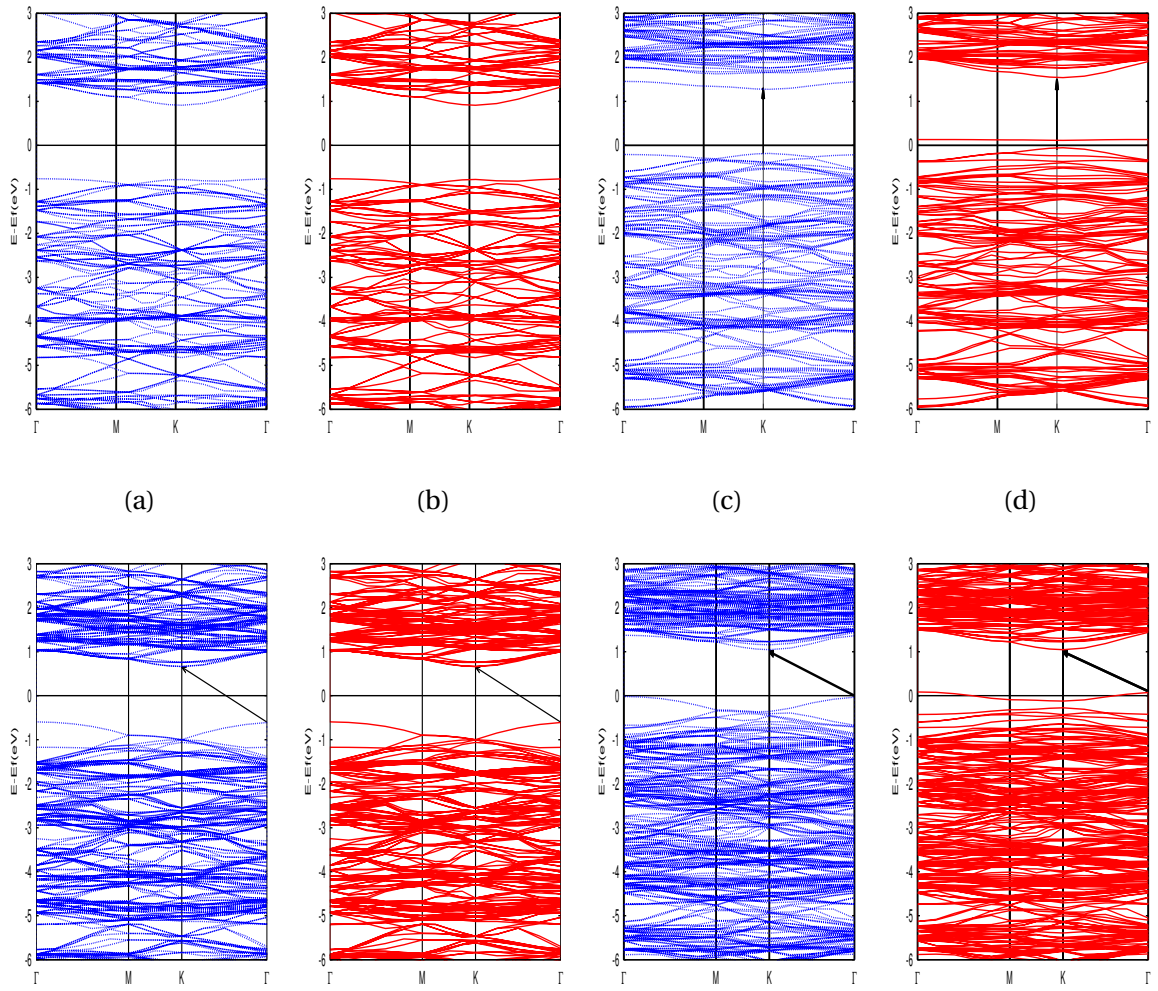

Fig. 4.4: Band structures of $4 \times 4 \times 1$ ML and BL MoS_2 supercell: (a) and (b) pure ML MoS_2, (c) and (d) one-V-doped ML MoS_2 , (e) and (f) pure BL MoS_2, (g) and (h) one-V-doped BL MoS_2 respectively .The blue and red lines represent the spin-up and spin-down components respectively

4.2 Conclusion

In conclusion, we have shown that Vanadium(V) dopant in monolayer(ML) and bilayer(BL) MoS_2 are more energetically favorable to occupy the substitutional lattice site(Mo) both S- and Mo for all impurity configurations.

The injection of vanadium atom in Mo site introduces magnetism and turns semiconductor behavior of host MoS_2 to half metallic nature.

The magnetic interaction between a pair of dopants (V atoms) in doped monolayer and bilayer MoS_2 oscillates from ferromagnet to antiferromagnet depending on the separation between dopants.

We have also found that interlayer interaction in V doped bilayer MoS_2 affects its magnetic properties.The calculated T_c show that,T_c increases with increasing dopant concentration. Based on our result, we suggest Vanadium doped monolayer and bilayer MoS_2 are promising candidates for nearly room temperature 2D dilute magnetic semiconductor for spintronics applications.

5

Valley and Spin Hall effect in doped monolayer MoS_2

5.1 Theoretical Model

We consider effective tight binding model in the vicinity of K^+ and K^- valleys of 2D hexagonal MoS_2 Brillouin zone including spin orbital coupling originate from transition metal element Mo 4d states and the dopant introduced Hamiltonian.In symmetry based three band tight binding(TB) model,the conduction bands are dominated by $4dz^2$,and the valance bands are dominated $4d_{xy}$ and $4dx^2 - y^2$ as shown in Fig.(5.1) .Since three band TB model is enough to capture the band-edge properties in the vicinity of $K^{\pm}$ valleys [85–87] including energy dispersions, Berry curvature as well as Valley Hall and spin Hall conductivity [118]. Therefore,it is convenient to use this model to study desired properties in the vicinity of those valleys.

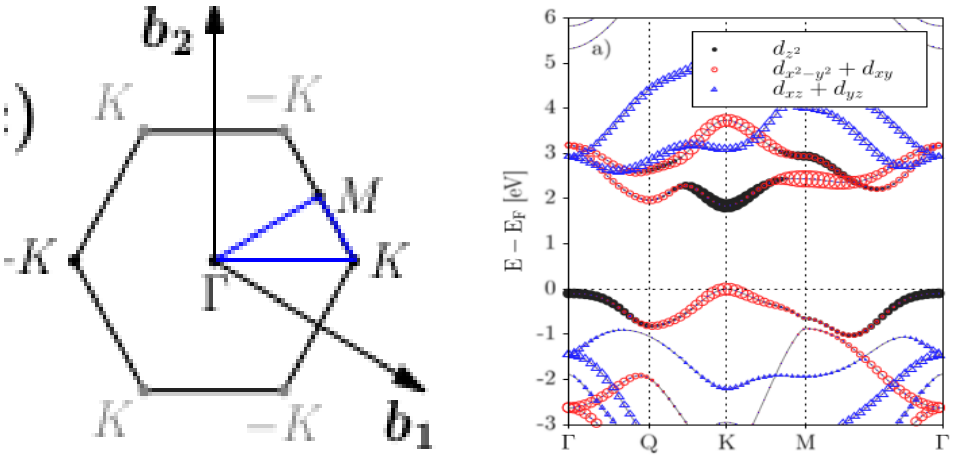

(a) (b)

Fig. 5.1: The color on line: the left panel 2D first Brillouin zone with special k points. b_1 and b_2 are the reciprocal basis vectors. The two inequivalent valleys K and K^- are shown in black and their equivalent counterparts in gray,the right panel atomic orbitals weights in the energy bands of MoS_2

Thus our Hamiltonian is of the form of

$$\hat{H} = \hat{H}_{k.p} + \hat{H}_{So} + \hat{H}^{dop}_{exc}. \tag{5.1}$$

Following [118,119] the low energy effective Hamiltonian in K.P theory of the system reads

$$\hat{H}_{k.p} = at(\nu\tau_x k_x + \tau_y k_y) + \Delta_m \tau_z.$$

and spin-orbital term Hamiltonian can be written as

$$\hat{H}_{so} = \nu\lambda_{so}(1-\tau_z)s_z.$$

whereas special contribution originating from dopant magnetic exchange energy are assumed to be

$$\hat{H}^{dop}_{ex} = -\nu s_z h_{ex}\sigma_z.$$

Here $\hat{H}^{dop}_{exc}$ is magnetic dopant(Mn,V)induced magnetic exchange energy is the energy splitting resulting from exchange interaction between dopants. Thus our approach is based on mean field treatment and magnetization along perpendicular to k_x and k_y plane or along z axis(along the direction of quantization) . Here t and a are first order valence(conduction) band effective hopping and lattice constant for MoS_2 respectively Δ_m and λ_{so} are mass correction for Dirac Hamiltonian and spin-orbit coupling parameter which is also linear in k respectively. Where as $\nu = \pm 1$ designates the value index for $K^{\pm}$,$\tau_{x,y,z}$ and $\sigma_{x,y,z}$ are Pauli matrices in lattice space and spin space respectively. Paul Dirac matrices, $\hat{\sigma}_x$,$\hat{\sigma}_y$ and $\hat{\sigma}_z$ are given by

$$\hat{\sigma}_x = \begin{pmatrix} 0 & 1 \\ 1 & 0 \end{pmatrix}, \qquad \hat{\sigma}_y = \begin{pmatrix} 0 & -i \\ i & 0 \end{pmatrix}, \qquad \hat{\sigma}_z = \begin{pmatrix} 1 & 0 \\ 0 & -1 \end{pmatrix}. \tag{5.2}$$

Upon substitution of Eq.(5.2) into Eq. (5.1),the matrix form of Hamiltonian read,

$$\hat{H}(k) = \begin{pmatrix} \Delta_m - \nu s_z h_{ex} & atk^{\nu}_{-} \\ atk^{\nu}_{+} & \nu s_z(h_{ex} - \lambda_{so}) - \Delta_m \end{pmatrix}. \tag{5.3}$$

where we have introduced short notation $k_{-}^{\nu} = k_x\nu - ik_y$ and its complex conjugate $k_{+}^{\nu} = k_x\nu + ik_y$ .The energy eigen function of Hamiltonian in Eq.(5.3) can be expressed in terms of product of periodic part(Bloch wave) and plane wave as

$$\Psi_p(k) = \frac{1}{\sqrt{A}} exp(ik.r) u_p^v(k), \tag{5.4}$$

where A is area of the two dimensional system and $\frac{1}{\sqrt{A}} exp(ik.r)$ is the plane wave solution corresponding to kinetic (hopping term) of Hamiltonian in Eq.(5.1) and $u_s^{\nu}(k)$ is periodic part of Bloch state can be written as two component way considering spin-resolved form of the wave function as

$$u_p^{\nu}(k) = \begin{pmatrix} c_{ap}(k) \\ \\ c_{bp}(k) \end{pmatrix}, \tag{5.5}$$

where ,cofficient $c_{ap}(k)$ and $c_{bp}(k)$ are determined after solving eigenvalue equation By diagonalizing the Hamiltonian given in Eq. (5.3), we obtain the eigenvalues

$$\zeta_p^{\nu}(k) = -\nu s_z \frac{1}{2}\lambda_{so} + p\sqrt{\left(\Delta_m + \nu\ s_z(\frac{1}{2}\lambda_{so} - h_{ex})\right)^2 + a^2t^2k^2}. \tag{5.6}$$

Here $(p = \pm)$ designates conduction and valence band index respectively. After series of mathematical operation, the corresponding normalized eigenfunctions are obtained as

$$\psi_p^{\nu}(k) = \frac{exp(ik.r)}{W} \begin{pmatrix} at(\nu k_x - i_{ky}) \\ \\ \zeta_p^{\nu}(k) + \nu s_z(h_{ex} - \Delta_m) \end{pmatrix}, \tag{5.7}$$

where

$$W = \sqrt{\left(\nu s_z(h_{ex} - \frac{1}{2}\lambda_{so}) - \Delta_m + pD_{s_z}^{\nu}(k)\right)^2 + a^2t^2k^2}. \tag{5.8}$$

$$D_{s_z}^{\nu}(k) = \sqrt{\left(\Delta_m + \nu s_z(\frac{1}{2}\lambda_{so} - \nu h_{ex})\right)^2 + a^2t^2k^2}. \tag{5.9}$$

Eigen vector in Eq.(5.9) can be rewritten in the terms of phase angle as

$$|\psi_p^{\nu}(k)\rangle = \frac{exp(ik.r)}{W} \begin{pmatrix} ate^{-i\gamma_{\nu}} \\ \\ \zeta_p^{\nu}(k) + \nu s_z(h_{ex} - \Delta_m), \end{pmatrix} \tag{5.10}$$

where Arctan $(\gamma) = \frac{k_y}{\nu k_x}$, which denotes the direction angle of k and its complex conjugate will be

$$\langle\psi_p^\nu(k)|= \frac{exp(-ik.r)}{W}\left(ate^{i\gamma_\nu}, \zeta_p^\nu(k) + \nu s_z(h_{ex} - \Delta_m) \right). \tag{5.11}$$

5.2 Berry potential

The Gauge invariant quantity, Berry potential in momentum space along α, β and γ where α, β and γ designates x,y and z coordinate system respectively were defined in terms of periodic spinor Bloch state and in band n and in parametric space R is defined as [120].

$$\mathbf{A}_n(R) = i\langle n(R)|\bigtriangledown_{\mathbf{R}}|n(R)\rangle \tag{5.12}$$

In Eq.(5.12) $\bigtriangledown_R$ is a short form of notation for $\frac{\partial}{\partial R}$,where R is parameter which characterize the Hamiltonian ,$\langle n(R)|$ and its complex conjugate are periodic part of Bloch state related to lattice periodicity in real crystal. Now, letting wave vector (**k** in the reciprocal-space(Brillouin zone) play the role of the parameter R and using the periodic part of normalized eigen vectors obtained in section (5.1),the Berry potential for doped monolayer MoS_2 along k_x,k_y and k_z where k_x,k_y and k_z designates wave vectors along x,y,z in the vicinity of $K^{\pm}$ valleys

$$A_{p,x}^\nu(k) = i\langle u_p^\nu(k)|\bigtriangledown_{k_x}|u_p^\nu(k)\rangle \tag{5.13}$$

$$A_{p,y}^\nu(k) = i\langle u_p^\nu(k)|\bigtriangledown_{k_y}|u_p^p(k)\rangle \tag{5.14}$$

$$A_{p,z}(k) = i\langle u_p(k)|\bigtriangledown_{k_z}|u_p(k)\rangle \tag{5.15}$$

Where,$\bigtriangledown_{k_x}$, $\bigtriangledown_{k_y}$ and $\bigtriangledown_{k_z}$ are short form of notation for $\frac{\partial}{\partial k_x}$, $\frac{\partial}{\partial k_y}$ and $\frac{\partial}{\partial k_z}$ respectively ,and $|u_p^\nu(k)\rangle$ and $\langle u_p^\nu(k)$ are the periodic part of Eqs.(5.10) and 5.(11) respectively.up on substitution of those Eqs. (5.10) and (5.11) into Eqs.5.(13-15) and after some mathematical manipulation we have obtained that

$$A_{p,x}^\nu = p\frac{\nu a^2t^2(k_x + k_+^\nu)}{\left(\nu s_z(h_{ex} - \frac{1}{2}\lambda_{so})^2 - \Delta_m + pD_{s_z}^\nu(k)\right)^2 + a^2t^2k^2} \tag{5.16}$$

$$A^{\nu}_{p,y} = -\frac{a^2t^2(pk_y - ik^{\nu}_{+})}{\left(\nu s_z(h_{ex} - \frac{1}{2}\lambda_{so})^2 - \Delta_m + pD^{\nu}_{s_z}(k)\right)^2 + a^2t^2k^2} \tag{5.17}$$

and $A_z = 0$,since we are considering 2D case ,the wave function $\langle u_s(k)|$ and $|u_s(k)\rangle$ are independent of wave vector along z (k_z)

5.2.1 Berry curvature in the vicinity of K^- and K^+ Valleys of doped Monolayer MoS_2

The general expression for Berry curvature ,analogical with real space magnetic field(B),along e_γ or along perpendicular to α and β plane is found to be

$$\vec{\Omega}^{n}_{\alpha,\beta} = -2Im\sum_{m\neq n}\frac{\langle u_n(k)|\nabla_\alpha\hat{H}(k)|u_m(k)\rangle\langle u_m(k)|\nabla_\beta\hat{H}(k)|u_n(k)\rangle}{(\varepsilon_{mk} - \varepsilon_{nk})^2}e_\gamma. \tag{5.18}$$

For detail derivation see **appendix A.1** of this dissertation.

Eq.(5.18) is general expression for K-space Berry curvature in 2D system. Now facilitating this expression to Berry curvature along z-axis(meaning carriers lied in x and y plane of hexagonal lattice, whose spin polarization is along z axis),for transitions metal(TM) doped MoS_2 in the vicinity of K^- and K^+ hexagonal Brillouin zone (BZ) using eigenvalues and eigenvectors obtained so far in section 5.1. Therefore,making transformation, $\epsilon_{nk} - \epsilon_{mk} \rightarrow \zeta^{\nu}_{+}(k) - \zeta^{\nu}_{-}(k), \nabla_\alpha \longrightarrow \frac{\partial}{\partial kx}$ and $\nabla_\beta \longrightarrow \frac{\partial}{\partial ky}$ using those variable changes in Eq.(5.18) we shall rewrite Berry curvature for upper band,CBM, and VBM in the vicinity of K^- and K^+ valleys as

$$\Omega^{\nu}_{x,y}(z) = -2Im\frac{\langle u^{\nu}_{+}(k)|\frac{\partial}{\partial kx}(\hat{H}(k))|u^{\nu}_{-}(k)\rangle\langle u^{\nu}_{-}(k)|\frac{\partial}{\partial ky}(\hat{H}(k))|u^{\nu}_{+}(k)\rangle}{(\zeta^{\nu}_{+}(k) - \zeta^{\nu}_{-}(k))^2}e_z. \tag{5.19}$$

using orthogonality relation we can have $|u^{\nu}_{+}(k)\rangle\langle u^{\nu}_{+}(k)| = |u^{\nu}_{-}(k)\rangle\langle u^{\nu}_{-}(k)| = 1$ from Eq.(5.19) and rewrite it as spin splited form,

$$\Omega^{\nu}_{+}(z) = -2Im\frac{\langle u^{\nu}_{+}(k)|\frac{\partial}{\partial kx}\hat{H}(k)\frac{\partial}{\partial ky}\hat{H}(k)|u^{\nu}_{+}(k)\rangle}{(\zeta^{\nu}_{+}(k) - \zeta^{\nu}_{-}(k))^2}e_z. \tag{5.20}$$

$$\Omega^{\nu}_{-}(z) = -2Im\frac{\langle u^{\nu}_{-}(k)|\frac{\partial}{\partial kx}\hat{H}(k)\frac{\partial}{\partial ky}\hat{H}(k)|u^{\nu}_{-}(k)\rangle}{(\zeta^{\nu}_{-}(k) - \zeta^{\nu}_{+}(k))^2}e_z. \tag{5.21}$$

The velocity operator along x,y and z can be obtained either using $\hat{v}_{x,y,z} = \frac{1}{i\hbar}[r, H]$ or using the relation between wave vector dependent Hamiltonian $(\hat{H}(k))$ and momentum operator $(\hat{p})$ as, $\hat{v}_{x,y,z} = \frac{\partial\hat{H}(k)}{\partial\hat{p}} = \frac{\partial\hat{H}(k)}{\hbar\partial\hat{k_{x,y,z}}}$ and using the model Hamiltonian in

Eq.(5.1) x,y components of velocity operators obtained as

$$\hat{v}_x = \frac{\partial \hat{H}(k)}{\hbar \partial \hat{k}} = \nu \frac{1}{\hbar} at \hat{\tau}_x \tag{5.22}$$

$$\hat{v}_y = \frac{\partial \hat{H}(k)}{\hbar \partial \hat{k}} = \frac{1}{\hbar} at \hat{\tau}_y \tag{5.23}$$

Substituting Eqs.(5.22 and 5.23) into Eq.(5.19) together with simple manipulation ,yields the Berry curvature for upper and lower band ($\pm$) as,

$$\Omega^{\pm}_{x,y} = \mp \frac{\nu a^2 t^2}{\hbar^2 D^2_{s_z \nu}} e_z, \tag{5.24}$$

where $D^{\nu}_{s_z}(k) = \sqrt{\left(\Delta_m + \nu s_z(\frac{1}{2}\upsilon\lambda_{so} - h_{ex})\right)^2 + a^2t^2k^2}$. In Eq.(5.24) e_z is unit vector along Z axis, to obtain the expression e_z explicitly ,we introduce three dimensional unit vector along x,y and z in two dimensional plane in k space in terms of eigenvalues as follows

$$\hat{n}(k) = \{\frac{\nu a t k_x}{D^{\nu}_{s_z}(k)}, \frac{a t k_y}{D^{\nu}_{s_z}(k)}, \frac{\Delta_m + s_z \nu(\frac{1}{2}\lambda_{so} - h_{ex})}{D^{\nu}_{s_z}(k)}\}. \tag{5.25}$$

Using Eqs.(5.25) into Eq.(5.24), we found

$$\Omega^{p}_{\nu}(z) = -p\nu \frac{a^2t^2(\Delta_m + \nu s_z(\frac{1}{2}\lambda_{so} - h_{ex})}{2D^{\nu}_{s_z}(k)^3}. \tag{5.26}$$

Wher $p = \pm 1$,p=1 for conduction band curvature and p=-1 for valnce band curvature.In the same valley, the Berry curvature is dependent on spin through the spin-dependent band gap:$(\Delta_m + s_z(\nu\frac{1}{2}\lambda_{so} - \nu M), s_z = +$ for spin up electrons(holes) and $s_z = -1$ for spin down electrons(holes).

5.3 The Kubo formula and Anomalous Hall Conductivity

Starting from linear response theory,the most general form of Quantum Kubo formula for current-Current correlated system is found to be

$$\sigma_{\mu v}(q, \varpi)) = \frac{i\hbar}{V^d} \sum_{n,m} \left\langle \frac{f(E_n) - f(E_m)}{(E_n - E_m)(E_n - E_m + \hbar(\omega + i\eta)} J^{nm}_{\mu}(q) J^{mn}_{v}(-q) \right\rangle_c. \tag{5.27}$$

for detail derivation see **appendix B**. Where,$\langle\rangle_C$ impurity averaging. However,the anomalous Hall conductivity related with Berry phase(curvature) is believed to be

intrinsic properties of carriers due to spin-orbit (SO) interaction and magnetic texture in system under the consideration. Therefore,at low impurity concentration(dilute limit)impurity averaging (disorder effect is not considerable here).Hence it is convenient to remove impurity varying from expression (5.27) and rewrite it as ,

$$\vec{\sigma}_{\alpha,\beta}(\omega) = \frac{lim}{\eta \to 0^+} \frac{\hbar}{V^d} \sum_n \sum_m \frac{(f_n - f_m)}{\epsilon_m - \epsilon_n} . Im \frac{\langle n|\hat{J}_\alpha|m\rangle\langle m|\hat{J}_\beta|n\rangle}{(\varepsilon_n - \varepsilon_m) + \hbar(\omega + i\eta)}. \tag{5.28}$$

Here,V is volume of system,d is the dimensionality $|n\rangle$is basis of eigenvectors of the one particle Hamiltonian $\hat{H}$ of eigenvalues ϵ_n i.e $\hat{H}|n\rangle = \epsilon_n|n\rangle, f_n$ and f_m are Fermi Dirac distribution function respectively given by $f_n = \frac{1}{1+exp(\frac{\varepsilon_n - \mu}{K_B T})}$ and$f_m = \frac{1}{1+exp(\frac{\varepsilon_m - \mu}{K_B T})}$,$\hat{J}_\alpha$ and $\hat{J}_\beta$ are single particle current operators given by $\hat{J}_\alpha = q\hat{v}_\alpha$ and $\hat{J}_\beta = q\hat{v}_\beta$.

Now we specialize Eq.(5.28),for system of two dimensional spin polarized monolayer(ML) MoS_2 DMSs subjected to spin-orbit coupling resulted from TM (Mo atom) and exchange field (h_{ex}) introduced by substitution of Mo atom by magnetic dopant (Mn,V). a particular,we employ the following variables change $_n \to f_{\zeta^\nu_+(k)}$ and $f_m \to f_{\zeta^\nu_-(k)}$, $\langle n| \longrightarrow \langle\psi^\nu_{+,k'}|$ and $|m\rangle \to \psi^\nu_{-,k'}\rangle$ .In addition to this, for clean sample making $\eta = 0$ and static limit ($\omega = 0$) Eq.(5.28) can be rewritten as,

$$\vec{\sigma}_{\alpha,\beta} = \frac{\hbar q^2}{V^d} \sum_{kk'} \sum_{n \neq m} (f_{\zeta^\nu_+(k)} - f_{\zeta^\nu_-(k')}) . Im \frac{\langle\psi^\nu_{+,k'}|\hat{v}_\alpha|\psi^\nu_{-,k}\rangle\langle\psi^\nu_{-,k}|\hat{v}_\beta|\psi^\nu_{+,k'}\rangle}{(\zeta^\nu_-(k) - \zeta^\nu_+(k))^2}. \tag{5.29}$$

After mathematical operation together with simplification for $k = k'$, Eq.(5.29) will be rewritten in terms of periodic part of wave function as

$$\sigma_{\alpha,\beta} = \frac{q^2}{\hbar V^d} \sum_k (f_{\epsilon_{km}} - f_{\epsilon_{kn}}) . \left(Im \sum_{n \neq m} \frac{\langle u_{nk}|\nabla_\alpha \hat{H}(k)|u_{km}\rangle\langle u_{mk}|\nabla_\beta \hat{H}(k)|u_{nk}\rangle}{(\varepsilon_{km} - \varepsilon_{kn})^2} \right) \tag{5.30}$$

Therefore,z components of Anomalous Hall conductivity can be written in terms of unit vector along e_z as

$$\sigma^\nu_{x,y}(z) = \frac{q^2}{\hbar V^d} \sum_k (f_{\zeta^\nu_-(k)} - f_{\zeta^\nu_+(k)}) . \left(Im \sum_{+\neq-} \frac{\langle u^\nu_{+k}|\nabla_x \hat{H}(k)|u^\nu_{k-}\rangle\langle u^\nu_{-,k}|\nabla_y \hat{H}(k)|u^\nu_{+k}\rangle}{(\zeta^\nu_-(k) - \zeta^\nu_+(k))^2} \right) e_z \tag{5.31}$$

On account of Eq.(5.19),right side of Eq.(5.31) inside the bracket gives $(-\frac{\Omega^n(\gamma)}{2})$ .Thus Eq.(5.31) becomes,

$$\sigma^p_\nu(z) = -\frac{q^2}{2\hbar V}\sum_k (f_{(\zeta_{k_-})} - f_{(\zeta_{k_+})})\Omega^p_\nu(z) \tag{5.32}$$

This recovers the conductance formula in terms of the Berry curvature,the intrinsic Anomalous Hall conductance is sum of Berry curvature of all occupied states .Here after we replace the band idices n via $\pm = p$ which designates conduction/valance band respectively in the vicinity of $K^+$and K^- valleys indexed by ν .Eq. (5.32) rewritten as both spin and Valley split form:

$$\sigma^p_{AHC}(z) = \frac{q^2}{2\hbar V}\sum_k (f_{(\zeta_{k_+})} - f_{(\zeta_{k_-})}\Omega^p_{\nu S_z}(z)). \tag{5.33}$$

Considering the presence of many atoms in system under consideration (continuous limit) it is convenient to replace summation in Eq.(5.33) into integration

$$\sum_k \to V^D \int \frac{d^D k}{(2\pi)^D} \tag{5.34}$$

For 2D case

$$\sum_k \to V^2 \int \frac{d^2 k}{(2\pi)^2} \tag{5.35}$$

Using Eq.(5.35) into Eq.(5.33) and Considering spherical symmetry in which carriers propagating d^2k can be rewritten as $d^2k = \int_o^{2\pi} d\phi \int kdk = 4\pi \int kdk$,thus Eq.(5.33) becomes

$$\sigma^p_{AHC} = \frac{q^2}{2h}\int (f_{(\zeta_{k_+})} - f_{(\zeta_{k_-})}\Omega^p_{\nu s_z}(z))kdk \tag{5.36}$$

5.4 Spin and valley Hall Conductivity

Following [118] spin Hall conductivity and valley Hall conductivity can be defined by

$$\sigma^{spin}(z) = \sum_\nu (\sigma(\nu,\uparrow) - \sigma(\nu,\downarrow) \tag{5.37}$$

$$\sigma^{valley}(z) = \sum_{s_z} (\sigma(\nu = +, s_z) - \sigma(\nu = -1, s_z) \tag{5.38}$$

After rearranging we shall obtain

$$\sigma^{spin}(z) = ((\sigma^{+}_{\uparrow}(z) - \sigma^{+}_{\downarrow}(z)) + ((\sigma^{-}_{\uparrow}(z) - \sigma^{-}_{\downarrow}(z)). \tag{5.39}$$

$$\sigma^{valley}(z) = ((\sigma^{+}_{\uparrow}(z) + \sigma^{+}_{\downarrow}(z)) - ((\sigma^{-}_{\uparrow}(z) + \sigma^{-}_{\downarrow}(z)). \tag{5.40}$$

Where $\pm$ designates short notation for K^+ and K^- valleys respectively and both spin and valley split form of anomalous Hall conductivity, ,$\sigma^{\pm}_{\uparrow,\downarrow}$,are evaluated by making use of Eq.(5.36). To calculate total valley and spin Hall conductivity using Eqs.(5.39) and (5.40) together with Eq.(5.36), we have considered different limiting cases based on temperature dependence and state occupancy based Fermi Dirac distribution function.

5.4.1 Spin and Valley Hall conductivity in ML MoS_2 when Fermi level is in the gap

At absolute zero,T=0K, in undoped ML MoS_2 system all electron states below the Fermi level will contribute (i.e.,it is a Fermi sea property)to Anomalous Hall conductivity and we can assume that the upper band is empty,since the system is gaped,the temperature is null and Fermi energy μ lies in the gap. Therefore,in this limit it is convenient to use the following logical approximation for $f_{(\zeta_{k_\pm})}$ entering in Eq.(5.36) as, $\zeta_{k+} >> \epsilon_F$ and $\zeta_{k-} << \epsilon_F$

For upper band $\zeta_{k+} >> \epsilon_F$

$$f(E_{k+}) = \frac{1}{1 + exp\beta(\zeta_{k+} - \epsilon_F)}$$
$$f(\zeta_{k+}) = \frac{1}{1 + e^{\infty}} = 0 \tag{5.41}$$

For lower occupied band $\zeta_{k-} << \epsilon_F$

$$f(\zeta_{k-}) = \frac{1}{1 + exp\beta(E_{k-} - \epsilon_F)}$$
$$f(\zeta_{k-}) = \frac{1}{1 + e^{-}\infty)} = 1 \tag{5.42}$$

Therefore,using Eqs.(5.41) and (5.42) into Eq.(5.36) ,$\vec{\sigma}_{AH}(z)$

$$\sigma^{p}_{\nu}(z) = -\frac{q^2}{2h}\int \Omega^{p}_{\nu s_z}(z) k dk \tag{5.43}$$

Now up on substituting Eq.(5.26) into Eq.(5.43),we have

$$\sigma_{\nu}^{p}(z)=\frac{p\nu q^{2}}{2h}(\Delta_{m}+\nu s_{z}(\frac{1}{2}\lambda_{so}-h_{ex}))\int_{0}^{\infty}\frac{a^{2}t^{2}kdk}{2\Bigg((\Delta_{m}+\nu s_{z}(\frac{1}{2}\upsilon\lambda_{so}-h_{ex}))^{2}+a^{2}t^{2}k^{2}\Bigg)^{\frac{3}{2}}}. \tag{5.44}$$

Anomalous Hall conductivity in the vicinity of K^{+} valleys in occupied valance band ,for spin up electrons(holes) $\sigma_{\uparrow}^{+}$ can be calculated using $\nu=1$,p=-1,$s_{z}=1$ in Eq. (5.44)

$$\sigma_{\uparrow}^{+}(z)=-\frac{q^{2}}{2h}(\Delta_{m}+(\frac{1}{2}\lambda_{so}-h_{ex})\int_{0}^{\infty}\frac{a^{2}t^{2}kdk}{2\Bigg((\Delta_{m}+(\frac{1}{2}\lambda_{so}-h_{ex}))^{2}+a^{2}t^{2}k^{2}\Bigg)^{\frac{3}{2}}}. \tag{5.45}$$

letting $u=(\Delta_{m}+\frac{1}{2}\upsilon\lambda_{so}-h_{ex})^{2}+a^{2}t^{2}k^{2}$ and $du=2a^{2}t^{2}kdk$,integral in Eq.(5.45) evaluated to give,

$$\sigma_{\uparrow}^{+}(z)=+\frac{q^{2}}{h}(\Delta_{m}+(\frac{1}{2}\lambda_{so}-h_{ex})\Bigg(\frac{1}{\sqrt{u(\infty)}}-\frac{1}{\sqrt{u(0)}}\Bigg),$$

$$\sigma_{\uparrow}^{+}(z)=-\frac{q^{2}}{h}\Bigg(\frac{(\Delta_{m}+(\frac{1}{2}\lambda_{so}-h_{ex})}{\sqrt{u(0)}}\Bigg),$$

$$\Rightarrow\sigma_{\uparrow}^{+}(z)=-\frac{q^{2}}{h}, \tag{5.46}$$

whereas,substitution of $\nu=1$,p=-1,$s_{z}=-1$ into eq.(5.44) and after similar mathematical manipulation expression for $\sigma_{\downarrow}^{+}(z)$ obtained as

$$\Rightarrow\sigma_{\downarrow}^{+}(z)=-\frac{q^{2}}{h}. \tag{5.47}$$

Similarly anomalous Hall conductivity in the vicinity of K^{-} valleys in occupied valance band ,for spin up and spin down electrons(holes) $\sigma_{\uparrow(\downarrow)}^{-}$ respectively can be calculated by substituting $\nu=-$,p=-1,$s_{z}=\pm1$ in eq. (5.44) and after straight forward algebra

$$\sigma_{\uparrow}^{-}(z)=\frac{q^{2}}{h}. \tag{5.48}$$

$$\sigma_{\downarrow}^{-}(z)=\frac{q^{2}}{h}, \tag{5.49}$$

spin Hall conductivity and Valley Hall conductivity respectively are obtained by substituting Eqs.(5.46-5.49) into Eq.(5.39) and Eq.(5.40)

$$\sigma^{spin}(z)=0. \tag{5.50}$$

$$\sigma^{valley}(z) = -4\frac{q^2}{h}. \tag{5.51}$$

5.4.2 Spin and Valley Hall conductivity in Mn doped ML MoS_2 at T=0

From DFT result we have found that Mn doped ML MoS_2 the Fermi level shift to conduction band .Therefore,in this limit both spin hall and valley hall conductivity should be calculated by taking consideration of both occupied band from ($-\infty$ to 0 plus the conduction band until (ϵ_F) or (k_F).Hence in this limit Eq.(5.36) rewritten as

,

$$\sigma^p_{AHC}(z) = \frac{q^2}{2\hbar V}\sum_{-\infty<k<0}(f_{(\zeta_{k_+})}\Omega^p_{\nu S_z}(z) - \sum_{0<K_F}(f_{(\zeta_{k_-})}\Omega^p_{\nu S_z}(z). \tag{5.52}$$

Using Eqs.(5.41) and (5.69) and after transforming summation into integration

$$\sigma^p_{AHC}(z) = \frac{q^2}{2h}\int_{-\infty}^{0}\Omega^p_{\nu S_z}(z) - \int_0^{k_F}\Omega^p_{\nu S_z}(z) \tag{5.53}$$

substituting Eq.(5.26) into Eq.(5.53) yields

$$\sigma^p_{\nu s_z}(z) = -\frac{p\nu q^2}{2h}(\Delta_m + \nu s_z(\frac{1}{2}\lambda_{so} - h_{ex})\int_{-\infty}^{0}\frac{a^2t^2kdk}{2\Big((\Delta_m + \nu s_z(\frac{1}{2}\lambda_{so} - h_{ex}))^2 + a^2t^2k^2\Big)^{\frac{3}{2}}}$$

$$+\frac{p\nu q^2}{2h}(\Delta_m + \nu s_z(\frac{1}{2}\lambda_{so} - h_{ex})\int_0^{k_F}\frac{a^2t^2kdk}{2\Big((\Delta_m + \nu s_z(\frac{1}{2}\lambda_{so} - h_{ex}))^2 + a^2t^2k^2\Big)^{\frac{3}{2}}}. \tag{5.54}$$

Hence for Mn-doped ML MoS_2 (n-doped) $\sigma^+_\uparrow(z), \sigma^+_\downarrow(z), \sigma^-_\uparrow(z)$ and $\sigma^-_\downarrow(z)$ are evaluated by varying the values of ν and s_z in Eq.(5.54). To evaluate $\sigma^+_\uparrow$ from Eq.(5.54) we use $\nu = 1, s_z = 1$,p=-1 for the first term and p=1 for the second part

$$\sigma^+_\uparrow(z) = \frac{q^2}{2h}(\Delta_m + \frac{1}{2}\lambda_{so} - h_{ex})\int_{-\infty}^{0}\frac{a^2t^2kdk}{2\Big((\Delta_m + \frac{1}{2}\lambda_{so} - h_{ex})^2 + a^2t^2k^2\Big)^{\frac{3}{2}}}$$

$$+\frac{q^2}{2h}(\Delta_m + \frac{1}{2}\lambda_{so} - h_{ex})\int_0^{k_F}\frac{a^2t^2kdk}{2\Big((\Delta_m + (\frac{1}{2}\lambda_{so} - h_{ex})^2 + a^2t^2k^2\Big)^{\frac{3}{2}}}. \tag{5.55}$$

letting $u = (\Delta_m + (\frac{1}{2}\lambda_{so} - h_{ex})^2 + a^2t^2k^2$ and $du = 2a^2t^2kdk$,integral in Eq.(5.57) yields

$$\sigma^+_\uparrow(z) = -\frac{q^2}{h}\Delta_m + \frac{1}{2}\lambda_{so} - h_{ex}\Big(\frac{1}{\sqrt{u(0)}} - \frac{1}{\sqrt{u(-\infty)}} + \frac{1}{\sqrt{u(k_F)}} - \frac{1}{\sqrt{u(0)}}\Big).$$

$$= -\frac{q^2}{h}\left(\frac{\Delta_m + \frac{1}{2}\lambda_{so} - h_{ex}}{\sqrt{u(k_F)}}\right).$$

$$\Rightarrow \sigma_{\uparrow}^{+}(z) = -\frac{q^2}{h}\frac{\Delta_m + \frac{1}{2}\lambda_{so} - h_{ex}}{\sqrt{(\Delta_m + \frac{1}{2}\lambda_{so} - h_{ex})^2 + a^2t^2k_F^2}}. \tag{5.56}$$

Similarly substitution of $\nu = 1, s_z = -1$,results expression for spin down electrons in in the vicinity of K^+ valleys as

$$\sigma_{\downarrow}^{+}(z) = \frac{q^2}{2h}\Delta_m - \frac{1}{2}h_{ex} - \lambda_{so})\int_{-\infty}^{0}\frac{a^2t^2kdk}{2\left((\Delta_m - (\frac{1}{2}h_{ex} - \lambda_{so}))^2 + a^2t^2k^2\right)^{\frac{3}{2}}}$$

$$+ \frac{q^2}{2h}(\Delta_m + \frac{1}{2}\lambda_{so} - h_{ex})\int_{0}^{k_F}\frac{a^2t^2kdk}{2\left((\Delta_m + \frac{1}{2}\lambda_{so} - h_{ex}))^2 + a^2t^2k^2\right)^{\frac{3}{2}}} \tag{5.57}$$

letting $u = (\Delta_m + h_{ex} - \frac{1}{2}\lambda_{so})^2 + a^2t^2k^2$ and $du = 2a^2t^2kdk$ integral in eq.(5.55) yields

$$\sigma_{\downarrow}^{+}(z) = -\frac{q^2}{h}(\Delta_m + h_{ex} - \frac{1}{2}\lambda_{so})\left(\frac{1}{\sqrt{u(0)}} - \frac{1}{\sqrt{u(-\infty)}} + \frac{1}{\sqrt{u(k_F)}} - \frac{1}{\sqrt{u(0)}}\right)$$

$$= -\frac{q^2}{h}\left(\frac{(\Delta_m + h_{ex} - \frac{1}{2}\lambda_{so})}{\sqrt{u(k_F)}}\right)$$

$$\Rightarrow \sigma_{\downarrow}^{+}(z) = -\frac{q^2}{h}\frac{(\Delta_m + h_{ex} - \frac{1}{2}\lambda_{so})}{\sqrt{(\Delta_m + h_{ex} - \frac{1}{2}\lambda_{so})^2 + a^2t^2k_F^2}}. \tag{5.58}$$

Following the same procedure ,$\sigma_{\uparrow}^{-}(z)$ and $\sigma_{\downarrow}^{-}(z)$ are found to be,

$$\sigma_{\uparrow}^{-}(z) = \frac{q^2}{h}\frac{(\Delta_m + h_{ex} - \frac{1}{2}\lambda_{so})}{\sqrt{(\Delta_m + h_{ex} - \frac{1}{2}\lambda_{so})^2 + a^2t^2k_F^2}}. \tag{5.59}$$

$$\sigma_{\downarrow}^{-}(z) = \frac{q^2}{h}\frac{(\Delta_m + \frac{1}{2}\lambda_{so} - h_{ex})}{\sqrt{(\Delta_m + \frac{1}{2}\lambda_{so} - h_{ex})^2 + a^2t^2k_F^2}}. \tag{5.60}$$

Spin Hall conductivities for the Fermi level in the conduction band at zero temperature can be obtained as by substituting Eqs.(5.56-5.60)) into Eq.(5.39)

$$\sigma^{spin}(z) = -\frac{q^2}{h}\left(\frac{\Delta_m + \frac{1}{2}\lambda_{so} - h_{ex}}{\sqrt{(\Delta_m + \frac{1}{2}\lambda_{so} - h_{ex})^2 + a^2t^2k_F^2}} - \frac{(\Delta_m + h_{ex} - \frac{1}{2}\lambda_{so})}{\sqrt{(\Delta_m + h_{ex} - \frac{1}{2}\lambda_{so})^2 + a^2t^2k_F^2}}\right).$$

$$+ \frac{q^2}{h}\left(\frac{(\Delta_m + h_{ex} - \frac{1}{2}\lambda_{so})}{\sqrt{(\Delta_m + h_{ex} - \frac{1}{2}\lambda_{so})^2 + a^2t^2k_F^2}} - \frac{(\Delta_m + \frac{1}{2}\lambda_{so} - h_{ex})}{\sqrt{(\Delta_m + \frac{1}{2}\lambda_{so} - h_{ex})^2 + a^2t^2k_F^2}}\right) \tag{5.61}$$

which can be rewritten as more compact form,

$$\sigma^{spin}(z) = \frac{2q^2}{h}\left(\frac{(\Delta_m + h_{ex} - \frac{1}{2}\lambda_{so})}{\sqrt{(\Delta_m + h_{ex} - \frac{1}{2}\lambda_{so})^2 + a^2t^2k_F^2}} - \frac{\Delta_m + \frac{1}{2}\lambda_{so} - h_{ex}}{\sqrt{(\Delta_m + \frac{1}{2}\lambda_{so} - h_{ex})^2 + a^2t^2k_F^2}}\right). \tag{5.62}$$

Finally Valley Hall conductivity can be calculated by making use of those Eqs.(5.56-5.60) into Eq.(40),

$$\sigma^{valley}(z) = -\frac{q^2}{h}\left(\frac{\Delta_m + \frac{1}{2}\lambda_{so} - h_{ex}}{\sqrt{(\Delta_m + \frac{1}{2}\lambda_{so} - h_{ex})^2 + a^2t^2k_F^2}} + \frac{(\Delta_m + h_{ex} - \frac{1}{2}\lambda_{so})}{\sqrt{(\Delta_m + h_{ex} - \frac{1}{2}\lambda_{so})^2 + a^2t^2k_F^2}}\right).$$
$$-\frac{q^2}{h}\left(\frac{(\Delta_m + h_{ex} - \frac{1}{2}\lambda_{so})}{\sqrt{(\Delta_m + h_{ex} - \frac{1}{2}\lambda_{so})^2 + a^2t^2k_F^2}} + \frac{(\Delta_m + \frac{1}{2}\lambda_{so} - h_{ex})}{\sqrt{(\Delta_m + \frac{1}{2}\lambda_{so} - h_{ex})^2 + a^2t^2k_F^2}}\right)$$

After rearranging we have,

$$\sigma^{valley}(z) = -\frac{2q^2}{h}\left(\frac{(\Delta_m + h_{ex} - \frac{1}{2}\lambda_{so})}{\sqrt{(\Delta_m + h_{ex} - \frac{1}{2}\lambda_{so})^2 + a^2t^2k_F^2}} + \frac{\Delta_m + \frac{1}{2}\lambda_{so} - h_{ex}}{\sqrt{(\Delta_m + \frac{1}{2}\lambda_{so} - h_{ex})^2 + a^2t^2k_F^2}}\right). \tag{5.63}$$

5.5 Discussion

First, we discuss the energy eigenvalues obtained in Eq. (5.7) for the $K^{\pm}$ point to explore the effect of dopant introduced magnetic exchange field(h_{ex}) on low energy band structure. The energy is plotted as a function of dimensionless wave number ($\frac{ka}{\pi}$) in Fig. (5.2). In Figs. (5.2a) and (5.2b), we found that for zero spin-orbital coupling (lo=0) and zero dopant introduced exchange field (h_{ex}=0),both bands (K^+ and K^-) valleys are degenerate. On the other hand,for nonzero spin-orbit coupling and zero exchange field Fig.(4c) and (4b),conduction band K^+ point eigenvalues are identical to those of the K^- point if spin up and down are exchanged but the degeneracy in valence band hole state in K^+ and K^- valleys are lifted due to spin-orbital coupling resulting from transition metal(Mo) orbitals. However,for finite spin-orbit coupling(lo) and finite dopant introduced exchange field degeneracy in both valance band holes and conduction band electrons in valley K^+ and K^- are lifted a seen in Figs. (5.2e) and (5.2f). Moreover,to understand the role of dopant introduced magnetic exchange field (h_{ex}) on momentum space Berry curvature,we

have plotted the Berry curvature as function of wave number ($\frac{ka}{\pi}$) in the vicinity of K^+ and K^- valleys for spining up holes in valence band Fig. (5.3) ,enhancement of curvature with rise in dopant introduce exchange field(0 to 0.16 eV) for state in the vicinity K^+ valleys are observed Fig.(5.3a),since Berry curvature is related with both spin hall and Valley hall through relation Eq. (5.36). Therefore, the spin and valley Hall conductivity expected to increase with dopant introduced exchange field for state in the vicinity of K^+ valleys. In contrast with Berry curvature for state in the vicinity of K^+ valley,the Berry curvature of state in the vicinity of K^- valley suppress with rise in dopant introduced exchange field (0 to 0.16eV). Therefore, the degeneracy of curvature in K^+ and K^- are lifted under dopant introduced magnetic exchange field in other words unequal number of spin up states are accumulated in K^+ and K^- curvature. Employing the Kubo linear response theorem within the low-energy effective model, we have investigated the Berry curvature mediated spin Hall and valley Hall conductivities (effect),in which electrons from different valleys (the region about the inequivalent K^+ and K^-= K points of the hexagonal Brillouin zone) flow to opposite transverse edges when the system is subjected to a longitudinal electric field in the presence of intrinsic spin-orbit coupling (SOC) in vicinity of $K^\pm$ valleys. At absolute zero (T=0K) and insulating regime where the chemical potential is in gap,Eqs.(5.46-5.49),show that the universal value of conductivity $\frac{q^2}{h}$ is obtained if for single spin and single valleys. Hence, we can say Hall conductivity is quantized in this limit and the sign of conductivity in K^+ and K^- are opposite indicating that both of valleys are related with time reversal symmetry. On the other hand, From Eqs. (5.50) and (5.51) and the total spin Hall conductivity vanishes identically. Whereas,total valley Hall conductivity is integral multiple of quantum conductivity ($4\frac{q^2}{h}$) the term 4 appear from two-fold valley degree of freedom (DOF) corresponding to the K^- and K^+ valleys of the Brillouin zone and two fold spin degree of freedom of those carriers. In addition,we have calculated both spin and valley Hall conductivity considering shift of chemical potential(Fermi level) mediated

by magnetic dopant atoms,in this scenario in contest to conductivity in insulating regime,the Hall conductivity calculated in single spin state (↑ / ↓) and in single valley (K^-) are not quantized but depend on the parameters (Δ_m,λ_{so},h_{ex}, k_F,a and t) see Eqs.5.(56-5.59). The calculated total spin Hall conductivity and total valley hall conductivity in Eqs. (62) and (63) can be written in more compact form as

$$\sigma^{spin}(z) = \frac{2q^2}{h}\left\{\left(1+\frac{a^2t^2k_F^2}{(\Delta_m + h_{ex} - \frac{1}{2}\lambda_{so})^2}\right)^{-\frac{1}{2}} - \left(1+\frac{a^2t^2k_F^2}{(\Delta_m + \frac{1}{2}\lambda_{so} - h_{ex})^2}\right)^{-\frac{1}{2}}\right\}. \quad (5.64)$$

$$\sigma^{val}(z) = -\frac{2q^2}{h}\left\{\left(1+\frac{a^2t^2k_F^2}{(\Delta_m + h_{ex} - \frac{1}{2}\lambda_{so})^2}\right)^{-\frac{1}{2}} + \left(1+\frac{a^2t^2k_F^2}{(\Delta_m + \frac{1}{2}\lambda_{so} - h_{ex})^2}\right)^{-\frac{1}{2}}\right\}. \quad (5.65)$$

From Eq.(5.64) and Eq.(5.65) ,total spin Hall conductivity and Valley conductivity depends on parameters : Δ_m,λ_{so},h_{ex},k_F,a and t,for particular limit $h_{ex} = \lambda_{so}$=0 and $h_{ex} = 2\lambda_{so}$ total spin hall conductivity in Eq.(5.64) vanishes whereas the total valley hall conductivity simplified to $-\frac{4q^2}{h}(\frac{\Delta_m^2+a^2t^2k_F^2}{atk_F})^{\frac{1}{2}}$, which indicates the interplay between spin-orbit coupling and dopant introduced magnetic exchange field are crucial for existence of spin hall conductivity.

5.6 Conclusion

The existence of dopant introduced exchange field breaks the time inversion symmetry and decouples the energetically degenerated valleys,elucidating the occurrence of valley polarization. The Berry curvature of occupied state resulting from transverse motion unequal number of of carriers in both valleys of 2D hexagonal lattice are responsible for existence of valley and spin hall conductivity. At low temperature ,in insulating regime valley Hall conductivity in a single valley is quantized. At finite dopant concentration,the strength of the spin orbit coupling together with the exchange energy determine the valley polarization,which in turn controls valley and spin Hall conductivity in doped ML MoS_2 system.The spin Hall and valley hall conductivity are dissipationless in the absence of any external magnetic field. This effect could enable a new generation of low power electronic devices.

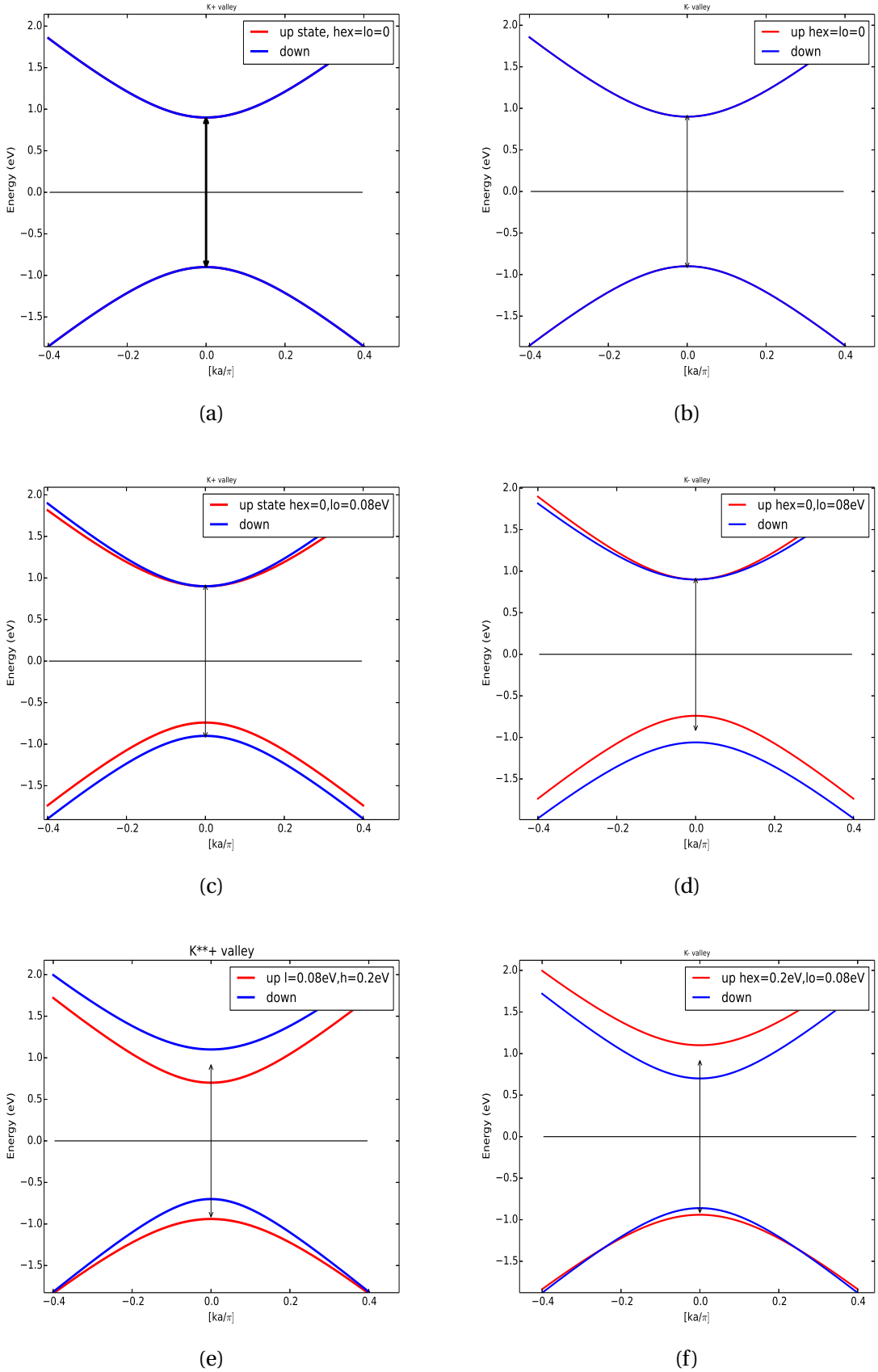

Fig. 5.2: Electronic band structure near valley $K^{\pm}$: a) and b)for zero both spin-orbit coupling and hexchange field (lo=h_{ex}=0),c) and d) for spin-orbit coupling(lo=0.08eV,) and zero exchange field ,and e) and f) for spin-orbit coupling(lo=0.08eV) and exchange field(h_{ex}=0.2eV). Red: spin up electron(hole) states, blue: spin down electron(hole) states,right panel for K^{+} and left panel for K^{-} valley.

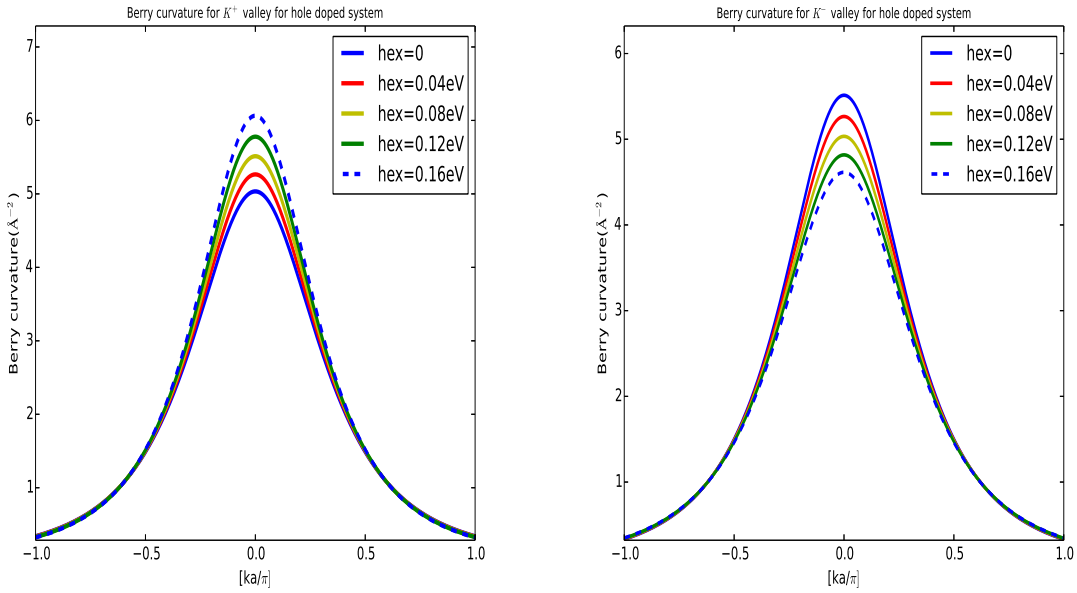

(a) (b)

Fig. 5.3: Berry Curvature as function of ($\frac{ka}{\pi}$) for different values of exchange field(h_{ex}) ,right panel for K^+ and left panel for K^- valley.

6

Summary and future work

Transition metal dichlcogenides(TMDs),MoS_2, are new class of open band gap semiconductors materials very essential for transistor applications and other semiconductor technology. However, those materials are non magnetic in their pure state. Hence it is necessary to introduce magnetism to this system to make it dilute magnetic semiconductors so that to broaden its application to spintronics.

In the first part of this work,chapter three and chapter four,the effect of magnetic dopants (V,Mn) on structural ,electronic and magnetic property are investigated in detail from stand point of defect formation energy calculations,electronic structure and magnetic energy calculations considering different impurity configurations and dopant concentrations. Moreover, the effect of layer number on magnetic interactions between dopants are also accessed.

The calculated dopant formation energy indicate Mn and V dopants in ML(BL) MoS_2 phase are energetically favorable to occupy the substitutional lattice site(Mo) and strongly bonded with host system(MoS_2).

It is found that,the magnetic interaction between Mn dopants in doped ML and BL MoS_2 are always ferromagnetic irrespective of dopant configurations. In contrast, in V doped case the magnetic interaction oscillates from ferromagnet to Antiferromagnet depending on the separation between dopants.

It is found that the interlayer interaction in (V,Mn) doped bilayer MoS_2 system affect the magnetic interactions between dopants .

The calculated ferromagnetic transition temperature (T_C) in Mn doped ML and BL MoS_2 cases are found to be above the room temperature (RT), whereas in V doped

cases T_C closer to RT. In addition, T_C increases with doping concentrations in a range of dilute limit (6.5%) of magnetic atoms for doped ML and BL MoS_2 ,which agree with latest experimental observed RT T_C.

In second part of this dissertation,using low energy effective tight binding model together with consideration of dopant introduced exchange field introduced magnetic exchange field it is found that ,dopant introduced exchange field breaks the time inversion symmetry and decouples the energetically degenerated valleys.

In addition to this ,we found that the strength of spin-orbit coupling together with exchange energy determine the valley polarization,which in turn controls valley and spin Hall conductivity in doped ML MoS_2 system. Our results are step towards information processing based on the valley degree of freedom.

Finally,it is worth noting that DFT underestimate the band gap value and to overcome the short coming of GGA functionals we have employed DFT+U formalism with U=3 and 4 eV for V and Mn to describe the strong electronic exchange correlation interaction in 3d state of V and Mn .However,for future we want to extend to GW method(Green function with self energy).

Bibliography

[1] A. K.Geim and I.V.Grigorieva,Nature,419-425(2013).

[2] K. S.Novoselov, et al., Science 306,666(2004).

[3] Tay-Rong Chang,Hsin Lin,Horng-Tay Jeng and A. Bansil,scientific reports 4,6270(2014).

[4] Po-Chun Yeh et al,Phys.Rev.B 91, 041407(R)(2015).

[5] B.Radisavljevic, M. B.Whitwick,and A. Kis, ACS Nano 5,9934(2011).

[6] Debora Pierucci et al.,Nano Lett.16 (7), 4054-4061(2016).

[7] A Shankara,Pradeep L Menezes,Kry,Sima and Satish V Kailas,Sadhana 33,207-220(2008).

[8] H.G. M.Fischer and R. P. Russell, US Pat.2 ,322-622(1943).

[9] B. Radisavljevic,A. Radenovic, J. Brivio, V. Giacometti and A. Kis, Nat. Nanotechnol 6,147150(2011).

[10] T.Bo ker et al,Phys. Rev.B 64, 235305(2001).

[11] F. E. Wickman and D. K. Smith, Am. Mineral.,55,18431856(1970).

[12] Sefaattin Tongay, Sima S. Varnoosfaderani,Bill R. Appleton,Junqiao Wu and Arthur F. Hebard,App. Phys. Lett 101,123105(2012).

[13] K.F. Mak, C. Lee, J. Hone, J. Shan and T.F. Heinz, Phys. Rev. Lett. 105,136805(2010).

[14] Wang etal,Nat. Nanotechnol.7,699-712(2012).

[15] Aiming Yan,Wei Chen,Colin Ophus,Jim Ciston,Yuyuan Lin,Kristin Persson,Phys.Rev.B 93,041420(2016).

[16] K. S.Novoselov,etal., Sciences of the United States of America 102, 30, 10451(2005).

[17] Y.-H. Lee et al, Adv. Mater.24,2320(2012).

[18] Wencan Jin,et al.,Phys.Rev.Lett 111, 106801(2013).

[19] D.Le,T.B. Rawal,T.S. Rahman, J. Phys. Chem. C118,5346-5351(2014).

[20] C. Ataca, S. Ciraci, J. Phys. Chem. C 115 , 13303-13311(2011)

[21] K. F. Mak, C. Lee, J. Hone, J. Shan, and T. F. Heinz, Phys. Rev.Lett.105,136805(2010).

[22] A. Splendiani, L. Sun, Y. B. Zhang, T. S. Li, J. Kim, C. Y. Chim,G. Galli, and F. Wang, Nano Lett.10,1271(2010).

[23] Q.H. Wang, K. Kalantar-Zadeh, A. Kis,J. N. Coleman and M. S. Strano, Nat. Nanotechnol.,7, 699712(2012).

[24] Z.Y. Zhu, Y. C. Cheng, and U. Schwingenschlo gl, Phys.Rev. B 84, 153402 (2011).

[25] D.Xiao, G. B. Liu, W. Feng, X. Xu, and W. Yao, Phys.Rev. Lett. 108, 196802(2012).

[26] Bui Dinh Hoi,Kavoos Mirabbaszadeh, Mohsen Yarmohammadi ,J Supercond Nov Magn.,7-4092(2017).

[27] Intek Song, ab Chibeom Park ab and Hee Cheul Choi, RSC Adv.,5, 7495(2015).

[28] S.Leb egue and O. Eriksson, Phys. Rev. B 79,115409(2009).

[29] J. He, K.Hummer, and C. Franchini,Phys. Rev. B 89, 075409(2014).

[30] Jin Xiao, Mengqiu Long, Xinmei Li, Qingtian Zhang, Hui Xu1 and K S Chan,Phys.: Condens. Matter 26,405302 (2014).

[31] Jiaxu Yan,Juan Xia,Xingli Wang,Lei Liu,Jer-Lai Kuo,Beng Kang Tay,Shoushun ChenŁ,Wu Zhou,Zheng Liu,and Ze Xiang Shen., Nano Lett.,15 (12),81558161(2015).

[32] S.F. Wu,J. S. Ross,G. B. Liu,G. Aivazian, A. Jones, Z. Fei, W. Zhu, D. Xiao, W. Yao, D.Cobden and X. Xu: Nat.Phys.9,149 (2013).

[33] Xiaofeng Fan,W.T.Zheng ,Jer-Lai Kuo,David J. Singh , C.Q. Sun ,W. Zhu,www.nature.com(scientificreports)(2016).

[34] S. W. Han, H.Kwon,S. K. Kim,S. Ryu,W. S.Yun,D. H. Kim,J. H. Hwang,J. S. Kang, J.Baik,H.J.Shin and S. C. Hong, Phys.Rev. B Vol. 84,045409(2011).

[35] K.Liu, L. Zhang, T. Cao, C. Jin, D. Qiu, Q. Zhou, A. Zettl,P. Yang, S. G. Louie, and F. Wang,Nat. Commun.5,4966(2014).

[36] A. M. van der Zande,et al.,Nano Lett.14,3869(2014).

[37] A. M. van der Zande,et al.,Nano Lett. 14,3869(2014).

[38] Sanfeng Wu and Jason S. Ros,s ,Nature Phys. 9,149-153(2013).

[39] Jin Xiao1, Mengqiu Long, Xinmei Li, Qingtian Zhang, Hui Xu1 and K S Chan, Phys. Condens. Matter 26,405302 (2014).

[40] WuS et al, Nat. Phys. 9149(2013).

[41] Tao Chu, Hesameddin Ilatikhameneh, Gerhard Klimeck, Rajib Rahman,and Zhihong ,Chen,Nano Lett.15 (12), 8000-8007(2015).

[42] W. Bao, X. Cai, D. Kim, K. Sridhara, and M. S. Fuhrer, Appl.Phys. Lett. 102,42104(2013).

[43] Jieqiong Wang,et al App. Phys. Lett. 109,092401(2016).

[44] Ashwin Ramasubramaniam ,Phys. Rev. B 87,195201(2013).

[45] Xu Zhao a,n ,Congxin Xia a , Tianxing Wang a , Xianqi Dai,Solid State Communications 220,31-35(2015).

[46] Xiang, ZhongCheng and Zhang, Zhong and Xu, XiJin and Zhang, Qin and Wang, QingBao and Yuan, Chengwu ,Phys. Chem. Chem. Phys., 17, 15822-15828(2015).

[47] Halbo Shu,Pengfei Luo, Pei Liang, Dan Cao, and Xiaoshuang Chen,ACS Appl. Mater.Interfaces,7,7534-7541(2015).

[48] Min Luo,Yu Hao Shen,and Jun Hao Chu,Japanese Journal of App.Phys.55,093001(2016).

[49] Hallam etal.Appl. Phys. Lett. 111,203101(2017).

[50] J.G.He,K.C. Wu, R.J. Sa, Q. H. Li and Y. Q.,Phys. Rev. Lett.,96,082504(2010).

[51] C. Ataca and S. Ciraci, Journal of Physical Chemistry C 11527),13303-13311 (2011).

[52] Wang, XQ.,Chen, WG., Zhu, ZL.et al. Acta Metall.Sin.,Engl. Lett.28:793(2015).

[53] Yanzong Wanget al,Journal of.physecal E.63,276-282(2014).

[54] H.Guo,T.Yang,P.Tao,Y.Wang,Z.Zhang, J. Appl. Phys. 113,013709(2013).

[55] Z T Wang et al,J. Phys.: Condens. Matter,24, 215801(2012).

[56] H. Ohno, D. Chiba, F. Matsukura, T. Omiya, E. Abe,T.Dielt,Nature,408, 944(2000).

[57] H. Ohno,Science,281, 951(1998).

[58] K. Sato, L. Bergqvist, J. Kudrnovsk, P. H. Dederichs, O. Eriksson, I. Turek, B. Sanyal, G. Bouzerar, H. Katayama-Yoshida, V. A. Dinh, T. Fukushima, H. Kizaki, and R. Zeller, Rev. Mod. Phys. 82, 1633(2010).

[59] S G Hu etal Nanotechnology 28 214001(2017).

[60] Y. C. Cheng, Z. Y. Zhu, W. B. Mi, Z. B. Guo, and U. Schwingenschlögl,Phys. Rev. B 87, 100401(R)(2013).

[61] Chang-Soo Park, Dongil Chu, Yoon Shon, Juwon Lee, and Eun Kyu Kim ,App. Phys. Lett 110, 222104 (2017).

[62] B Belhadji,LBergqvist,R Zeller, P H Dederichs,KSato and H Katayama-Yoshida, Phys.: Condens. Matter19,436227 (12)(2007).

[63] Luo, M., Xu, Y.E. and Shen, Y.H, J. Supercond Nov Magn.30, 2849(2017).

[64] Zener C ,Phys. Rev.81440(1951).

[65] Dietl T, Ohno H, Matsukura F,Cibert J and Ferrand D Science 287 1019(2000).

[66] B Belhadji et al, Kanamori J and Terakura K ,J.Phys.Soc.Japan 70 1433(2001).

[67] Kanamori J,J. Phys. Chem. Solids 1087(1959).

[68] Goodenough J B ,Phys. Rev.100564(1955).

[69] R. Mishra, W. Zhou, S. J. Pennycook, S. T. Pantelides and J.-C.Idrobo,Phys. Rev. B: Condens. Matter Mater. Phys.,88,144409(2013).

[70] Tiantian Zhang, etal,Proc. SPIE 10024,1002444(2016).

[71] A.H.Castro Neto, F.Guinea,N. M. R. Peres, K. S.Novoselov, A. K. Geim,Rev. Mod. Phys. 81, 109-162(2009).

[72] Di Xiao, Gui-Bin Liu, Wanxiang Feng, Xiaodong Xu, and Wang Yao,Phys.Rev.Lett 108,196802(2012).

[73] K. F. Mak, K. L. McGill, J. Park, P. L. McEuen, Science. 344 ,1489-1492 (2014).

[74] Xiao, W. Yao, and Q. Niu,Phys. Rev. Lett.99, 236809(2007).

[75] W. Yao, D. Xiao, and Q. Niu,Phys. Rev. B 77, 235406(2008).

[76] Min, J. E. Hill, N. A. Sinitsyn, B. R. Sahu, L. Kleinman,and A. H. MacDonald,Phys. Rev. B 74,165310(2006).

[77] Y. Yao, F. Ye, X.-L. Qi, S.-C. Zhang, and Z. Fang,Phys.Rev. B75, 041401(2007).

[78] 1.Mak, K. F., He, K., Shan, J. , Heinz, T. F.Nat. Nanotech.7, 494498 (2012).

[79] Zeng, H., Dai, J., Yao, W., Xiao, D.Cui, X. Nat. Nanotech. 7, 490493 (2012).

[80] Cao,T.et al., Nat. Comm. 3, 887 (2012).

[81] Kin Fai Mak1,Keliang He,Jie Shan2 and Tony F.Heinz1,NNANO.96,(2012).

[82] G.Kioseoglou, A. T.,Hanbicki, M. Currie, A. L.Friedman and B. T. Jonker,scientificreports(2016).

[83] Xiao,WY and Niu,Phys.Rev.Lett.99,236809(2007).

[84] Srivastava, A. et al , Phys. 11, 141-147(2015).

[85] Aivazian, G. et al. Phys. 11, 148152(2015).

[86] MacNeill, D. et al. Phys. Rev. Lett. 114, 037401(2015).

[87] Li, Y. et al. Phys. Rev. Lett. 113,266804(2014).

[88] Kathleen M. McCreary et al.,ACS Nano (2017).

[89] P. Hohenberg and W. Kohn, Phys. Rev.B, 136, 864(1964).

[90] W.Kohn and L.J.Sham, Phys. Rev. 140, A1133(1965).

[91] S.W. Peterson and H. A. Levy, Acta Crystallographica 10,70(1957).

[92] J.P. Perdew, J.A. Chevary, S. H. Vosko, K. A. Jackson, M. R. Pederson, D. J. Singh, and C. Fiolhais, Phys. Rev. B 66,165117 (2002).

[93] Anisimov, V. I.; Zaanen, J.; Andersen, O. K. Phys. Rev. B: Condens. Matter,44, 943-54(1991).

[94] Solovyev, I. V.; Dederichs, P. H.; Anisimov, V. I. Physical Review B 1994, 50,16861-16871(1994).

[95] V.I. Anisimov, F. Aryasetiawan, and A.I. Lichtenstein,J. Phys.: Condens. Matter9,767(1997).

[96] Journal of the Korean Physical Society, Vol. 62, No. 12,2155-2159(2013).

[97] H.J. Monkhorst and J. D. Pack, Phys. Rev.B 13, 5188(1976).

[98] N.Troullier and Jose Luriaas Martins.Phys.Rev. B, 43 (2006).

[99] David Vanderbilt. Phys.Rev. B, 41:7892-7895(1990).

[100] Rui Wang, Xiaoyu Zhou, Xiaoyong Xu, Jingguo Hu and Jing Pan,Phys. D: Appl. Phys.50,7, 095102(2017).

[101] P. Giannozzi et al., J. Phys.:Condens. Matter 21 395502 (2009).

[102] S. Grimme, J. Antony, S. Ehrlich and H. Krieg,J. Chem. Phys.,132, 154104(2010).

[103] H. J. Monkhorst and J. D. Pack, Phys. Rev.B 13,5188(1976).

[104] Kapildeb Dolui, Ivan Rungger, Chaitanya Das Pemmaraju, and Stefano Sanvito,Phys.Rev.B 88, 075420 (2013).

[105] Fanetal.,Nanoscale Research Letters 11,154 (2016).

[106] Adam J. Jackson,Davide Tiana and Aron Walsh,Chem. Sci.,7,1082(2016).

[107] Rohan Mishra, Wu Zhou, Stephen J. Pennycook, Sokrates T. Pantelides,and Juan-Carlos Idrobo ,Phys.Rev.B 88,144409 (2013).

[108] Deng Jiajun, Chen Pei, Wang Wenjie, Hu Bing,Che Jiantao, Chen Lin ,Wang Hailong and Zhao Jianhua,journal of Semiconductors.34, No. 8,(2013).

[109] Chang-Soo Park, Dongil Chu, Yoon Shon, Juwon Lee, and Eun Kyu Kim ,App.phys.Lett110, 222104 (2017).

[110] G.C. Hadjipanayis et al.,Science and Technology of Nanostructured Magnetic Materials,Springer Science and Business Media New York (1991).

[111] J.B. Goodenough, Phys. Rev. 100, 564 (1955).

[112] Kanamori, J. Phys. Chem. Solid 10, 87(1959).

[113] Changlong Tan,Dan Sun ,Long Zhou,Xiaohua Tian ,Yuewu Huang ,Superlattices and Microstructures 98,416-422(2016).

[114] Heng-Fu Lin, Woon-Ming Lau and Jijun Zhao,Scientific Reports 2017,Yiren Wang,Sean Li,1 and Jiabao Yia ,Sci. Rep. 6,24153 (2016).

[115] Neil.W Aschcroft ,N.David Memer, Solid State Physics, Harcourt college publisher, New York, 699-718(1976).

[116] M. Shahjahan,I.M. Razzakul, M.M. Rahman,Computational Condensed Matter 9 ,67-71(2016).

[117] K.S.Novoselov, A.K. Geim, S. V.Morozov, D.Jiang, Y. Zhang, S. V. Dubonos, I. V.Grigorieva, and A. A.Firsov,Science 306,666-669(2004).

[118] Di Xiao, Gui-Bin Liu Wanxiang Feng,Xiaodong Xu, and Wang Yao,PRL 108, 196802 (2012).

[119] Andor Kormnyos ,Guido Burkard ,Martin Gmitra,Jaroslav Fabian,Viktor Zlyomi Neil D Drummond and Vladimir Falko 3,2D Mater. 2 , 022001((2015).

[120] Y. Yao, L. Kleinman, A. H. MacDonald, J. Sinova, T. Jungwirth, D.-s. Wang, E.Wang, and Q. Niu, Phys. Rev. Lett. 92, 037204(2004).

[121] Manish Chhowalla,Zhongfan Liu and Hua Zhang,Chem. Soc. Rev.,44, 260(2015).

[122] M. Tahir, A. Manchon, K. Sabeeh, and U. Schwingenschlö gl ,App.Phys.Lett 102, 162412(2013).

[123] R.I. Eglitis, Applied Surface Science 358, 556 (2015).

[124] R.I. Eglitis, Int. J. Mod. Phys. B 28, 1430009 (2014).

6.1 List of publications

1. Sintayehu Mekonnen, P. Singh,Berry Approach to Intrinsic Anomalous Hall Conductivity in Dilute Magnetic Semiconductors,**World Journal of Condensed Matter Physics**,Vol. **5**,pp. 1790-186(2015).

2. Sintayehu and P.Singh,Electronic structure and nearly room temperature Ferromagnetism in V doped monolayer and bilayer MoS_2
   international journal of modern physics B,accepted may 20,2018

3. Sintayehu and p.Singh,Dopant induced Valley polarization ,spin and Valley Hall conductivity in doped monolayer MoS_2 ,**Advance in condensed matter physics** ,accepted may 2,2018

Other(non thesis related)

4. Sintayehu ,Nat. Science Vol.6 No.5(2014),

A

Appendix

A.1 Derivation of Berry curvature in two dimensional k-space

In this particular section we shall derive the general expression to Berry curvature for two dimensional (2D) system in terms of Berry potential A_α and A_β ,here α, β and γ designates x,y and z coordinates respectively .The Berry curvature along perpendicular to α, β plane is defined using analogical expression for real space magnetic field($\vec{B}$)

$$\Omega_{\alpha,\beta,\gamma} = \bigtriangledown_{\alpha,\beta,\gamma} \times A_{\alpha,\beta,\gamma} \tag{A.1}$$

In two dimensional system,

$$\vec{\Omega}_{\alpha,\beta} = (\bigtriangledown_{\alpha,\beta,} \times A_{\alpha,\beta})e_\gamma$$

$$\vec{\Omega}_{\alpha,\beta} = (\bigtriangledown_\alpha A_\beta - \bigtriangledown_\beta A_\alpha)e_\gamma \tag{A.2}$$

Where A_α and A_β are given by

$$\mathbf{A}_\alpha(k) = i\langle u_n(k)|\bigtriangledown_\alpha|u_n(k)\rangle \tag{A.3}$$

$$\mathbf{A}_\beta(k) = i\langle u_n(k)|\bigtriangledown_\beta|u_n(k)\rangle \tag{A.4}$$

Substituting Eqs. (A.3) and (A.4) into (A.2),

$$\vec{\Omega}_{\alpha,\beta} = i(\bigtriangledown_\alpha(\langle u_n(k)|\bigtriangledown_\beta|u_n(k)\rangle) - \bigtriangledown_\beta(\langle u_n(k)|\bigtriangledown_\alpha|u_n(k)\rangle)e_\gamma \tag{A.5}$$

Using properties of partial derivative ,Eq.(A.5) can be written as

$$\vec{\Omega}_{\alpha,\beta} = i\Big(\langle\bigtriangledown_\alpha u_n(k)|\bigtriangledown_\beta|u_n(k)\rangle + \langle u_n(k)|\bigtriangledown_\alpha \bigtriangledown_\beta |u_n(k)\rangle \tag{A.6}$$

$$-\langle \bigtriangledown_\beta u_n(k)|\bigtriangledown_\alpha|u_n(k)\rangle - \langle u_n(k)|\bigtriangledown_\beta \bigtriangledown_\alpha |u_n(k)\rangle\Big)e_\gamma$$

Collecting the same terms together,we have

$$\vec{\Omega}_{\alpha,\beta} = i\Big(\langle \bigtriangledown_\alpha u_n(k)|\bigtriangledown_\beta|u_n(k)\rangle - \langle \bigtriangledown_\beta u_n(k)|\bigtriangledown_\alpha|u_n(k)\rangle$$

$$+ \langle u_n(k)|\bigtriangledown_\alpha \bigtriangledown_\beta |u_n(k)\rangle - \langle u_n(k)|\bigtriangledown_\beta \bigtriangledown_\alpha |u_n(k)\rangle\Big)e_\gamma, \tag{A.7}$$

Which can be written as compact form after introducing commutator

$$\vec{\Omega}_{\alpha,\beta} = i\Big(\langle \bigtriangledown_\alpha u_n(k)|\bigtriangledown_\beta|u_n(k)\rangle - \langle \bigtriangledown_\beta u_n(k)|\bigtriangledown_\alpha|u_n(k)\rangle + \langle u_n(k)[\bigtriangledown_\alpha, \bigtriangledown_\beta]u_n(k)\rangle\Big)e_\gamma. \tag{A.8}$$

Since $\bigtriangledown_\alpha$ and $\bigtriangledown_\beta$ are commutate to each other ,hence the term $i(\langle u_n(k)[\bigtriangledown_\alpha, \bigtriangledown_\beta]u_n(k)\rangle)$ appeared in Eq.(A.8) vanishes and we left with

$$\vec{\Omega}_{\alpha,\beta} = i(\langle \bigtriangledown_\alpha u_n(k)|\bigtriangledown_\beta|u_n(k)\rangle - \langle \bigtriangledown_\beta u_n(k)|\bigtriangledown_\alpha|u_n(k)\rangle)e_\gamma \tag{A.9}$$

Introducing identity $\sum_m |u_m(k)\rangle\langle u_m(k)| = 1$ into Eq.(A.9)

$$\vec{\Omega}_{\alpha,\beta} = i\sum_{m\neq n}(\langle \bigtriangledown_\alpha u_n|u_m(k)\rangle\langle u_m(k)|(k)|\bigtriangledown_\beta|u_n(k)\rangle - \langle \bigtriangledown_\beta u_n(k)|u_m(k)\rangle\langle u_m(k)|\bigtriangledown_\alpha|u_n(k)\rangle)e_\gamma \tag{A.10}$$

Any complex number Z and its complex conjugate $Z*$ can be written as,

$$Z - Z* = i2ImZ \tag{A.11}$$

In the view of Eq.(A.11) ,Eq.(A.10) can be written as

$$\vec{\Omega}^n_{\alpha,\beta} = -2Im\sum_{m\neq n}(\langle \bigtriangledown_\alpha u_n|u_m(k)\rangle\langle u_m(k)|(k)|\bigtriangledown_\beta|u_n(k)\rangle e_\gamma \tag{A.12}$$

It is convenient to rewrite Eq.(A.12),in compact and more elegant form in terms of Eigenvalues and Eigenvectors , to do so we proceed further as follows,

$$\hat{H}(k)|\psi_{mk}(k)\rangle = \varepsilon_{mk}|\psi_{mk}(r)\rangle \tag{A.13}$$

where eigenfunction $|\psi_{mk}(r)\rangle$ are given by $\frac{1}{\sqrt{A}}exp(ik.r)u_m(k)\rangle$,and taking momentum derivative $\frac{\partial}{\partial k}$ on both sides of Eq.(A.13),we have

$$\frac{\partial}{\partial k}(\hat{H}(k)|\psi_{mk}(r)\rangle) = \frac{\partial}{\partial k}(\varepsilon_{mk}|\psi_{mk}(r)\rangle). \tag{A.14}$$

Eq.(A.14) can be rewritten using properties of partial derivative as

$$\frac{\partial}{\partial k}\hat{H}(k))|\psi_{mk}(r)\rangle + \hat{H}(k)\frac{\partial}{\partial k}|\psi_{mk}(r)\rangle) \tag{A.15}$$
$$= \frac{\partial}{\partial k}\varepsilon_{mk})|\psi_{mk}(r)\rangle + \varepsilon_{mk}\frac{\partial}{\partial k}|\psi_{mk}(r)\rangle).$$

Then overlapping with $\langle\psi_{nk'}(r)|$ from left,Eq.(A.15),we have

$$\langle\psi_{nk'}(r)|\frac{\partial}{\partial k}\hat{H}(k))|\psi_{mk}(r)\rangle + \langle\psi_{nk'}(r)|\hat{H}(k)\frac{\partial}{\partial k}|\psi_{mk}(r)\rangle) \tag{A.16}$$
$$= \langle\psi_{nk'}(r)|\frac{\partial}{\partial k}\varepsilon_{mk})|\psi_{mk}(r)\rangle + \langle\psi_{nk'}(r)|\varepsilon_{mk}\frac{\partial}{\partial k}|\psi_{mk}(r)\rangle)$$

Using Eigenfunction $\langle\psi_{nk'}(r)|$ and its complex conjugates into Eq.(A.16) together with implementing relation $\langle\psi_{nk'}(r)|\hat{H}(k)$=$En(k')\langle\psi_{nk'}|$ and straight forward simplification at($k = k'$) yields

$$\langle u_n(k)|\frac{\partial}{\partial k}\hat{H}(k)|u_m(k)\rangle + \varepsilon_{nk}\langle u_n(k)|\frac{\partial}{\partial k}|u_m(k)\rangle \tag{A.17}$$
$$= (\frac{\partial}{\partial k}\varepsilon_{mk})\langle u_n(k)|u_m(k)\rangle + \varepsilon_{mk}\langle u_n(k)|\frac{\partial}{\partial k}|u_m(k)\rangle$$

After rearranging

$$\langle u_n(k)|\frac{\partial}{\partial k}\hat{H}(k)|u_m(k)\rangle = (\frac{\partial}{\partial k}\varepsilon_{mk})\langle u_n(k)|u_m(k)\rangle + (\varepsilon_{mk}-\varepsilon_{nk})\langle u_n(k)|\frac{\partial}{\partial k}|u_m(k)\rangle \tag{A.18}$$

since($\varepsilon_{mk} \neq \varepsilon_{nk}$),their overlap should vanish i.e $\langle u_n(k)|u_m(k)\rangle = 0$. Therefore ,Eq.(A.18) reduced to

$$\langle u_n(k)|\frac{\partial}{\partial k}\hat{H}(k)|um_n(k)\rangle = (\varepsilon_{nk} - \varepsilon_{nk})\langle u_n(k)|\frac{\partial}{\partial k}|u_m(k)\rangle$$
$$\Rightarrow \langle u_n(k)|\frac{\partial}{\partial k}|u_m(k)\rangle = \frac{\langle u_n(k)|\frac{\partial}{\partial k}\hat{H}(k)|u_m(k)\rangle}{(\varepsilon_{mk} - \varepsilon_{nk})} \tag{A.19}$$

Using orthogonality relation one can show that

$$\langle\frac{\partial}{\partial k}u_n(k)|u_m(k)\rangle = -\langle u_n(k)|\frac{\partial}{\partial k}u_m(k)\rangle \tag{A.20}$$

On the view of Eq.(A.19), we can write Eq.(A.20) and its complexcongugate respectively as

$$\langle\nabla_\alpha u_n(k)|u_m(k)\rangle = -\frac{\langle u_n(k)|\nabla_\alpha\hat{H}(k)|u_m(k)\rangle}{(\varepsilon_{mk} - \varepsilon_{nk})}. \tag{A.21}$$

$$\langle u_m(k)|\nabla_\beta|u_n(k)\rangle = \frac{\langle u_m(k)|\nabla_\beta \hat{H}(k)|u_n(k)\rangle}{(\varepsilon_{mk} - \varepsilon_{nk})}. \tag{A.22}$$

Where we have introduced short notation($\frac{\partial}{\partial k_\alpha} \rightarrow \nabla_\alpha$, $\frac{\partial}{\partial k_\beta} \rightarrow \nabla_\beta$). Using those Eqs.(A.21) and (A.22) into Eq.(A.12) the general expression for Berry curvature along e_γ as

$$\vec{\Omega}^n_{\alpha,\beta} = -2Im \sum_{m\neq n} (\frac{\langle u_n(k)|\nabla_\alpha \hat{H}(k)|u_m(k)\rangle\langle u_m(k)|\nabla_\beta \hat{H}(k)|u_n(k)\rangle}{(\varepsilon_{mk} - \varepsilon_{nk})^2} e_\gamma. \tag{A.23}$$

B

Appendix

B.1 Linear response theory to derivative Kubo formula for Hall conductivity

linear response theory is based on the idea that the external perturbation, for example an external electric field, is small enough so we can only take into account the linear perturbation term.Assuming that the Hamiltonian operator of system under-consideration can be decomposed into the Hamiltonian of unperitubed system ,$\hat{H}_0$ and operator related to general time dependent perturbation,$\hat{H}^{'}(t)$.

$$\hat{H}(t) = \hat{H}_0 + \hat{H}^{'}(t). \tag{B.1}$$

Using grand canonical ensembele ,the density operator of unperitubed system can be written using the Van Newmann equation of motion for density matrix,

$$\varrho(t) = \frac{exp(-\beta H_0)}{Z}. \tag{B.2}$$

Where β=$\frac{1}{K_B T}$,T is temperature and K_B the Blothmann constant ,wheras Z is given by $Z = Tr(exp(\beta H_0))$. In the Schrdinger picture the equation of motion for density operator $\varrho(t)$ with respect to H(t) is given by ,

$$i\hbar\frac{\partial\varrho(t)}{\partial t} = [H(t), \varrho(t)]. \tag{B.3}$$

We know that in absence of perturbation ,the density operator $\varrho(t)$ is just $\varrho(0)$.Therefore,$\varrho(t)$ can be written as

$$\varrho(t) = \varrho(0) + \varrho^{'}(t) \tag{B.4}$$

Now substituting Eqs.(B.1) and (B.4) into Eq.(B.3),

$$i\hbar\frac{\partial}{\partial t}\bigg(\varrho(0)+\varrho_I^{'}(t)\bigg)=[\hat{H}_0+\hat{H}^{'}(t),\varrho(0)+\varrho_I^{'}(t]. \tag{B.5}$$

Making use of $[H_0,\varrho_0]=0$,we shall get first order in $H^{'}(t)$ as

$$i\hbar\frac{\partial}{\partial t}\varrho^{'}(t))=[\hat{H}_0,\varrho^{'}(t)]+[\hat{H}^{'}(t),\varrho(0)] \tag{B.6}$$

It is now worth to switch interaction (or Dirac) picture,

$$\varrho(t)=\varrho(0)+\varrho_I'(t) \tag{B.7}$$

$$\varrho_I^{'}(t)=exp(\frac{i}{\hbar}H_0t)\varrho^{'}(t)exp(\frac{-i}{\hbar}H_0t) \tag{B.8}$$

Evaluting $i\hbar\frac{\partial}{\partial t}\varrho_I^{'}(t)$ using above as follows,

$$i\hbar\frac{\partial}{\partial t}\varrho_I^{'}(t)=i\hbar\frac{\partial}{\partial t}\bigg(exp(\frac{i}{\hbar}H_0t)\varrho^{'}(t)exp(\frac{-i}{\hbar}H_0t)\bigg) \tag{B.9}$$

After expanding right side of Eq. (B.9) can be written as ,

$$\begin{aligned}i\hbar\frac{\partial}{\partial t}\varrho_I^{'}(t)&=i\hbar\frac{\partial}{\partial t}exp(\frac{i}{\hbar}H_0t)\varrho^{'}(t)exp(\frac{-i}{\hbar}H_0t)\\&+exp(\frac{i}{\hbar}H_0t)(i\hbar\frac{\partial}{\partial t}\varrho^{'}(t))exp(\frac{-i}{\hbar}H_0t)\\&+i\hbar exp(\frac{i}{\hbar}H_0t)(\varrho^{'}(t)\frac{\partial}{\partial t}exp(\frac{-i}{\hbar}H_0t)\end{aligned} \tag{B.10}$$

Then performing derivative we have,

$$\begin{aligned}i\hbar\frac{\partial}{\partial t}\varrho_I^{'}(t)&=-H_0exp(\frac{i}{\hbar}H_0t)\varrho^{'}(t)exp(\frac{-i}{\hbar}H_0t)\\&+exp(\frac{i}{\hbar}H_0t)(i\hbar\frac{\partial}{\partial t}\varrho^{'}(t))exp(\frac{-i}{\hbar}H_0t)\\&+exp(\frac{i}{\hbar}H_0t)(\varrho^{'}(t)exp(\frac{-i}{\hbar}H_0t)H_0\end{aligned} \tag{B.11}$$

In view of Dirac(interaction)picture ,Eq.(B.11),becomes,

$$i\hbar\frac{\partial}{\partial t}\varrho_I^{'}(t)=-H_0\varrho_I^{'}(t)+exp(\frac{i}{\hbar}H_0t)(i\hbar\frac{\partial}{\partial t}\varrho^{'}(t))exp(\frac{-i}{\hbar}H_0t)+\varrho_I^{'}(t)H_0 \tag{B.12}$$

which can be written in compact form after introducing commutator as,

$$i\hbar\frac{\partial}{\partial t}\varrho_I^{'}(t)=[\varrho_I^{'}(t),H_0]+exp(\frac{i}{\hbar}H_0t)(i\hbar\frac{\partial}{\partial t}\varrho^{'}(t))exp(\frac{-i}{\hbar}H_0t) \tag{B.13}$$

Plugging Eq.(B.6),into Eq.(B.13),we obtain,

$$i\hbar\frac{\partial}{\partial t}\varrho_I^{'}(t) = [\varrho_I^{'}(t), H_0] + exp(\frac{i}{\hbar}H_0t)\Big([\hat{H}_0, \varrho^{'}(t)] + [\hat{H}^{'}(t), \varrho(0)]\Big)exp(\frac{-i}{\hbar}H_0t) \tag{B.14}$$

which can be written as

$$i\hbar\frac{\partial}{\partial t}\varrho_I^{'}(t) = [\varrho_I^{'}(t), H_0]+[\hat{H}_0, exp(\frac{i}{\hbar}H_0t)\varrho^{'}(t)exp(\frac{-i}{\hbar}H_0t)]+[exp(\frac{i}{\hbar}H_0t)\hat{H}^{'}(t)exp(\frac{-i}{\hbar}H_0t), \varrho(0)] \tag{B.15}$$

Recaling Dirac(interaction) picture, Eq.(B.15) becomes

$$i\hbar\frac{\partial}{\partial t}\varrho_I^{'}(t) = [\varrho_I^{'}(t), H_0] + [\hat{H}_0, \varrho_I^{'}(t)] + [\hat{H}_I^{'}(t), \varrho(0)] \tag{B.16}$$

Using properties of cumutation relation,Eq.(B.16) simplified to,

$$i\hbar\frac{\partial}{\partial t}\varrho_I^{'}(t) = [\hat{H}_I^{'}(t), \varrho(0)] \tag{B.17}$$

The solution of the above equation with the boundary condition $\varrho_I^{'}(t) \to 0$ as $t \to -\infty$ (in other words as t goes to ∞ there is no perturbation)can be given as

$$\varrho_I^{'}(t) = \frac{-i}{\hbar}\int_{-\infty}^{t} dt'[\hat{H}_I^{'}(t'), \varrho(0)] \tag{B.18}$$

Therefor, Eq.(B.18) can be approximated as first order as

$$\varrho(t) = \varrho_0 - \frac{i}{\hbar}\int_{-\infty}^{t} dt' exp(\frac{-i}{\hbar}H_0t)[\hat{H}_I^{'}(t'), \varrho(0)]exp(\frac{i}{\hbar}H_0t). \tag{B.19}$$

The time evolution of physical observable ,say A(t) associated with Hermitian operator can be defined as expection vlue,

$$\langle A(t)\rangle = Tr(\varrho A) \tag{B.20}$$

Using Eq.(B.19) into Eq.(B.20) we have

$$A(t) = Tr(\varrho_0 A) - \frac{i}{\hbar}\int_{-\infty}^{t} dt' Tr\Big(exp(\frac{-i}{\hbar}H_0t)[\hat{H}_I^{'}(t'), \varrho(0)]exp(\frac{i}{\hbar}H_0t)\Big)A. \tag{B.21}$$

Aftre introducing interaction,Dirac picture, Eq.(B.21),

$$A(t) = A_0 - \frac{i}{\hbar}\int_{-\infty}^{t} dt' Tr\Big([\hat{H}_I^{'}(t'), \varrho(0)]A_I(t)\Big). \tag{B.22}$$

Where,$A_0 = Tr(\varrho_0 A)$ and $A_I(t) = exp(\frac{i}{\hbar}H_0 t)Aexp(\frac{-i}{\hbar}H_0 t)$. Applying identity

$$Tr([A,B]C) = Tr(ABC - BAC) = Tr(BCA - BAC) = Tr(B[C,A]). \tag{B.23}$$

Change of expection value of operator $\delta A(t)$,from Eq.(B.22) togher with employing relation Eq.(B.23) we have ,

$$A(t) - A_0 = \delta A(t) = -\frac{i}{\hbar}\int_{-\infty}^{t} dt' Tr\bigg(\varrho(0[A_I(t)), \hat{H}_I'(t')]\bigg). \tag{B.24}$$

The Quantum Kubo's formula

Applying Heisenberg picture instead of Dirac(interaction) picture Eq.(B.24) become

$$\delta A(t) = -\frac{i}{\hbar}\int_{-\infty}^{t} dt' Tr\bigg([\varrho_0, \hat{H}_H'(t')]\hat{A}_H(t)\bigg). \tag{B.25}$$

Where operators are taken to be in Heisenberg picture with respect to the unpertubed system. Kubo's identity state that for any observable $X_H(t)$ in Heisenberg picture can be written as

$$\frac{i}{\hbar}[\varrho, X_H(t)] = \varrho\int_0^{\beta} d\lambda \dot{X}_H(t - i\lambda\hbar) \tag{B.26}$$

$$\dot{X}_H(t) = -\frac{i}{\hbar}[X_H(t), \hat{H}]. \tag{B.27}$$

Where the density operator is given by

$$\varrho = -\frac{exp(-\beta H)}{Tr(exp(-\beta H))}, \tag{B.28}$$

$$X_H(t) = exp(\frac{i}{\hbar}H_0 t)X(t)exp(\frac{-i}{\hbar}H_0 t). \tag{B.29}$$

Applying Kubo's identity in Eq.(B.26),Eq.(B.25),yields,

$$\delta A(t) = -\int_{-\infty}^{t} dt' \int_0^{\beta} d\lambda Tr\bigg(\varrho_0 \dot{\hat{H}}'(t - i\lambda\hbar)\hat{A}_H(t)\bigg). \tag{B.30}$$

After performing properties of Trace of an operator we shall obtain,

$$\delta A(t) = -\int_{-\infty}^{t} dt' \int_0^{\beta} d\lambda Tr\bigg(\varrho_0 \dot{\hat{H}}'(t'))\hat{A}(t - t' + i\lambda\hbar)\bigg). \tag{B.31}$$

To Introduce the concept of current-current correclation,we assuming that when time varing electric field applied to solid.Obviously this induce currents ,which in

turn emits electric field.Taking account of the variation of current density due to applied electric field the μ^{th} components of corrent density J_μ can be written as

$$\hat{J}_\mu(r,t) = -\int_{-\infty}^{t} dt' \int_0^\beta d\lambda Tr\Big(\varrho_0 \dot{\hat{H}}'(t')\hat{J}_\mu(r,t-t'+i\lambda\hbar)\Big). \tag{B.32}$$

To obtain explicit form of $\dot{H}$ we assume that the total electric field (internal plus external electric field) (E(r,t)is related to perturbation through a scalar potential($\phi(r,t)$) E(r,t)=$-\bigtriangledown\phi(r,t)$.

$$\begin{aligned} H'(t) &= \int Q\phi(r,t)d^3r \\ &= \int (nq)\phi(r,t)d^3r \\ &= \int d^3rqn(r,t)\phi(r,t) \\ &= \int d^3r\rho(r)\phi(r,t) \end{aligned} \tag{B.33}$$

where ,$\rho(r)$ is charge density (in coulumb per meter),n(r,t) is number density. Taking time derivative in both sides of Eq.(B.33),

$$\dot{H}'(t) = \int d^3r\dot{\rho}(r)\phi(r,t) \tag{B.34}$$

To obtain the explicit form of $\dot{\rho}(r)$ we shall use continity equation which relates the number density to electron current density

$$\frac{d\rho}{dt} = -\nabla_r J(r) \tag{B.35}$$

Substitution of Eq.(B.35) into Eq.(B.34) yields

$$\begin{aligned} \dot{H}'(t) &= -\int d^3r\nabla_r\phi(r,t)J(r) \\ &= \int d^3rE(r,t)J(r) \end{aligned} \tag{B.36}$$

Now substituting Eq.(B.36) into Eq.(B.32),we have

$$\hat{J}_\mu(r,t) = \sum_v \int_{-\infty}^{t} dt' \int_0^\beta d\lambda Tr\Big(\varrho_0 \int d^3rE_v(r,t)J_v(r)\hat{J}_\mu(r,t-t'+i\lambda\hbar)\Big). \tag{B.37}$$

On the other hand,using Ohm's law ,one can write μ^{th} component of current density as

$$\hat{J}_{\mu}(r,t) = \sum_{v} \int_{-\infty}^{t} dt' \int d^3r' \sigma_{\mu v}(r,r',t,t') E_v(r',t'). \tag{B.38}$$

Comparision of Eq.(B.37) and Eq.(B.38) yields space-time correlation function as

$$\sigma_{\mu v}(r,r',t,t') = \theta(t-t') \int_0^{\beta} d\lambda Tr\Big(\varrho_0 J_{v,o}(r) \hat{J}_{\mu}(r,t-t'+i\lambda\hbar)\Big). \tag{B.39}$$

Assuming that $\sigma_{\mu v}(r,r',t,t')$ is homogenous in space i.e,$\sigma_{\mu v}(r,r',t,t') = \sigma_{\mu v}(r-r',t-t')$ Fourier transformation $\hat{J}(r,t)$ can be written as

$$J_{\mu}(q,\omega) = \frac{1}{V} \int_{\infty}^{\infty} dt \int d^3r J_{\mu}(r,t) exp(-iq.r + i\omega t) \tag{B.40}$$

From which we shall obtain the Fourier transform of cunductivity tensor as,

$$\sigma_{\mu v}(q,\varpi) = \frac{1}{V} \int_0^{\infty} dt exp(i\omega t) \int_0^{\beta} d\lambda Tr\Big(\varrho_0 J_v(q,0) \hat{J}_{\mu}(q,t+i\hbar\lambda)\Big) \tag{B.41}$$

Using the value of ϱ_0 ,

$$\varrho_0 = \frac{exp(-\beta H_0)}{Z} \tag{B.42}$$

Where,Z is partition function given by $Z = Tr(exp(-\beta H_0))$ and using the relation

$$\hat{J}_{\mu}(q,t+i\hbar\lambda) = exp(-\beta\lambda) \hat{J}_{\mu}(q,t) exp(\beta\lambda) \tag{B.43}$$

After substituting Eqs.(B.26) and (B.43) into) Eq.(B.41) togther with some mathematical algebra,

$$\sigma_{\mu v}(q,\varpi) = \frac{i}{\hbar V} \int_0^{\infty} dt exp(i\omega t) \int_t^{\infty} dt' Tr\Big(\varrho_0 \Big[J_{\mu}(q,t'), J_v(-q,0)\Big]\Big) \tag{B.44}$$

Employing integration by part technique

$$\int_a^b f(t)\dot{g}(t)dt = f(t)g(t)\Big|_a^b - \int_a^b \dot{f}(t)g(t)dt \tag{B.45}$$

On the view of Eq.(B.45),Eq.(B.44)) can be written as

$$\sigma_{\mu v}(q,\varpi) = \frac{1}{\hbar V\omega}\Big(exp(i\omega t) \int_t^{\infty} dt' Tr\Big(\varrho_0 \Big[J_{\mu}(q,t'), J_v(q,0)\Big]\Big)\Big)\Big|_0^{\infty}$$
$$+\frac{1}{\hbar V\omega} \int_0^{\infty} dt exp(i\omega t) Tr\Big(\varrho_0 \Big[J_{\mu}(q,t'), J_v(q,0)\Big]\Big)$$

$$= \frac{1}{\hbar V\omega}\int_0^\infty dt exp(i\omega t) Tr\Big(\varrho_0\Big[J_\mu(q,t'),J_v(-q,0)\Big]\Big) - \frac{1}{\hbar V\omega}\int_0^\infty dt' Tr\Big(\varrho_0\Big[J_\mu(q,t'),J_v(-q,0)\Big]\Big) \tag{B.46}$$

Now defing current-current correlation function as

$$C_{\mu v}(q,\omega) = \frac{1}{\hbar V}\int_0^\infty dt exp(i\omega t) Tr\Big(\varrho_0\Big[J_\mu(q,t'),J_v(-q,0)\Big]\Big) \tag{B.47}$$

From which at $\omega = 0$,the correlation function becomes

$$C_{\mu v}(q,0) = \frac{1}{\hbar V}\int_0^\infty dt Tr\Big(\varrho_0\Big[J_\mu(q,t),J_v(-q,0)\Big]\Big) \tag{B.48}$$

Using Eqs.(B.47) and (B.48) conductivity can be written in terms of current-current correlation as function as

$$\sigma_{\mu v}(q,\varpi) = \frac{1}{\omega}\Big(C_{\mu v}(q,\omega) - C_{\mu v}(q,0)\Big) \tag{B.49}$$

To tackle Eq.(B.47) here after we introduce independent particle approximation ,which appears for a system of independent Fermions by defining one particle operators and the corresponding Dirac Distribution function.For this we use $f(H_0) = \frac{1}{exp\beta(H_0-\mu)+1}$ insetead of $\varrho_0 = \frac{exp(-\beta H_0)}{Z}$ and employing basis of eigenfunction and eigenvalue equations ,

$$H_0|n\rangle = E_n|n\rangle \tag{B.50}$$

$$\langle m|n\rangle = \delta_{nm}, \tag{B.51}$$

$$\sum_n |n\rangle\langle n| = I \tag{B.52}$$

Using thus basis we shall evaluate the cumutation relation in current-current corelation function in Eq.(B.47) as follows,

$$Tr\Big(\varrho_0\Big[J_\mu(q,t'),J_v(-q,0)\Big]\Big) = \sum_n \langle n|\varrho_0\Big[J_\mu(q,t'),J_v(-q,0)\Big]|n\rangle \tag{B.53}$$

using commutation relation Eq.(B.53) can be expanded as,

$$Tr\Big(\varrho_0\Big[J_\mu(q,t'),J_v(-q,0)\Big]\Big) = \sum_n \langle n|f(H_0)J_\mu(q,t')J_v(-q,0)|n\rangle - \sum_n \langle n|f(H_0)J_v(-q,0)J_\mu(q,t')|n\rangle. \tag{B.54}$$

Introducing completeness relation $\sum_n|n\rangle\langle n| = \sum_m|m\rangle\langle m| = \sum_Q|Q\rangle\langle Q| = I$ Into right side of Eq.(B.54) ,

$$Tr\bigg(\varrho_0\bigg[J_\mu(q,t'),J_v(-q,0)\bigg]\bigg) = \sum_n\sum_m\langle n|f(H_0)J_\mu(q,t')|m\rangle\langle mJ_v(-q,0)|n\rangle - \sum_m\sum_n\langle m|f(H_0)J_v(-q \tag{B.55}$$

$$= \sum_n\sum_m\sum_Q\langle n|f(H_0)|Q\rangle\langle Q|J_\mu(q,t')|m\rangle\langle mJ_v(-q,0)|n\rangle$$
$$- \sum_m\sum_n\sum_Q\langle m|f(H_0)|Q\rangle\langle Q|J_v(-q,0)|n\rangle\langle nJ_\mu(q,t')|m\rangle \tag{B.56}$$

Using interaction (Dirac) picture we rewrite $J_\mu(q,t)$ and $J_\mu(q,o)$ as

$$J_\mu(q,t') = exp(-iH_0t')J_\mu(q)exp(iH_0t') \tag{B.57}$$

plugging Eq.(B.57) into Eq.(B.56),we have

$$Tr\bigg(\varrho_0\bigg[J_\mu(q,t'),J_v(-q,0)\bigg]\bigg) = \sum_n\sum_m\sum_Q\langle n|f(H_0)|Q\rangle\langle Q|exp(-iH_0t')J_\mu(q)exp(iH_0t')|m\rangle\langle mJ_v(-q$$
$$- \sum_m\sum_n\sum_Q\langle m|f(H_0)|Q\rangle\langle Q|J_v(-q,0)|n\rangle\langle nexp(-iH_0t')J_\mu(q)exp(iH_0t')|m\rangle \tag{B.58}$$

Using the relation $\langle n|f(H_0)|Q\rangle = f(E_n)\delta_{Qn}$ and $\langle m|f(H_0)|Q\rangle = f(E_m)\delta_{Qm}$, Eq.(B.58) can be rewritten,

$$= \sum_{n,m,Q} f(E_n)\delta_{Qn}exp(-iE_Qt')J_\mu^{Qm}(q)exp(iE_mt')J_v^{mn}(-q)$$
$$- \sum_{m,n,Q} f(E_m)\delta_{Qm}J_v^{Qn}(-q)exp(-iE_Qt')J_\mu^{mn}(q)exp(iE_nt') \tag{B.59}$$
$$= \sum_{n,m} f(E_n)exp(-iE_nt')J_\mu^{nm}(q)exp(iE_mt')J_v^{mn}(-q)$$
$$- \sum_{m,n} f(E_m)J_v^{Qn}(-q)exp(-iE_nt')J_\mu^{nm}(q)exp(iE_mt') \tag{B.60}$$

Which can be written in more compact form as

$$Tr\bigg(\varrho_0\bigg[J_\mu(q,t'),J_v(-q,0)\bigg]\bigg) = \sum_{n,m}(f(E_n) - f(E_m)exp(\frac{i(E_m-E_n)}{\hbar})t'J_\mu^{nm}(q)J_v^{mn}(-q) \tag{B.61}$$

Where $J_\mu^{nm}(q) = \langle n|J_\mu(q)|m\rangle$,$J_\mu^{mn}(q) = \langle m|J_\mu(q)|n\rangle$. Using Eq.(B.61) into (B.47) of current-current correlation function ,we obtain

$$C_{\mu v}(q,\omega) = \frac{1}{\hbar V}\int_0^\infty dtexp(i\omega t)\sum_{n,m}(f(E_n) - f(E_m)exp(\frac{i(E_m-E_n)}{\hbar})t'J_\mu^{nm}(q)J_v^{mn}(-q) \tag{B.62}$$

when the perturbation is switched on,we have (t=t'),after rearranging ,

$$C_{\mu v}(q,\omega) = \frac{1}{\hbar V}\sum_{n,m}(f(E_n) - f(E_m)' J_{\mu}^{nm}(q) J_{v}^{mn}(-q) \int_0^{\infty} dt exp(\frac{i(E_n - E_m + \hbar\omega)}{\hbar})t \tag{B.63}$$

Using laplace transformation with respect t for $s > 0$

$$\int_0^{\infty} dt exp(\frac{i(-s + E_n - E_m + \hbar\omega)}{\hbar})t = \frac{exp(\frac{i(-s+E_n-E_m+\hbar\omega)t}{\hbar})}{(-s + E_n - E_m + \hbar\omega)} \tag{B.64}$$

At t=0, $s \approx 0$,the right side of Eq.(B.64) becomes $\frac{1}{\frac{i}{\hbar}(E_n - E_m + \hbar\omega)}$ and substituting this into Eq.(B.63),

$$C_{\mu v}(q,\omega) = \frac{1}{iV}\sum_{n,m}\frac{f(E_n) - f(E_m)}{i(E_n - E_m + \hbar\omega)} J_{\mu}^{nm}(q) J_{v}^{mn}(-q) \tag{B.65}$$

$$C_{\mu v}(q,0) = \frac{1}{iV}\sum_{n,m}\frac{f(E_n) - f(E_m)}{i(E_n - E_m)} J_{\mu}^{nm}(q) J_{v}^{mn}(-q) \tag{B.66}$$

Finally plugging Eqs.(B.65) and (B.66) into Eq.(B.49) and straight forward manipulation yields Kubo formula for Hall conductivity

$$\sigma_{\mu v}(q,\varpi)) = \frac{i\hbar}{V}\sum_{n,m}\left\langle \frac{f(E_n) - f(E_m)}{(E_n - E_m)(E_n - E_m + \hbar\omega)} J_{\mu}^{nm}(q) J_{v}^{mn}(-q) \right\rangle_c . \tag{B.67}$$